

**PHASE SPACE ANALYSIS AND CLASSIFICATION
OF SONAR ECHOES IN SHALLOW-WATER
CHANNELS**

by

Greg Okopal

B.S. in Computer Engineering, Villanova University, 2002

M.S. in Electrical Engineering, University of Pittsburgh, 2007

Submitted to the Graduate Faculty of
the Swanson School of Engineering in partial fulfillment
of the requirements for the degree of

Doctor of Philosophy

University of Pittsburgh

2009

UNIVERSITY OF PITTSBURGH
SWANSON SCHOOL OF ENGINEERING

This dissertation was presented

by

Greg Okopal

It was defended on

June 29, 2009

and approved by

P. J. Loughlin, Ph.D., Professor

J. R. Boston, Ph.D., Professor

A. A. El-Jaroudi, Ph.D., Associate Professor

Z. H. Mao, Ph.D., Assistant Professor

J. Pitton, Ph.D., Principal Engineer, Applied Physics Laboratory, University of
Washington, Affiliate Assistant Professor, Department of Electrical Engineering, University
of Washington

Dissertation Director: P. J. Loughlin, Ph.D., Professor

Copyright © by Greg Okopal
2009

PHASE SPACE ANALYSIS AND CLASSIFICATION OF SONAR ECHOES IN SHALLOW-WATER CHANNELS

Greg Okopal, PhD

University of Pittsburgh, 2009

A primary objective of active sonar systems is to detect, locate, and classify objects, such as mines, ships, and biologics, based on their sonar backscatter. A shallow-water ocean channel is a challenging environment in which to classify sonar echoes because interactions of the sonar signal with the ocean surface and bottom induce frequency-dependent changes (especially dispersion and damping) in the signal as it propagates, the effects of which typically grow with range. Accordingly, the observed signal depends not only on the initial target backscatter, but also the propagation channel and how far the signal has propagated. These propagation effects can increase the variability of observed target echoes and degrade classification performance. Furthermore, uncertainty of the exact propagation channel and random variations within a channel cause classification features extracted from the received sonar echo to behave as random variables.

With the goal of improving sonar signal classification in shallow-water environments, this work develops a phase space framework for studying sound propagation in channels with dispersion and damping. This approach leads to new moment features for classification that are invariant to dispersion and damping, the utility of which is demonstrated via simulation. In addition, the accuracy of a previously developed phase space approximation method for range-independent pulse propagation is analyzed and shown to be greater than the accuracy of the standard stationary phase approximation for both large and small times/distances. The phase space approximation is also extended to range dependent propagation. Finally, the phase space approximation is used to investigate the random nature of moment features

for classification by calculating the moments of the moment features under uncertain and random channel assumptions. These moments of the moment features are used to estimate probability distribution functions for the moment features, and we explore several ways in which this information may be used to improve sonar classification performance.

TABLE OF CONTENTS

PREFACE	xi
1.0 INTRODUCTION	1
1.1 Background	1
1.2 Summary of this Work	3
2.0 WAVE PROPAGATION	7
2.1 Wigner Distribution	10
2.2 Single Mode	12
2.2.1 Wigner Approximation	13
3.0 MOMENTS OF THE WIGNER DISTRIBUTION	14
3.1 Global Moments	14
3.1.1 Temporal Moments	15
3.1.1.1 Approximate Temporal Moments	16
3.1.1.2 Stationary Phase Approximation	16
3.1.2 Spectral Moments	19
3.2 Exact and Approximate Local Temporal Moments	20
3.2.1 Approximate Local Temporal Moments	21
3.3 Moments as Classification Features	21
4.0 PROPAGATION INVARIANT CLASSIFICATION	24
4.1 Moments Invariant to Dispersion	24
4.2 Moments Invariant to Dispersion and Damping	26
4.2.1 Exponential Attenuation	26
4.2.2 Power-law Attenuation	28

4.2.3	Cepstral Moments	29
4.2.4	Relation Between ADIMs and Cepstral Moments	30
4.3	Classification Simulations	32
4.3.1	Simulation Setup	32
4.3.2	Simulation Results	35
5.0	MOMENTS OF MOMENTS	42
5.1	Uncertain Channels	43
5.1.1	Uncertain Channel Model	43
5.1.2	Moments of Moments of the Wigner Distribution	44
5.1.2.1	Temporal Moment Features	44
5.1.2.2	Frequency Moments	46
5.1.3	Example 1	47
5.1.4	Example 2	49
5.1.4.1	First Temporal Moment Feature	50
5.1.4.2	Second Temporal Moment Feature	51
5.1.4.3	Real Dispersion Relation	53
5.2	Random Channels	55
5.2.1	Randomly Varying Channels	55
5.2.2	Pulse Propagation	58
5.2.2.1	Wigner Distribution for Randomly Varying Channels	59
5.2.3	Moments of Moments	60
5.2.4	Example	62
6.0	FEATURE DISTRIBUTIONS	65
6.1	Bayesian Classification	65
6.2	Feature Distributions	69
6.3	Feature Set Design	71
6.3.1	Accuracy	72
6.3.2	Redundancy	72
7.0	ACOUSTIC PROPAGATION IN A WEDGE-SHAPED OCEAN	74
7.1	Dispersion Relation	75

7.1.1 Comparison to Parallel-Plate Waveguide	78
7.2 Acoustic Field Due to a Point Source	79
7.3 Wigner Distribution and Approximation	81
7.4 Numerical Simulations	83
8.0 CONCLUSION	89
8.1 Future Work	90
APPENDIX. DERIVATIONS	92
A.1 Temporal	92
A.2 Frequency	94
BIBLIOGRAPHY	95

LIST OF TABLES

1	Global moments	18
2	Local moments	22
3	Physical parameters used in simulations	33
4	Geometry of shells used in simulations	33
5	Area Under ROC for classification simulations	40

LIST OF FIGURES

1	Comparison of DIMs performance for $\beta = 0$ and $\beta = 10^{-8} \text{ m}^{-1}\text{Hz}^{-1}$	25
2	An overview of the simulations	32
3	Waveforms generated by cylinder 1(1.25 km, 2.5 km)	35
4	Waveforms generated by cylinder 2 (1.25 km, 2.5 km)	36
5	Augmented waveform generated by cylinder 1 (1.25 km, 2.5 km)	36
6	Augmented waveform generated by cylinder 2 (1.25 km, 2.5 km)	37
7	ROC curves for $\beta = 10^{-8} \text{ m}^{-1}\text{Hz}^{-1}$	38
8	ROC curves for $\beta = 10^{-7} \text{ m}^{-1}\text{Hz}^{-1}$	39
9	ROC curves for $\beta = 10^{-8} \text{ m}^{-1}\text{Hz}^{-1}$ in a wedge	41
10	Schematic of a fluctuating channel	57
11	Scattering regimes in Λ - Σ space	58
12	Feature distributions and possible outcomes of a likelihood ratio test	68
13	Schematic of the perfect wedge	76
14	A comparison of the parameters for depth and range	78
15	Diagram of the first example showing source and receiver positions	84
16	Exact Wigner and approximation, example 1	85
17	Diagram of the second example showing source and receiver positions.	86
18	Exact Wigner and approximation, example 2	87
19	Exact Wigner and spectrogram, example 1	88

PREFACE

To my parents, thank you for everything.

1.0 INTRODUCTION

In active sonar, detection and classification of objects via their backscattered sonar signatures can be complicated by propagation effects such as dispersion and frequency-dependent attenuation. These effects are especially significant in shallow water channels. It is in the interest of improved classification that methods be derived to estimate and compensate for these effects. Because these effects are best characterized in a time-frequency (or position-wavenumber) space, we develop a phase space propagation model based on the Wigner distribution. We then use this model to develop propagation-invariant features and to characterize the statistical nature of ordinary moment features in uncertain and randomly-varying channels. Finally, we consider the range-dependent case by developing a phase space approach and approximation for propagation in a wedge.

1.1 BACKGROUND

Because sound waves propagate far more efficiently than electromagnetic waves in water, the primary means for exploring and communicating in undersea environments is sonar [52]. Modern sonar systems are broadly characterized as either passive or active. Passive sonar listens for acoustic energy emanating from entities in the underwater environment. In contrast, active sonar creates a sound in the water via an explosion or a transducer and then listens for the reflection of the acoustic energy [54]. Characteristics of the echo may be used to identify objects in the sea because the interaction of acoustic energy with an object is unique to the object's size, shape, and material composition.

One of the primary objectives of a sonar system is to distinguish between sounds emanating from or reflected by objects of interest (which, in this work, we will generally refer to as targets) from sounds emanating from or reflected by other non-target objects in the undersea environment (which we will generally refer to as clutter). This process is called classification. The variety of approaches to sonar classification that have been pursued is quite large. A common method for classification is the matched filter or correlator-receiver approach, in which an observed signal is correlated with a reference signal, and then the correlation coefficient is compared to a threshold [53]. Another method involves the construction of a partitioned feature space from labeled training data. Observed data is classified by computing the feature vector and choosing the label corresponding to the location of the vector in the feature space. The latter method is the method with which we are concerned.

Sound waves propagating through an ocean channel may exhibit nonstationarities, that is, time- or spatially-varying spectral changes. These changes may complicate the task of classifying echoes, because features computed from these echoes may reflect information about the channel in addition to the object from which the sound wave reflected. Therefore, it is logical to account for these nonstationarities in order to improve classification. Two basic approaches can be taken: one is to use knowledge of the propagation environment to compensate for channel effects on the observed wave; a second is to extract features from the wave that are invariant to channel effects. We study both approaches in this work.

In one of the earlier papers on sonar classification, Hoffman [30] studied the problem in the time domain by comparing the quadrature components of a received echo to the quadrature components of reference echoes for known targets and computing a likelihood ratio. Chestnut *et al.* [9, 10] studied the problem in the frequency domain using feature vectors derived from filterbanks and autoregressive modeling of the spectra of sonar echoes. The feature vector of a received echo was then compared to the feature vector of known targets via a distance metric.

Classification techniques in the joint time-frequency domain have also been explored. Altes [1] proposed a method for signal detection (or classification) using the spectrogram. In general, the method involves computing a statistic that is a function of the spectrograms of a reference signal and the received signal and comparing that statistic to a threshold. In cases

where some parameters of the signal to be detected are random (e.g., delay and Doppler shift), the statistic incorporates probability distributions for each of these parameters. In the case of a known signal propagating in a noisy channel, the statistic is computed by correlating the spectrogram of the received signal with an ensemble average spectrogram of the output of the channel when the known signal is applied as input. In order to account for channel effects with this method, the scattering function of the channel must be known.

To account for bottom reverberation with no specific *a priori* knowledge of the channel, Chevret [11] proposed using a time-frequency filtering method. The Wigner distribution of the free-field response of targets of interest is used to highlight areas of interest in the time-frequency plane. These areas correspond to the regions that will be passed by the filter. To detect or classify signals, the filter representing each target of interest slides along the received signal in the time dimension. The output of the filter is then compared to the reference free-field response using an error measure. The minimum error indicates detection of the target corresponding to that filter. The possible misclassification of reverberation echoes is handled by a signal-to-reverberation ratio; possible detections of signal components whose amplitudes are less than this ratio are ignored.

1.2 SUMMARY OF THIS WORK

An approximate propagation model based on the Wigner distribution has recently been given [40] that is applicable to range-independent shallow water channels. This model quantifies in time-frequency space the changes induced in a propagating wave by dispersion and damping, two frequency-dependent propagation effects that are characterized by the real and imaginary parts of the dispersion relation, respectively. Time-frequency distributions such as the Wigner distribution capture important characteristics of an evolving wave that may not be obvious in the time series or spectrum. Statistical moments computed from these distributions quantify these characteristics and, therefore, may be used as features for classification. It is important to understand how these moments can change in a deterministic propagation channel. Using the global and local moments of a propagating wave, we quantify the

impact of dispersion and damping on the Wigner distribution and evaluate the accuracy of the Wigner approximation under these conditions, and we also show that the Wigner approximation is more accurate at short propagation distances than the stationary phase approximation. We show that the spectral moments of the Wigner approximation are exact for arbitrary dispersion and damping. We also show that the first order temporal moment is exact for arbitrary dispersion and damping and that the second order temporal moment is exact for arbitrary dispersion and damping that is linear with frequency. Temporal moments higher than second order are not exact.

Using the knowledge of how the moments change due to dispersion and damping, we develop a feature extraction process that is invariant to dispersion and certain important forms of damping. We demonstrate the effectiveness of this process via simulation and comparison to ordinary moments.

The effects of dispersion and damping are dependent upon various parameters of the environment such as attenuation coefficients, sound speed profiles, channel depth, and range of propagation. Uncertainty and randomness in these parameters leads to uncertainty and randomness in the evolution of the wave as it propagates, which finally leads to increased variability in features computed from the wave. We develop an analytical framework for estimating the probability distribution functions (pdfs) of classification features using estimates of the uncertainty or randomness of the environmental parameters by calculating the moments of the features.

We make a distinction between an uncertain channel and a randomly-varying channel. Uncertainty in propagation channels may cause variability in classification features. Propagation effects such as dispersion and damping cause a wave to change as it propagates. As the wave changes, the values of the features computed from that wave change as well. The magnitude and nature of the changes are dependent upon the specific properties of the channel, which are represented in the channel model by various parameters such as the sound speed profile and the dispersion relation. The degree to which those parameters change over the course of training directly affects the pdfs computed for the features used by the classifier, and changes in the channel parameters during application of a classifier will directly affect the classification performance.

In contrast to the uncertain channel model, we also investigate the effects of randomly-varying channels. The ocean environment is complex and fluctuating, and the random variations that occur in an ocean channel also induce variability in moment features. The primary cause of ocean channel variability is internal waves, but other phenomena such as ocean currents and planetary waves (large-scale water waves caused by the rotation of the Earth) also induce variability. Using accepted models of random ocean acoustic propagation [18], we may extend the moments of moments approach derived for uncertain channels to randomly-varying channels. The expressions for the moments of the moment features are found in terms of the moments of the signal in a corresponding deterministic channel and the two-frequency mutual coherence function. The two-frequency mutual coherence function is a commonly used measure to characterize fluctuating media, and its form is known and has been experimentally verified for ocean channels [2, 18]. We also show how the two-frequency mutual coherence function is related to the Wigner distribution by a Fourier transform.

The moments of moments approach may be used to provide guidance toward designing feature sets. The characteristic function of a moment feature may be calculated via the moments of the moment features, and the inverse Fourier transform of the characteristic function is one estimate of the pdf of the moment feature. Another more general estimate is provided by the maximum entropy pdf that satisfies the moments. Generalizing this to higher dimensions and using joint moments, we may calculate the joint pdf and covariance of a set (two or more) of moment features. Using the pdfs and covariance, we may evaluate potential feature sets for their accuracy and redundancy. The accuracy of a feature is a measure of how well the feature discriminates between the target and clutter classes, and the redundancy of a feature is a measure of the discriminability gained by adding a certain feature to a feature set. The amount of training data necessary to properly train a classifier grows exponentially with the dimensionality of the feature set, and typically, training data is not available in abundance. Therefore, it is important to construct feature sets with minimal redundancy. Using these metrics to evaluate potential feature sets, we can build efficient, environmentally robust feature sets.

For many problems, the range-independent parallel plate waveguide is a sufficient approximation to shallow-water ocean channels. However, in coastal regions, the ocean often

has a sloping bottom, and thus a better approximation may be obtained by using a wedge shape as a model. The solution to this problem has been previously obtained by several authors using integral transforms and other methods [6, 4, 33]; however, it is also possible to obtain a solution that emphasizes propagation effects such as dispersion and damping using separation of variables. Using a transformation to polar coordinates and the technique of separation of variables, we derive the exact solution for the acoustic field in a two-dimensional wedge due to a point source at an arbitrary location. We then use this solution to derive the Wigner approximation for sloping bottom shallow water channels and use numerical simulation to compare the Wigner approximation to the exact solution.

Finally, we conclude this work with a look at future areas of research.

2.0 WAVE PROPAGATION

The acoustic wave equation may be formulated in terms of pressure, velocity, or displacement and in any coordinate system. The general form is derived from basic equations of motion and is expressed as [23]

$$\nabla^2 p = \frac{1}{c^2} \frac{\partial^2 p}{\partial t^2} \quad (2.1)$$

where Φ is the wave, c is the speed of sound in the medium, and t is time. The Laplacian, ∇^2 is defined as

$$\nabla^2 = \frac{\partial^2}{\partial x^2} + \frac{\partial^2}{\partial z^2} \quad (2.2)$$

in two-dimensional Cartesian coordinates where the x coordinate is range and the z coordinate is depth. The wave equation is, therefore,

$$\frac{\partial^2 p}{\partial x^2} + \frac{\partial^2 p}{\partial z^2} = \frac{1}{c^2} \frac{\partial^2 p}{\partial t^2} \quad (2.3)$$

The nature of this partial differential equation suggests a solution of the form

$$p(x, z, \omega, t) = U(x, z, \omega) e^{j\omega t} \quad (2.4)$$

where ω is radial frequency. Substituting this form of the solution into Eq. (2.3) and simplifying, we arrive at the Helmholtz equation:

$$\frac{\partial^2 U(x, z, \omega)}{\partial x^2} + \frac{\partial^2 U(x, z, \omega)}{\partial z^2} + k^2 U(x, z, \omega) = 0 \quad (2.5)$$

where $k = \frac{\omega}{c}$ is the acoustic wavenumber. We seek a solution of the acoustic field of the form

$$U(x, z, \omega) = \sum_{m=1}^{\infty} \Phi_m(x) \Psi_m(z) \quad (2.6)$$

where $\Psi_m(z)$ is one of a sequence of orthogonal functions called *eigenfunctions* or *modes*. We will initially focus on the m^{th} mode. The Helmholtz equation for the m^{th} mode is given by

$$\Psi_m(z) \frac{\partial^2 \Phi_m(x)}{\partial x^2} + \Phi_m(x) \frac{\partial^2 \Psi_m(z)}{\partial z^2} + k_m^2 \Phi_m(x) \Psi_m(z) = 0 \quad (2.7)$$

where k_m is the wavenumber in the direction of propagation for the m^{th} mode, and may be written in terms of the x and z components as

$$k_m^2 = k_{xm}^2 + k_{zm}^2 \quad (2.8)$$

Eq. (2.7) may be written as

$$\frac{1}{\Phi_m(x)} \frac{\partial^2 \Phi_m(x)}{\partial x^2} + \frac{1}{\Psi_m(z)} \left[\frac{\partial^2 \Psi_m(z)}{\partial z^2} + k_m^2 \Psi_m(z) \right] = 0 \quad (2.9)$$

and it is clear that the left-hand side of the equation is the sum of an x -dependent differential term and a z -dependent differential term. Therefore, to satisfy the right-hand side, the terms must be equal to the positive and negative values of a constant, k_{xm}^2 , which is the eigenvalue corresponding to $\Psi_m(z)$ [32]. We then obtain the following two partial differential equations:

$$\frac{1}{\Phi_m(x)} \frac{\partial^2 \Phi_m(x)}{\partial x^2} = -k_{xm}^2 \quad (2.10)$$

$$\frac{1}{\Psi_m(z)} \left[\frac{\partial^2 \Psi_m(z)}{\partial z^2} + k_m^2 \Psi_m(z) \right] = k_{xm}^2 \quad (2.11)$$

Simplifying, we obtain,

$$\frac{\partial^2 \Phi(x)}{\partial x^2} + k_{xm}^2 \Phi(x) = 0 \quad (2.12)$$

$$\frac{\partial^2 \Psi(z)}{\partial z^2} + k_{zm}^2 \Psi(z) = 0 \quad (2.13)$$

The general solutions to these second-order homogenous equations are given by

$$\Phi(x) = A_1 \cos(k_{xm}x) + A_2 \sin(k_{xm}x) \quad (2.14)$$

$$\Psi(z) = B_1 \cos(k_{zm}z) + B_2 \sin(k_{zm}z) \quad (2.15)$$

where the constants (A_1, A_2, B_1, B_2) are determined by the boundary conditions.

The full solution for the field at a given frequency is given by Eq. (2.6). To obtain a time domain solution for pulse propagation, we use Fourier synthesis. The impulse response at x is found by integrating the single frequency solution over all frequencies,

$$h(x, z, t) = \frac{1}{\sqrt{2\pi}} \int U(x, z, \omega) e^{-j\omega t} d\omega \quad (2.16)$$

and the time domain signal due to an arbitrary input pulse is given by

$$s(x, z, t) = \frac{1}{\sqrt{2\pi}} \int F(0, \omega) U(x, z, \omega) e^{-j\omega t} d\omega \quad (2.17)$$

where $F(0, \omega)$ is the spectrum of the initial pulse. Substituting the expression from Eq. (2.6) and changing the order of integration and summation, we obtain

$$s(x, z, t) = \frac{1}{\sqrt{2\pi}} \sum_m^{\infty} \Psi_m(z) \int F(0, \omega) \Phi_m(x) e^{-j\omega t} d\omega \quad (2.18)$$

Assuming no specific boundary conditions for the solution given in Eq. (2.14), we are free to choose the constants to be $A_1 = 1$ and $A_2 = j$, giving

$$\Phi(x) = e^{jk_{xm}x} \quad (2.19)$$

One can easily verify that this is a solution by substituting Eq. (2.19) in to Eq. (2.14). We then have that a wave at x and z is given in the time domain by

$$s(x, z, t) = \frac{1}{\sqrt{2\pi}} \sum_m^{\infty} \Psi_m(z) \int F(0, \omega) e^{jk_{xm}x} e^{-j\omega t} d\omega \quad (2.20)$$

The spectrum of the wave at (x, z) is given by

$$S(x, z, \omega) = \sum_m^{\infty} \Psi_m(z) F(0, \omega) e^{jk_{xm}(\omega)x} \quad (2.21)$$

where we have explicitly denoted the frequency dependence of the dispersion relation with the notation $k_{xm}(\omega)$. For free space, $k = \frac{\omega}{c}$, whereas, in bounded media, k is generally a nonlinear function of ω .

In the next section, we will develop the phase space solution of the propagating wave using the Wigner distribution, which illuminates the propagation effects of dispersion and damping.

2.1 WIGNER DISTRIBUTION

The Wigner distribution of the wave at (x, z) is given by [14]¹

$$W(t, \omega; x, z) = \frac{1}{2\pi} \int s\left(x, z, t + \frac{\tau}{2}\right) s^*\left(x, z, t - \frac{\tau}{2}\right) e^{j\omega\tau} d\tau \quad (2.22)$$

or equivalently in terms of the spectrum as [14]

$$W(t, \omega; x, z) = \frac{1}{2\pi} \int S^*\left(x, z, \omega + \frac{\theta}{2}\right) S\left(x, z, \omega + \frac{\theta}{2}\right) e^{jt\theta} d\theta \quad (2.23)$$

Plugging in the expression from Eq. (2.21), we obtain

$$\begin{aligned} W(t, \omega; x, z) &= \frac{1}{2\pi} \sum_{m_1=1}^{\infty} \sum_{m_2=1}^{\infty} \Psi_{m_1}(z) \Psi_{m_2}(z) \int F^*\left(0, \omega + \frac{\theta}{2}\right) F\left(0, \omega - \frac{\theta}{2}\right) \\ &\quad e^{-jk_{xm_1}^*(\omega + \frac{\theta}{2})x} e^{jk_{xm_2}(\omega - \frac{\theta}{2})x} e^{jt\theta} d\theta \end{aligned} \quad (2.24)$$

which represents the Wigner distribution for the entire acoustic field (all modes). The Wigner distribution of the initial pulse is given by

$$W_u(t, \omega; 0) = \frac{1}{2\pi} \int F^*\left(0, \omega + \frac{\theta}{2}\right) F\left(0, \omega + \frac{\theta}{2}\right) e^{jt\theta} d\theta \quad (2.25)$$

and, using Fourier relations, we have that

$$F^*\left(0, \omega + \frac{\theta}{2}\right) F\left(0, \omega + \frac{\theta}{2}\right) = \frac{1}{2\pi} \int W_u(t, \omega; 0) e^{-jt\theta} dt \quad (2.26)$$

The expression in Eq. (2.26) may be used to simplify Eq. (2.24),

$$\begin{aligned} W(t, \omega; x, z) &= \frac{1}{2\pi} \sum_{m_1=1}^{\infty} \sum_{m_2=1}^{\infty} \Psi_{m_1}(z) \Psi_{m_2}(z) \int \int W_u(t', \omega; 0) \\ &\quad e^{jx[k_{xm_1}(\omega - \frac{\theta}{2}) - k_{xm_2}^*(\omega + \frac{\theta}{2})]} e^{j\theta(t-t')} d\theta dt' \end{aligned} \quad (2.27)$$

and, therefore, we have that

$$W(t, \omega; x, z) = \frac{1}{2\pi} \sum_{m_1=1}^{\infty} \sum_{m_2=1}^{\infty} \Psi_{m_1}(z) \Psi_{m_2}(z) W_u(t, \omega; 0) *_t W_{h; m_1, m_2}(t, \omega; x) \quad (2.28)$$

¹The formula given in Eq. (2.22) differs slightly from the usual definition of the Wigner distribution as given in [14]; here, we prefer to define the Wigner distribution with a positive exponent in order to make the expression for the Wigner approximation more intuitive. We use the definition in Eq. (2.22) throughout this work.

where $*_t$ denotes time domain convolution and $W_{h;m_1,m_2}(t, \omega; x)$ is the cross-Wigner distribution of the channel for modes m_1 and m_2 , given by

$$W_{h;m_1,m_2}(t, \omega; x) = \frac{1}{2\pi} \int e^{jx[k_{xm_1}(\omega - \frac{\theta}{2}) - k_{xm_2}^*(\omega + \frac{\theta}{2})]} e^{j\theta t} d\theta \quad (2.29)$$

We may write the dispersion relation in terms of its real and imaginary parts as

$$k_{xm}(\omega) = k_{Rxm}(\omega) + jk_{Ixm}(\omega) \quad (2.30)$$

and substitute this into Eq. (2.29), giving

$$W_{h;m_1,m_2}(t, \omega; x) = \frac{1}{2\pi} \int e^{-x[k_{Ixm_1}(\omega - \frac{\theta}{2}) + k_{Ixm_2}^*(\omega + \frac{\theta}{2})]} e^{jx[k_{Rxm_1}(\omega - \frac{\theta}{2}) - k_{Rxm_2}^*(\omega + \frac{\theta}{2})]} e^{j\theta t} d\theta \quad (2.31)$$

Expanding the arguments of the exponentials in a Taylor series and keeping only lower-ordered terms, we have

$$k_{Ixm_1}\left(\omega - \frac{\theta}{2}\right) + k_{Ixm_2}\left(\omega + \frac{\theta}{2}\right) \approx k_{Ixm_1}(\omega) + k_{Ixm_2}(\omega) \quad (2.32)$$

$$-\frac{\theta}{2} (k'_{Ixm_1}(\omega) - k'_{Ixm_1}(\omega)) \quad (2.33)$$

$$k_{Rxm_1}\left(\omega - \frac{\theta}{2}\right) - k_{Rxm_2}\left(\omega + \frac{\theta}{2}\right) \approx k_{Rxm_1}(\omega) - k_{Rxm_2}(\omega) \quad (2.34)$$

$$-\frac{\theta}{2} (k'_{Rxm_1}(\omega) + k'_{Rxm_1}(\omega)) \quad (2.35)$$

Plugging this result into Eq. (2.31) and evaluating the integral over θ gives an approximate solution for the cross-Wigner distribution of the channel:

$$W_{h;m_1,m_2}(t, \omega; x) \approx e^{-x[k_{Ixm_1}(\omega) + k_{Ixm_2}(\omega)]} \delta\left(t + (k_{Rxm_1}(\omega) - k_{Rxm_2}(\omega)) - \frac{x}{2} (k'_{Rxm_1}(\omega) + k'_{Rxm_1}(\omega))\right) \quad (2.36)$$

For the special case of $m_2 = m_1$, Eq. (2.36) becomes

$$W_{h;m_1,m_1}(t, \omega; x) \approx e^{-2xk_{Ixm_1}(\omega)} \delta(t - k'_{Rxm_1}(\omega)x) \quad (2.37)$$

In the next section, we will use this expression to develop the Wigner approximation for a single mode.

2.2 SINGLE MODE

As is common in wave propagation, we study one mode at a time. Given an initial wave at $x = 0$,

$$u(0, t) = \frac{1}{\sqrt{2\pi}} \int F(0, \omega) e^{-j\omega t} d\omega \quad (2.38)$$

where $F(0, \omega)$ is the spectrum of $u(0, t)$, the wave for mode m at some other point x is given by

$$u_m(x, t) = \frac{1}{\sqrt{2\pi}} \int F_m(x, \omega) e^{-j\omega t} d\omega \quad (2.39)$$

$$= \frac{1}{\sqrt{2\pi}} \int F(0, \omega) e^{j(k_m(\omega)x - \omega t)} d\omega \quad (2.40)$$

where $k_m(\omega)$ is the dispersion relation for the m^{th} mode ($k_m(\omega) = \pm \frac{\omega}{c}$ for no dispersion). Therefore,

$$F_m(x, \omega) = F(0, \omega) e^{jk_m(\omega)x} \quad (2.41)$$

This is analogous to a linear, time-invariant systems approach with the impulse response of the channel given by

$$h_m(t) = \frac{1}{\sqrt{2\pi}} \int e^{j(k_m(\omega)x - \omega t)} d\omega \quad (2.42)$$

It will also be useful to write $F_m(x, \omega)$ in terms of amplitude $B_m(x, \omega)$ and phase $\psi_m(x, \omega)$, which further highlights the effects of dispersion and damping. Let

$$F_m(x, \omega) = B_m(x, \omega) e^{j\psi_m(x, \omega)} \quad (2.43)$$

where

$$\psi_m(x, \omega) = \arg F_m(x, \omega) \quad (2.44)$$

and

$$B_m(x, \omega) = F_m(x, \omega) e^{-j\psi_m(x, \omega)} \quad (2.45)$$

Accordingly, it follows that the amplitude and phase are

$$B_m(x, \omega) = B(0, \omega) e^{-k_{Im}(\omega)x} \quad (2.46)$$

$$\psi_m(x, \omega) = \psi(0, \omega) + k_{Rm}(\omega)x \quad (2.47)$$

2.2.1 Wigner Approximation

The Wigner distribution of the wave of a single mode at x is given by [14]

$$W_{um}(t, \omega; x) = \frac{1}{2\pi} \int u_m \left(x, t + \frac{\tau}{2} \right) u_m^* \left(x, t - \frac{\tau}{2} \right) e^{j\omega\tau} d\tau \quad (2.48)$$

or, equivalently in the frequency domain as [14]

$$W_{um}(t, \omega; x) = \frac{1}{2\pi} \int F_m^* \left(x, \omega + \frac{\theta}{2} \right) F_m \left(x, \omega - \frac{\theta}{2} \right) e^{j\theta t} d\theta \quad (2.49)$$

Using the expression from Eq. (2.41), we have that

$$W_{um}(t, \omega; x) = \frac{1}{2\pi} \int F^* \left(0, \omega + \frac{\theta}{2} \right) e^{-jk_m(\omega + \frac{\theta}{2})x} F \left(0, \omega - \frac{\theta}{2} \right) e^{jk_m(\omega - \frac{\theta}{2})x} e^{j\theta t} d\theta \quad (2.50)$$

The relationship reduces to a convolution in time between the Wigner distribution of the initial wave and the Wigner distribution of the impulse response,

$$W_{um}(t, \omega; x) = \int W_{hm}(t - \tau, \omega; x) W_u(\tau, \omega; 0) d\tau \quad (2.51)$$

By expanding the exponent of the transfer function in a Taylor series and keeping only the first order terms (as in the previous section), we obtain the Wigner approximation of the impulse response [39, 40, 37], as given in Eq. (2.37) for a single mode:

$$W_{hm}(t, \omega; x) \approx e^{-2k_{Im}(\omega)x} \delta(t - k'_{Rm}(\omega)x) \quad (2.52)$$

Substituting into Eq. (2.51), we find that the Wigner approximation of the wave for a single mode m at x is given by

$$W_{um}(t, \omega; x) \approx e^{-2k_{Im}(\omega)x} W(t - k'_{Rm}(\omega)x, \omega, 0) \quad (2.53)$$

This approximation has motivated the design of classification features that are invariant to dispersion and attenuation. These features will be covered in Chapter 4. The approximation will also be used to find approximate analytical expressions for the moments of moment features in Chapter 5.

3.0 MOMENTS OF THE WIGNER DISTRIBUTION

In this chapter we analytically quantify the impact of dispersion and damping on the global and local moments of a propagating wave, and we also evaluate the accuracy of the Wigner approximation under these conditions. We show that the spectral moments of the Wigner approximation are exact for arbitrary dispersion and damping. The first order temporal moment is exact for arbitrary dispersion and damping, and the second order temporal moment is exact for arbitrary dispersion and damping that is linear with frequency. Temporal moments higher than second order are not exact, and we quantify the error terms up to the third order moment.

We give the formulas for the global temporal and spectral moments of the exact Wigner distribution and of the approximation and evaluate these for low-order temporal moments. We compare the moments of the Wigner approximation to moments calculated from the stationary phase approximation (method of steepest descent) and show that the Wigner moments are more accurate for small propagation distances. At large propagation distances, the two approximations approach the same result. We also give the local temporal moments of the exact Wigner and approximation, with a few examples of the exact and approximate moment values.

3.1 GLOBAL MOMENTS

Global moments quantify characteristics of a wave such as arrival time, duration, and bandwidth. They are called “global” because they are calculated over the entire wave (or its spectrum) for all time and all frequencies (in contrast to the “local” moments described in

the next section, which are calculated from the time-frequency representation for specific frequencies). Moments have been used as features for automatic classification of objects. Our aim in this section is to examine the impact of propagation effects on the moments, which could have a deleterious impact on the utility of such features for classification, since the moments from two identical objects could differ simply because of different propagation effects. To accomplish our aim, we calculate the moments using the Wigner approximation, and compare these results with the exact results for low-order moments.

3.1.1 Temporal Moments

The global temporal moments are defined as [14]

$$\langle t^n \rangle_x = \int t^n |u(x, t)|^2 dt \quad (3.1)$$

Because the Wigner distribution satisfies the marginals, the temporal moments are equivalently given by

$$\langle t^n \rangle_x = \int \int t^n W(x, t, \omega) d\omega dt \quad (3.2)$$

Using Eq. (2.27), these may be written in terms of the Wigner distribution at $x = 0$ as [16]

$$\langle t^n \rangle_x = j^n \int \int W(0, t, \omega) \left[\frac{\partial^n}{\partial \theta^n} e^{-x[k_I(\omega - \frac{\theta}{2}) - k_I(\omega + \frac{\theta}{2})]} e^{-j\theta t'} e^{-jx[k^*(\omega + \frac{\theta}{2}) - k(\omega - \frac{\theta}{2})]} \right] d\omega dt \quad (3.3)$$

The above expression is exact, and this form facilitates easy calculation of the moments of the Wigner distribution at an arbitrary position x in terms of the moments of the initial Wigner distribution (at $x = 0$).

We may also define global central temporal moments as

$$\mu_x^n = \langle (t - \langle t \rangle_x)^n \rangle_x \quad (3.4)$$

3.1.1.1 Approximate Temporal Moments Global temporal moments may also be computed from the Wigner approximation. Using Eq. (3.2) and inserting the Wigner approximation, we obtain

$$\langle t^n \rangle_x^{wa} = \int \int t^n W_a(x, t, \omega) d\omega dt \quad (3.5)$$

$$= \int \int t^n e^{-2k_I(\omega)x} W(0, t - k'_R(\omega)x, \omega) d\omega dt \quad (3.6)$$

$$= \int \int (t + k'_R(\omega)x)^n e^{-2k_I(\omega)x} W(0, t, \omega) d\omega dt \quad (3.7)$$

3.1.1.2 Stationary Phase Approximation The stationary phase approximation is commonly used in acoustics to approximate integrals of the form of the integral in Eq. (2.40). The general form of the integral may be written as

$$u(x, t) = \frac{1}{\sqrt{2\pi}} \int F(0, \omega) e^{j\phi(\omega)} d\omega \quad (3.8)$$

where $\phi(\omega) = (k(\omega)x - \omega t)$ is the phase term and the dispersion relation is complex. The exponential term is highly oscillatory and the positive and negative contributions mostly cancel each other out; therefore, the majority of the contributions to the integral come from the points where the phase is approximately stationary, denoted ω_s :

$$\phi'(\omega_s) = 0 \quad (3.9)$$

Because we are investigating the moments of a wave propagating in a channel with a complex dispersion relation, we use the complex generalization of the stationary phase approximation known as the method of steepest descent. Evaluating Eq. (3.9) gives

$$k'_R(\omega_s) = \frac{t}{x} \quad (3.10)$$

where we have the real part of the dispersion relation because, for the method of steepest descent to be valid, the derivative of the imaginary part of the complex phase ϕ must be zero at the stationary point [5]. The approximate solution to the integral in Eq. (3.8) is given by the method of steepest descent to be [5]

$$u(x, t) \approx \frac{F(0, \omega_s)}{\sqrt{k''_R(\omega_s)x}} e^{j(k(\omega_s)x - \omega_s t)} \quad (3.11)$$

and the magnitude-squared signal is given by

$$|u(x, t)|^2 \approx \frac{|F(0, \omega_s)|^2}{|k_R''(\omega_s)x|} e^{-2k_I(\omega_s)x} \quad (3.12)$$

To calculate the global temporal moments using this approximate result, we use the moment formulation given in Eq. (3.1) with the result given in Eq. (3.12), giving,

$$\langle t^n \rangle_x^{sp} = \int t^n \frac{|F(0, \omega_s)|^2}{|k_R''(\omega_s)x|} e^{-2k_I(\omega_s)x} dt \quad (3.13)$$

Using Eq. (3.10), we have

$$t = k_R'(\omega_s)x \quad (3.14)$$

$$dt = k_R''(\omega_s)x d\omega_s \quad (3.15)$$

Therefore, using a change of variables in Eq. (3.13) and rearranging terms, we get

$$\langle t^n \rangle_x^{sp} = \int (k_R'(\omega_s)x)^n e^{-2k_I(\omega_s)x} |F(0, \omega_s)|^2 d\omega_s \quad (3.16)$$

$$= \langle (k_R'(\omega))^n d_x(\omega) \rangle_0 x^n \quad (3.17)$$

where, to simplify the notation of the moment values, we have defined

$$d_x(\omega) = e^{-2k_I(\omega)x} \quad (3.18)$$

In Table 1 we give the expressions for the first three global temporal moments of the exact solution and the Wigner approximation. The notation $\langle \cdot \rangle_0$ indicates that the quantity inside the brackets is averaged over the Wigner distribution of the initial wave (at $x = 0$). In general, for arbitrary function $g(t, \omega)$, the bracket notation indicates the following operation:

$$\langle g(t, \omega) \rangle_x = \int \int g(t, \omega) W(x, t, \omega) dt d\omega \quad (3.19)$$

Note, first, how the moments are highly dependent on the propagation environment – i.e., on the dispersion and damping. Also, we observe that the first moment of the approximation is exact, as is the second moment when there is no damping (it has been argued that this is one reason, among others, why the Wigner approximation is a good approximation for dispersive pulse propagation [16, 40]). The second moment of the approximation is also exact for damping that is linear with frequency ($k_I(\omega) \sim \omega$).

Table 1: Global moments

Quantity	Exact	Wigner Approx.	Stat. Phase
$\langle t \rangle_x$	$\langle t d_x(\omega) \rangle_0 + \langle k'_R(\omega) d_x(\omega) \rangle_0 x$	exact	$\langle (k'_R(\omega)) d_x(\omega) \rangle_0 x$
$\langle t^2 \rangle_x$	$\langle t^2 d_x(\omega) \rangle_0 + 2 \langle t k'_R(\omega) d_x(\omega) \rangle_0 x$ $+ \langle (k'_R(\omega))^2 d_x(\omega) \rangle_0 x^2$ $- \frac{1}{2} \langle k''_I(\omega) d_x(\omega) \rangle_0 x$	exact + $\frac{1}{2} \langle k''_I(\omega) d_x(\omega) \rangle_0 x$	$\langle (k'_R(\omega))^2 d_x(\omega) \rangle_0 x^2$
$\langle t^3 \rangle_x$	$\langle t^3 d_x(\omega) \rangle_0 + 3 \langle t^2 k'_R(\omega) d_x(\omega) \rangle_0 x$ $+ 3 \langle t (k'_R(\omega))^2 d_x(\omega) \rangle_0 x^2$ $+ \langle (k'_R(\omega))^3 d_x(\omega) \rangle_0 x^3$ $- \frac{3}{2} \langle t k''_I(\omega) d_x(\omega) \rangle_0 x$ $- \frac{3}{2} \langle k''_I(\omega) k'_R(\omega) d_x(\omega) \rangle_0 x^2$ $- \frac{1}{4} \langle k'''_R(\omega) d_x(\omega) \rangle_0 x$	exact + $\frac{3}{2} \langle t k''_I(\omega) d_x(\omega) \rangle_0 x^3$ $+ \frac{3}{2} \langle k''_I(\omega) k'_R(\omega) d_x(\omega) \rangle_0 x^2$ $+ \frac{1}{4} \langle k'''_R(\omega) d_x(\omega) \rangle_0 x$	$\langle (k'_R(\omega))^3 d_x(\omega) \rangle_0 x^3$

The moments calculated from the stationary phase approximation are the same as the approximate Wigner moments for large values of x because the stationary phase result only captures the highest ordered term. Hence, for large x , the two approximations approach the same result. For small values of x , the stationary phase approximation is not applicable.

3.1.2 Spectral Moments

Because the Wigner distribution satisfies the marginals, we have that the exact global spectral moments are given by

$$\langle \omega^n \rangle_x = \int \int \omega^n W(x, t, \omega) dt d\omega \quad (3.20)$$

$$= \int \omega^n |F(x, \omega)|^2 d\omega \quad (3.21)$$

$$= \int \omega^n e^{-2k_I(\omega)x} |F(0, \omega)|^2 d\omega = \langle \omega^n d_x(\omega) \rangle_0 \quad (3.22)$$

where we have made use of Eq. (2.41). Note that the spectral moments in general depend on propagation distance x . However, if there is dispersion but no damping ($d_x(\omega) = 1$), then the spectral moments at x are identical to those of the original wave for each mode: $\langle \omega^n \rangle_x = \langle \omega^n \rangle_0$.

For the Wigner approximation, the analogous calculation gives

$$\langle \omega^n \rangle_x^{wa} = \int \int \omega^n W_a(x, t, \omega) dt d\omega \quad (3.23)$$

$$= \int \int \omega^n e^{-2k_I(\omega)x} W(0, t - k'_R(\omega)x, \omega) dt d\omega \quad (3.24)$$

$$= \int \omega^n e^{-2k_I(\omega)x} |F(0, \omega)|^2 d\omega = \langle \omega^n d_x(\omega) \rangle_0 \quad (3.25)$$

which we observe is in fact exact: the Wigner approximation gives the exact spectral moments (because it gives the correct frequency marginal).

We may also calculate moments from the spectrum of the stationary phase/steepest descent approximation. The approximate spectrum is given by the Fourier transform of Eq. (3.11),

$$F(x, \omega) \approx \frac{1}{\sqrt{2\pi}} \int \frac{F(0, \omega_s)}{\sqrt{k''_R(\omega_s)x}} e^{j(k(\omega_s)x - \omega_s t)} e^{j\omega t} dt \quad (3.26)$$

Therefore, using a change of variables defined by Eqs. (3.14) and (3.15) in Eq. (3.26), the approximate spectrum is given by

$$F(x, \omega) \approx \frac{1}{\sqrt{2\pi}} \int \sqrt{k_R''(\omega_s)} x F(0, \omega_s) e^{jk(\omega_s)x} e^{jk_R'(\omega_s)x[\omega - \omega_s]} d\omega_s \quad (3.27)$$

In general, this spectrum is not equivalent to the exact spectrum, which is given by

$$F_m(x, \omega) = F(0, \omega) e^{jk_m(\omega)x} \quad (3.28)$$

and therefore we may conclude that the spectral moments of the stationary phase/steepest descent approximation are not exact.

3.2 EXACT AND APPROXIMATE LOCAL TEMPORAL MOMENTS

The local temporal moments quantify the temporal shape of the Wigner distribution at individual frequencies. The local temporal moments of the wave at x are defined as

$$\langle t^n \rangle_{\omega, x} = \frac{1}{\int W(x, t, \omega) dt} \int t^n W(x, t, \omega) dt \quad (3.29)$$

Note that this definition of the local moments includes a normalization by $\int W(x, t, \omega) dt = |F(x, \omega)|^2$. With this normalization, the local moments are related to the global moments by

$$\langle t^n \rangle_x = \int \langle t^n \rangle_{\omega, x} |F(x, \omega)|^2 d\omega \quad (3.30)$$

Following Eq. (3.3), we may write the local moments as

$$\begin{aligned} \langle t^n \rangle_{\omega, x} &= \frac{j^n}{e^{-2k_I(\omega)x} |F(0, \omega)|^2} \int W(0, t, \omega) \\ &\left[\frac{\partial^n}{\partial \theta^n} e^{-x[k_I(\omega - \frac{\theta}{2}) - k_I(\omega + \frac{\theta}{2})]} e^{-j\theta t'} e^{-jx[k^*(\omega + \frac{\theta}{2}) - k(\omega - \frac{\theta}{2})]} \right] dt \end{aligned} \quad (3.31)$$

The local central temporal moments are defined as

$$\mu_{\omega, x}^n = \langle (t - \langle t \rangle_{\omega, x})^n \rangle_{\omega, x} \quad (3.32)$$

3.2.1 Approximate Local Temporal Moments

Using the Wigner approximation in place of the exact Wigner distribution, we obtain approximate local temporal moments by

$$\langle t^n \rangle_{\omega, x}^{wa} = \frac{1}{e^{-2k_I(\omega)x} |F(0, \omega)|^2} \int t^n e^{-2k_I(\omega)x} W(0, t - k'_R(\omega)x, \omega) dt \quad (3.33)$$

$$= \frac{1}{|F(0, \omega)|^2} \int (t + k'_R(\omega))^n W(0, t, \omega) dt \quad (3.34)$$

Note that the normalization cancels out the damping term in the approximate moments.

In Table 2 we give the formulations for the first few local temporal moments. We also give the formulation for the second-order local central temporal moment, a moment that quantifies the duration of the wave at each frequency. As in the case of the global moments, we see that the first-order local moment of the Wigner approximation is exact, and higher-order moments of the Wigner approximation differ from the exact result by moments of higher derivatives of the real and imaginary parts of the dispersion relation.

3.3 MOMENTS AS CLASSIFICATION FEATURES

Propagation effects such as dispersion and damping may degrade sonar classification performance by increasing the variability of features extracted from a received waveform. Indeed, the results given in this chapter show that in general the temporal and spectral moments change as the wave propagates when there is dispersion and damping (as indicated by the x -dependence of the values given in Tables 1 and 2).

The temporal and spectral moments, which are often used for classification, are generally not invariant to arbitrary forms of both dispersion and damping. However, if there is no damping ($k_I(\omega) = 0$, resulting in a purely real dispersion relation), then the global frequency moments are dispersion-invariant:

$$\langle \omega^n \rangle_x = \langle \omega^n \rangle_0 \quad (3.35)$$

Table 2: Local moments

Quantity	Exact	Wigner Approx.
$\langle t \rangle_{\omega,x}$	$\langle t \rangle_{\omega,0} + k'_R(\omega)x$	exact
$\langle t^2 \rangle_{\omega,x}$	$\langle t^2 \rangle_{\omega,0} + 2\langle t \rangle_{\omega,0}k'_R(\omega)x$ $+ (k'_R(\omega))^2 x^2 - \frac{1}{2}k''_I(\omega)x$	exact $+ \frac{1}{2}k''_I(\omega)x$
$\langle t^3 \rangle_{\omega,x}$	$\langle t^3 \rangle_{\omega,0} + 3\langle t^2 \rangle_{\omega,0}k'_R(\omega)x + 3\langle t \rangle_{\omega,0} (k'_R(\omega))^2 x^2$ $+ (k'_R(\omega))^3 x^3 - \frac{3}{2}\langle t \rangle_{\omega,0}k''_I(\omega)x$ $- \frac{3}{2}k''_I(\omega)k'_R(\omega)x^2 - \frac{1}{4}k'''_R(\omega)x$	exact $+ \frac{3}{2}\langle t \rangle_{\omega,0}k''_I(\omega)x$ $+ \frac{3}{2}k''_I(\omega)k'_R(\omega)x^2$ $+ \frac{1}{4}k'''_R(\omega)x$
$\mu_{\omega,x}^2$	$\mu_{\omega,0}^2 - \frac{1}{2}k''_I(\omega)x$	exact $+ \frac{1}{2}k''_I(\omega)x$

Also, for the case of no damping or damping that is linear with frequency, the second-order *local* central temporal moment (local duration) is given by

$$\mu_{\omega,x}^2 = \mu_{\omega,0}^2 \tag{3.36}$$

and is, therefore, dispersion-invariant.

In previous papers, we have given formulations and algorithms for extracting moment-like classification features that are invariant to the effects of dispersion [15, 38, 44], and in the next chapter we derive moment-like features that are invariant to dispersion and certain forms of damping [42]. We also show through simulation that propagation-invariant features may lead to improved classification results.

4.0 PROPAGATION INVARIANT CLASSIFICATION

To improve classification in environments with certain propagation effects, features that are invariant to those effects may be extracted from the sonar echo. Features invariant to dispersion have previously been derived [43, 44]. We build on that result to develop features that are invariant to dispersion and certain important forms of damping.

4.1 MOMENTS INVARIANT TO DISPERSION

Ordinary moments of a wave, such as its duration, change with propagation in a dispersive environment. It is possible, however, to obtain temporal moment-like features that are invariant to dispersion; this has been done by Okopal et al., who defined the “dispersion invariant moments” by [44],

$$A_n(x) = \int F^*(x, \omega) \left(j \frac{\partial}{\partial \omega} - \langle t \rangle_{x, \omega} \right)^n F(x, \omega) d\omega \quad (4.1)$$

where $\langle t \rangle_{x, \omega}$ denotes the “local mean time” and is equal to the group delay of the wave, $\langle t \rangle_{x, \omega} = -\psi'(x, \omega)$. These moments are similar to ordinary central moments, with the important exception that, instead of centering about the mean time $\langle t \rangle_x$, they are centered about the local mean time (i.e., the group delay). This centering about the local mean time has the beneficial effect of removing the effects of dispersion; in particular [44],

$$A_n(x) = A_n(0) \quad (4.2)$$

for purely real dispersion relation (no damping).

While these moments are invariant to dispersion, they are not invariant to damping (frequency-dependent attenuation). To see the effect of damping, we consider the example in Okopal et al. [44] of distinguishing between two different sized cylinders in a Pekeris waveguide (however, in the following example, the maximum distance has been increased to 15 kilometers to highlight the effect of damping). To introduce damping, we make the dispersion relation complex, per Eq. (2.30), where $k_R(\omega)$ is the dispersion relation of the 25 m deep Pekeris waveguide used in previous simulations (reported in [44]), and the damping is given by $k_I(\omega) = \beta\omega$, where the constant parameter β determines the level of damping. In Fig. 1, we show the performance of the 2nd order DIM in a dispersive channel with no attenuation ($\beta = 0$, solid black line). Additionally, we give the performance of the same feature for $\beta = 10^{-8} \text{ m}^{-1}\text{Hz}^{-1}$ (dashed blue line), which corresponds to the average level of damping seen in sea water for frequencies in the range considered here [8]. Clearly, the

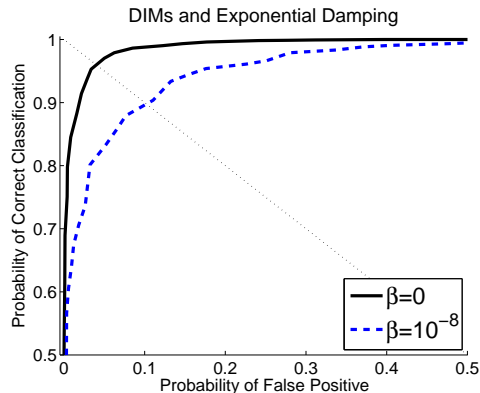


Figure 1: **Comparison of DIMs performance for $\beta = 0$ (no damping, solid black line) and $\beta = 10^{-8} \text{ m}^{-1}\text{Hz}^{-1}$ (dashed blue line).**

performance of the DIMs feature is reduced by the effect of damping. Accordingly, these moments, like spectral moments, can serve as propagation-invariant features for classification of waves propagating in dispersive channels. However, when there is damping in addition to dispersion, these time-domain moment-like features will in fact change with propagation distance, as will the spectral moments $\langle \omega^n \rangle_x$. In the next section, we consider features that are invariant to both frequency-dependent attenuation and dispersion.

4.2 MOMENTS INVARIANT TO DISPERSION AND DAMPING

Our aim is to develop a signal processing approach that will allow extraction of features that preserve the dispersion invariance of the DIMs, as well as achieve invariance to damping. To meet this aim, first note that the DIMs of Eq. (4.1) can be equivalently computed by [44],

$$A_n(x) = \frac{1}{2\pi} \int \int t^n |F(x, \omega)| e^{-j\omega t} d\omega dt \quad (4.3)$$

Thus, dispersion invariance is obtained by centering about the local mean time (or group delay), as in Eq. (4.1), or, equivalently, by computing features from the spectral magnitude (or its inverse Fourier transform) as in Eq. (4.3). Thus, the first step of the processing chain to achieve invariance to dispersion and damping is analogous to that of the DIMs processing; namely, we compute the magnitude-Fourier transform of the wave, to obtain the spectral amplitude, given by Eq. (2.46).

In order to achieve invariance to damping, we wish to process the spectral amplitude in order to separate the propagation effects of damping from the spectral properties of the initial backscatter embodied in $B_m(0, \omega)$. Accomplishing this aim for arbitrary (and unknown) damping $k_{Im}(\omega)$ is a daunting task. However, for two physically important forms of damping, a general processing algorithm is developed to achieve the desired invariance. The first form we consider is where the damping term is linear with frequency, and the second is where the damping term is proportional to log-frequency.

4.2.1 Exponential Attenuation

When the damping is linear, $k_I(\omega) = \beta\omega$, the spectral amplitude exhibits exponential attenuation,

$$B(x, \omega) = B(0, \omega) e^{-\beta\omega x} \quad (4.4)$$

Equivalently, the attenuation in dB is linear with frequency, which corresponds to physically relevant situations, including attenuation by seawater over a wide range of frequencies [8].

Features that are invariant to propagation effects are characterized by a lack of a dependence upon x . In order to obtain such features, we take the derivative of the natural logarithm of the spectral magnitude of the received signal to obtain

$$Z(x, \omega) = \frac{\partial}{\partial \omega} \ln B(x, \omega) = \frac{B'(x, \omega)}{B(x, \omega)} = \frac{B'(0, \omega)}{B(0, \omega)} - \beta x. \quad (4.5)$$

Note that the function $Z(x, \omega)$ does not change shape over frequency as x changes; instead, the βx term induces a constant level shift. This level shift may be eliminated by forcing the mean over ω to be zero,

$$Z_0(x, \omega) = Z(x, \omega) - \text{mean} \{Z(x, \omega)\} \quad (4.6)$$

This augmented spectral function of the received wave is now invariant to dispersion and exponential damping. At this stage, any features could be extracted from this function. We are interested in temporal features, so we exponentiate and transform back to the time domain

$$v(x, t) = \frac{1}{\sqrt{2\pi}} \int \exp(Z_0(x, \omega)) e^{-j\omega t} d\omega \quad (4.7)$$

[Note: one could skip the exponentiation step, which we discuss further in the following section.] The ADIMs are then computed as time-domain moments of the augmented signal $v(x, t)$,

$$T_n(x) = \int t^n |v(x, t)|^2 dt \quad (4.8)$$

Because the augmented signal $v(x, t)$ does not change with x , the moment features $T_n(x)$ are invariant to the effects of dispersion and exponential damping, i.e., $v(x, t) = v(0, t)$ and therefore $T_n(x) = T_n(0)$.

4.2.2 Power-law Attenuation

The second form of damping we consider is logarithmic, with $k_I(\omega) = p \log(\omega)$. Accordingly, the spectral attenuation is given by

$$B(x, \omega) = B(0, \omega) \omega^{-px}, \quad p > 0, \quad (4.9)$$

On a dB amplitude scale, the spectral attenuation is linear with log-frequency.

To compute propagation invariant features, we follow a similar procedure as in the exponential damping case. First, we compute the Z function by taking the partial derivative in ω of the log-magnitude spectrum of the signal at x , which yields,

$$Z(x, \omega) = \frac{\partial}{\partial \omega} \ln B(x, \omega) = \frac{B'(0, \omega)}{B(0, \omega)} - \frac{px}{\omega} \quad (4.10)$$

or equivalently,

$$\omega Z(x, \omega) = \omega \frac{B'(0, \omega)}{B(0, \omega)} - px \quad (4.11)$$

Analogous to the previous case, the x -dependence of the right-hand side of this equation is a level shift, which may be removed by subtracting the mean over frequency,

$$Z_0(x, \omega) = \omega Z(x, \omega) - \text{mean} \{ \omega Z(x, \omega) \} \quad (4.12)$$

As with the exponential attenuation case, this augmented spectral function of the received signal $u(x, t)$ is now independent of the effects of dispersion and damping; any desired features could be extracted from it to test their utility for classification. To obtain our time domain attenuation- and dispersion-invariant moments (ADIMs), we exponentiate Z_0 and transform back to the time domain to obtain the augmented signal:

$$v(x, t) = \frac{1}{\sqrt{2\pi}} \int \exp(Z_0(x, \omega)) e^{-j\omega t} d\omega \quad (4.13)$$

Temporal moments are then computed from the augmented signal in the usual way,

$$T_n(x) = \int t^n |v(x, t)|^2 dt \quad (4.14)$$

and because $v(x, t) = v(0, t)$, the features are likewise invariant: $T_n(x) = T_n(0)$.

4.2.3 Cepstral Moments

The frequency domain log operation of the ADIMs processing given previously is reminiscent of the cepstrum of a signal [45]. For $u(x, t)$, the cepstrum is given by

$$c_u(x, t) = \frac{1}{\sqrt{2\pi}} \int \ln B(x, \omega) e^{-j\omega t} d\omega \quad (4.15)$$

For purely real dispersion relations (i.e., no damping, $k_I(\omega) = 0$), it follows from Eq. (2.46) that the cepstrum is invariant to dispersion, and in turn, features calculated from the cepstrum are invariant to dispersion.

However, the cepstrum is not, in general, invariant to damping. When there is damping, the cepstrum is given by

$$c_u(x, t) = \frac{1}{\sqrt{2\pi}} \int \ln (B(0, \omega) e^{-k_I(\omega)x}) e^{-j\omega t} d\omega \quad (4.16)$$

$$= \frac{1}{\sqrt{2\pi}} \int \ln B(0, \omega) e^{-j\omega t} d\omega - \frac{x}{\sqrt{2\pi}} \int k_I(\omega) e^{-j\omega t} d\omega \quad (4.17)$$

$$= c_u(0, t) - I(x) \quad (4.18)$$

where

$$I(x) = \frac{x}{\sqrt{2\pi}} \int k_I(\omega) e^{-j\omega t} d\omega \quad (4.19)$$

Accordingly, in general $c_u(x, t) \neq c_u(0, t)$ when there is damping, and thus cepstral moments, computed from the cepstrum as

$$M_c(x; n) = \int t^n |c_u(x, t)|^2 dt \quad (4.20)$$

are also not generally invariant to damping.

Some cepstral moments are, however, invariant to the specific case of exponential attenuation, where $k_I(\omega) = \beta\omega$. For this case, the cepstrum at x is given by Eq. (4.18), with

$$I(x) = \frac{\beta x}{\sqrt{2\pi}} \int \omega e^{-j\omega t} d\omega \quad (4.21)$$

$$= j\beta x \delta'(t) \quad (4.22)$$

The cepstral moments are then given by

$$M_c(x; n) = \int t^n |c_u(0, t) - j\beta x \delta'(t)|^2 dt \quad (4.23)$$

$$= \int t^n c_u^2(0, t) dt + \beta^2 x^2 \int t^n (\delta'(t))^2 dt \quad (4.24)$$

For odd n , the integrand of the second integral is an odd function, and thus integrates to zero. Hence, the odd-order cepstral moments are invariant to dispersion and exponential damping,

$$M_c(x; n) = M_c(0; n), \quad [\text{for } n \text{ odd, exponential damping}] \quad (4.25)$$

4.2.4 Relation Between ADIMs and Cepstral Moments

Because the ADIMs and cepstral moments are computed via similar procedures (a log operation in the frequency domain is common to both), it is worthwhile to further explore the mathematical relationship between the two. As noted previously in the derivation of the time-domain ADIMs, we exponentiate the Z_0 function and then transform back to the time domain. Initially, this exponentiation step was done to “undo” in some sense the amplitude compression induced by the log operation in the earlier stage of the ADIMs processing. Moreover, we found in our simulations that it led to improved classification performance of our features in some cases. We can skip this exponentiation step and the zero-mean normalization step in the ADIMs processing and consider the moments from the Z function,

$$\langle t^n \rangle_Z = \int t^n |Z(x, t)|^2 dt \quad (4.26)$$

From the definition of the Z function given in Eq. (4.5) and the definition of the cepstrum given in Eq. (4.15), we have by Fourier properties that

$$Z(x, t) \sim j t c_u(x, t) \quad (4.27)$$

Hence, the n^{th} -order temporal moments of the Z function are the $(n + 2)$ -order moments of the cepstrum,

$$\langle t^n \rangle_Z = \int t^n |Z(x, t)|^2 dt \quad (4.28)$$

$$\sim \int t^n |t c_u(x, t)|^2 dt = \int t^{n+2} |c_u(x, t)|^2 dt \quad (4.29)$$

While this relationship is interesting and may be useful analytically, it is important to note that eliminating the mean-subtraction step of the ADIMs processing, as done here, will sacrifice the propagation-invariance to damping. Accordingly, we next examine the relation between the cepstral moments and the moments computed using full ADIMs processing.

Let

$$V(x, \omega) = e^{Z_0(x, \omega)} \quad (4.30)$$

Then the (complex) cepstrum of $V(x, \omega)$ is

$$c_v(x, t) = \int \log V(x, \omega) e^{j\omega t} d\omega = \int Z_0(x, \omega) e^{j\omega t} d\omega \quad (4.31)$$

Accordingly, if we skip the exponentiation step in the ADIMs processing prior to transforming to the time domain (Eq. 4.7), then the time-domain moments obtained from the $Z_0(x, \omega)$ function are equivalent to the temporal moments of the complex cepstrum of the function $V(x, \omega)$.

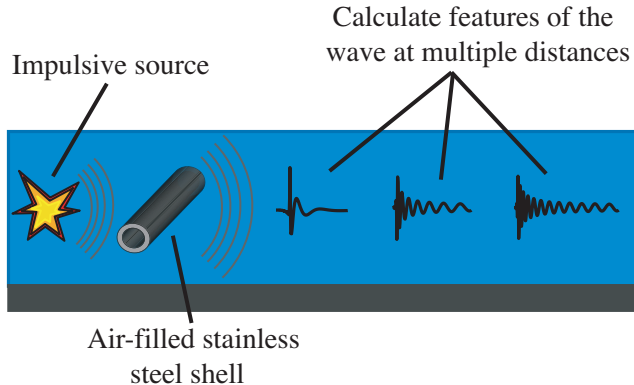


Figure 2: **An overview of the simulations.**

4.3 CLASSIFICATION SIMULATIONS

4.3.1 Simulation Setup

In this section, we present the results of simulations conducted to test the classification utility of the features for discriminating between two differently-sized cylinders in a shallow water channel model that includes dispersion and damping. Variability was introduced into the simulation by varying the propagation distance uniformly over the range from 5 to 2500 meters, sampled at 5 meter increments. An overview of the simulations is shown in Fig. 2.

The backscatter from cylindrical shells of different radii and thicknesses was computed using resonance scattering theory (RST) [22, 25, 24, 26, 51]. The physical parameters of the various materials are given in Table 3. The geometry of the shells used in the simulations was chosen to be similar to real world objects that might be encountered in an undersea environment. The inner and outer radii of the shells are given in Table 4, along with the value of h for each shell, defined by

$$h = \left(1 - \frac{r_{inner}}{r_{outer}}\right) \times 100\% \quad (4.32)$$

The backscatter from each shell was propagated to various distances within a simulated shallow water channel. For the simulation results presented in this paper, the channel is a

Table 3: Physical parameters used in simulations

	Water	Air	Steel
Density	$1000 \frac{kg}{m^3}$	$1.2 \frac{kg}{m^3}$	$7800 \frac{kg}{m^3}$
Speed of Sound Waves	$1500 \frac{m}{s}$	$340 \frac{m}{s}$	$5880 \frac{m}{s}$ (dilatational) $3140 \frac{m}{s}$ (shear)

Table 4: Geometry of shells used in simulations

	Inner Radius (m)	Outer Radius (m)	h
Cylinder 1	1.19	1.20	0.83%
Cylinder 2	1.43	1.45	1.4%

parallel-plate waveguide with a pressure-release top boundary and rigid bottom boundary, and the medium exhibits attenuation with an exponential dependence upon frequency. Thus, the dispersion relation of this channel is given by

$$k(\omega) = \frac{1}{c} \sqrt{\omega^2 - \omega_{0m}^2} + j\beta\omega \quad (4.33)$$

where $c = 1500$ [m/s] is the velocity of sound, β is the attenuation parameter, and ω_{0m} is the cut-off frequency of the mode m , given by

$$\omega_{0m} = \frac{(m - 0.5)\pi c}{D} \quad (4.34)$$

The first term in Eq. (4.33) is the expression for the dispersion relation of an ideal two-plate waveguide [50] and the second term represents exponential attenuation. Mode separation is implicit in our simulations, as we consider only the first propagated mode in the channel ($m = 1$ in Eq. 4.33). Also note that the two-plate channel model implicitly has a low-frequency cut-off, since $k(\omega)$ becomes purely imaginary when $\omega < \frac{(m-0.5)\pi c}{D}$. Hence, frequencies below this value do not propagate in the model.

The depth of the channel was fixed at 25 meters. Feature values were calculated at 5 meter increments over a range of 5 to 2500 meters. Therefore, for each shell, we obtain 500 values for each feature. The sampling frequency was fixed at 10 kHz, and an anti-aliasing filter was applied to limit the bandwidth of the backscattered echoes to 5 kHz.

The classification features extracted from each simulated propagated echo were ordinary central temporal moments given in Eq. (3.4) for $n = 2, 3, 4$, the corresponding ADIMs given by the procedures discussed in Sections 4.2.1 and 4.2.2, and cepstral moments computed per Eq. (4.20). All moments were normalized by the respective zero-order moment so that differences in signal energy between the classes would not contribute to classification performance. The classification performance of each feature was evaluated via receiver operating characteristic (ROC) curves, which plot the relationship between the probability of correct classification and the probability of false positive. The ROC curves were obtained by computing histograms of the feature values for each shell and sweeping a decision threshold across the histograms. At each position of the threshold, the probability of correct classification (correctly identifying a target) was calculated and plotted versus the probability of false alarm (incorrectly labeling a clutter echo as a target).

4.3.2 Simulation Results

For the first simulation, the attenuation parameter was set to $\beta = 10^{-8} \text{ m}^{-1}\text{Hz}^{-1}$. As the wave propagates to longer distances in the channel, the low frequencies are increasingly delayed due to dispersion and the higher frequencies are increasingly attenuated. These effects may be seen in Figs. 3 and 4, which show the backscatter at 1250 meters and the backscatter at 2500 meters of cylinder 1 and cylinder 2, respectively. The time series are significantly affected as the waves propagate to greater distances, and it stands to reason that ordinary temporal moments will not be effective classification features.

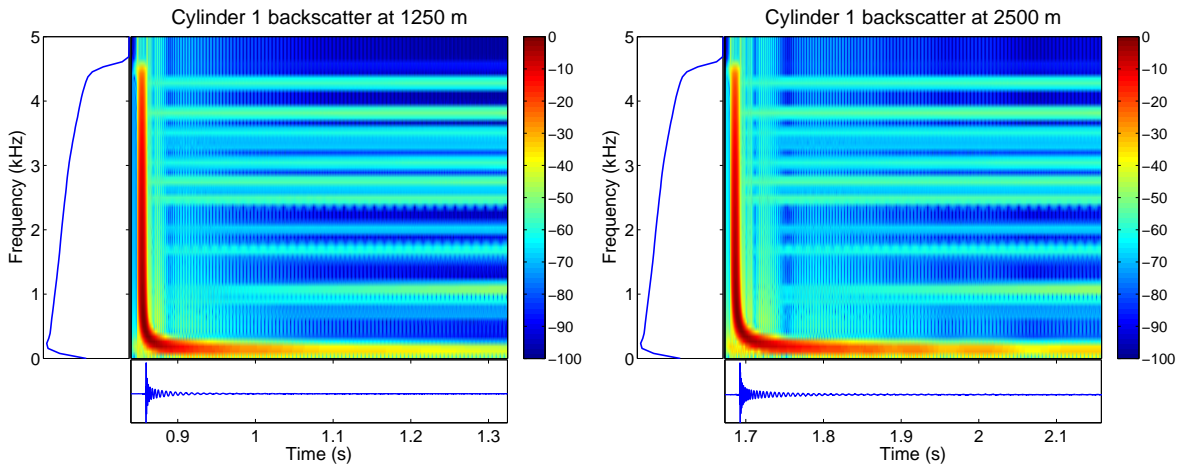


Figure 3: Waveforms generated by cylinder 1(1.25 km, 2.5 km).

The augmented wave, $v(x, t)$, as given in Section 4.2.1 by Eq. (4.7) is shown for the backscatter at 1250 meters and the backscatter at 2500 meters for cylinder 1 and cylinder 2 in Figs. 5 and 6, respectively. The time series of the augmented waves do not change significantly with greater propagation distance, and the spectrum and spectrogram of each augmented wave show that the processing enhances the natural resonances of the shells.

The ROC curves for this simulation are shown in Fig. 7. The cepstral moments and the ADIMs exhibit significantly better performance compared to the ordinary temporal moments.

A second simulation was performed in which all parameters were identical to the first simulation, except that the attenuation parameter was increased by an order of magnitude

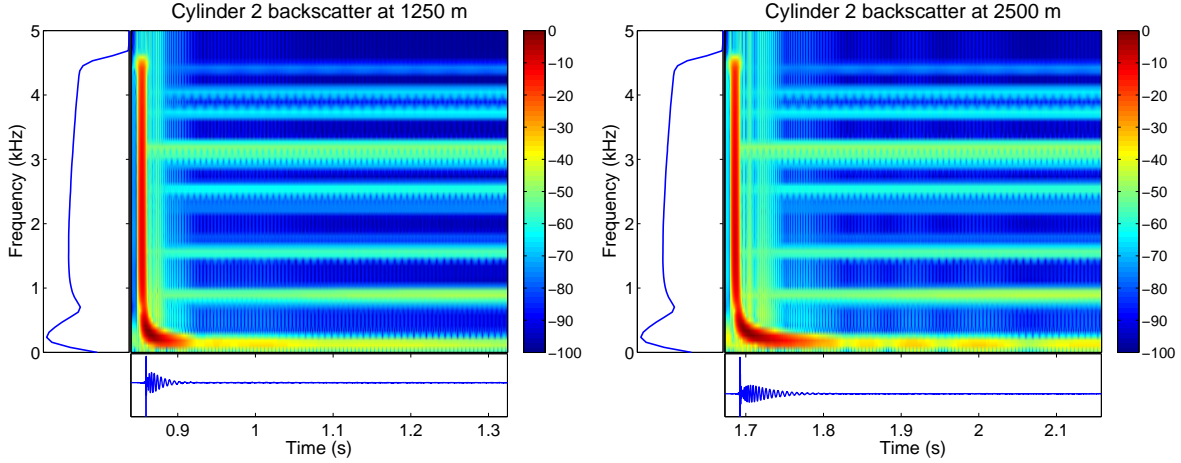


Figure 4: Waveforms generated by cylinder 2 (1.25 km, 2.5 km).

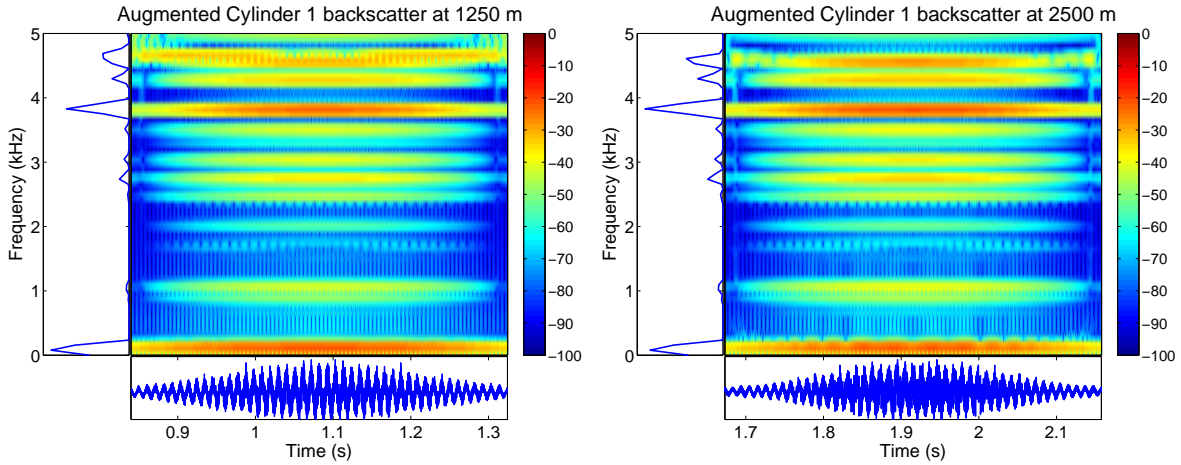


Figure 5: Augmented waveform generated by cylinder 1 (1.25 km, 2.5 km).

to $\beta = 10^{-7} \text{ m}^{-1}\text{Hz}^{-1}$. The ROC curves for this simulation are given in Fig. 8. The cepstral moments display less classification utility compared to their performance with $\beta = 10^{-8} \text{ m}^{-1}\text{Hz}^{-1}$, while the ADIMs are not affected by the increased attenuation. The ordinary temporal moments show no classification utility.

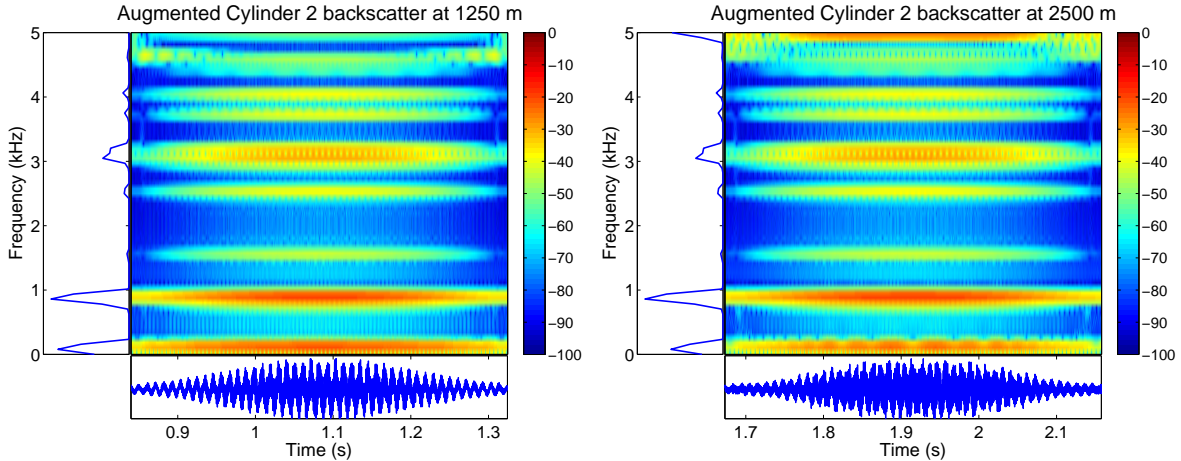


Figure 6: **Augmented waveform generated by cylinder 2 (1.25 km, 2.5 km).**

To provide easy comparison of the results, we give in Table 5 the area under the ROC curves for each result. These statistics are one way to express the quality of classification performance in a single number. An area under ROC score of unity is a perfect score, while a score of 0.5 represents chance. For each order of moment and attenuation parameter, the cepstral moments and ADIMs achieve better classification performance than the ordinary temporal moments.

In this chapter we have developed features, called ADIMs, that are invariant to dispersion and certain important types of damping. To the extent that the ADIMs can separate the classes in the free field, they will also separate the classes with dispersion and exponential or power-law damping. Thus, the use of these features may aid classification performance in complicated propagation channels such as shallow-water environments.

The ADIMs have been developed using a range-independent propagation model. If the assumption of range independence is violated, however, the ADIMs may no longer be invariant to propagation effects. As an example, we repeat the classification simulation presented above, but we replace the range-independent two-plate waveguide with a range-dependent wedge (the exact solution for the acoustic field in a wedge is given in Chapter 7). The angle of wedge in this simulation is 0.5 degrees. The source is located 3 km from the apex at

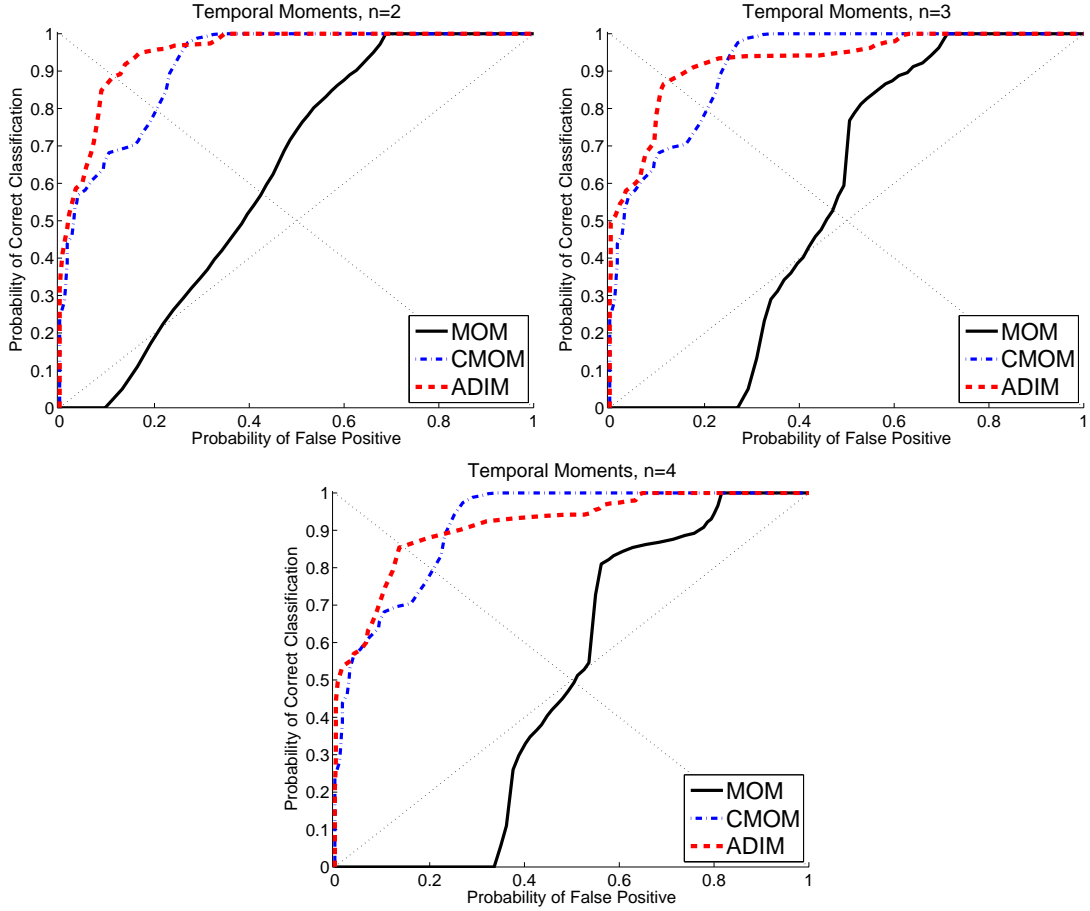


Figure 7: ROC curves showing classification performance of ordinary temporal moments (MOM), cepstral moments (CMOM), and attenuation and dispersion invariant temporal moments (ADIM) for $n = 2, 3$, and 4 in a channel with exponential attenuation, $\beta = 10^{-8} \text{ m}^{-1} \text{ Hz}^{-1}$.

0.25 degrees, and the signal is propagated at 5 meter increments to a total distance of 5.5 km from the apex. The ROC curves for $\beta = 10^{-8} \text{ m}^{-1} \text{ Hz}^{-1}$ are given in Fig. 9. Clearly, the performance of the ADIMs degrades in this range-dependent simulation, suggesting that they lose their invariance. These results motivate consideration of our extension of the phase space approach to the range-dependent case, as done in Chapter 7.

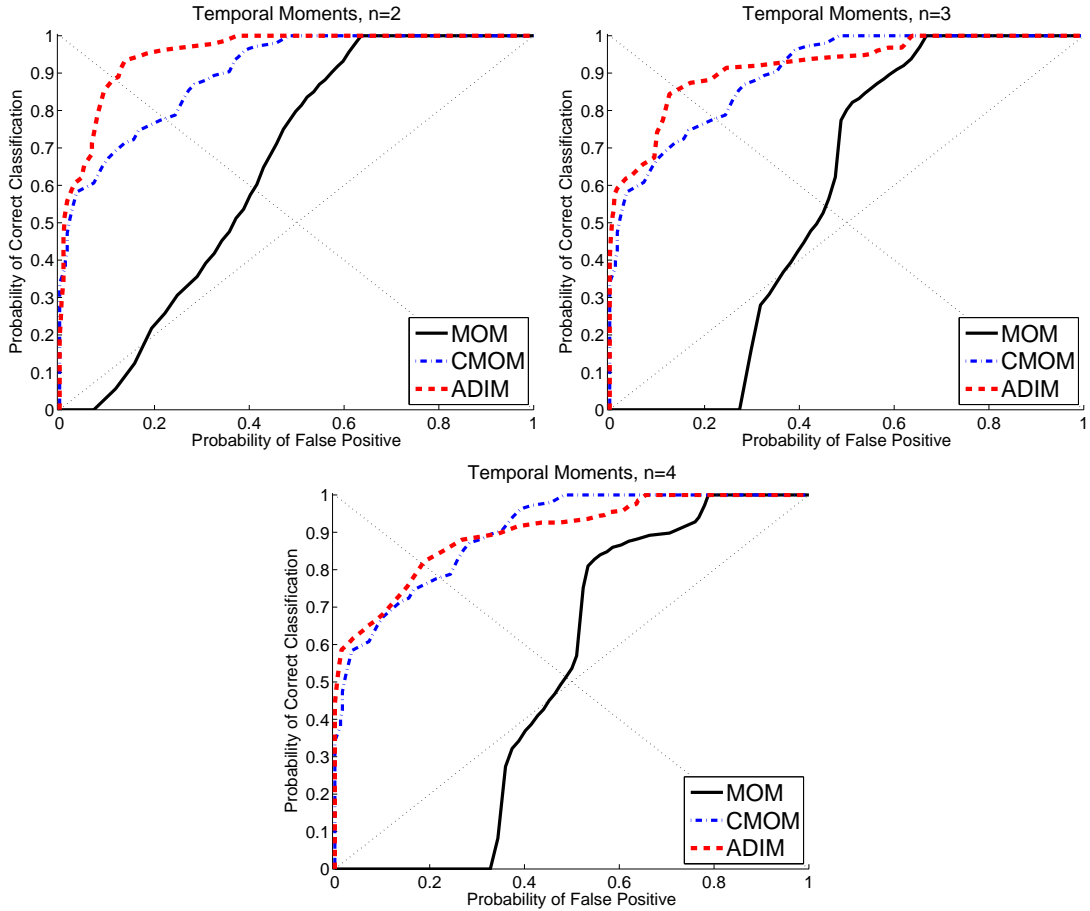


Figure 8: ROC curves showing classification performance of ordinary temporal moments (MOM), cepstral moments (CMOM), and attenuation and dispersion invariant temporal moments (ADIM) for $n = 2, 3$, and 4 in a channel with exponential attenuation, $\beta = 10^{-7} \text{ m}^{-1} \text{ Hz}^{-1}$.

Additionally, in cases where the ADIMs do not provide good free field class separation, other features that are potentially affected by propagation effects must be used. In the next chapter, we develop a method for estimating the impact of the propagation effects on a broad class of potential classification features—the temporal and spectral statistical moments.

Table 5: Area Under ROC for classification simulations.

	MOM	CMOM	ADIM
$n = 2, \beta = 10^{-8}$	0.6182	0.9159	0.9511
$n = 2, \beta = 10^{-7}$	0.6443	0.8994	0.9526
$n = 3, \beta = 10^{-8}$	0.5530	0.9157	0.9275
$n = 3, \beta = 10^{-7}$	0.5635	0.8996	0.9188
$n = 4, \beta = 10^{-8}$	0.4946	0.9154	0.9134
$n = 4, \beta = 10^{-7}$	0.5215	0.8998	0.8993

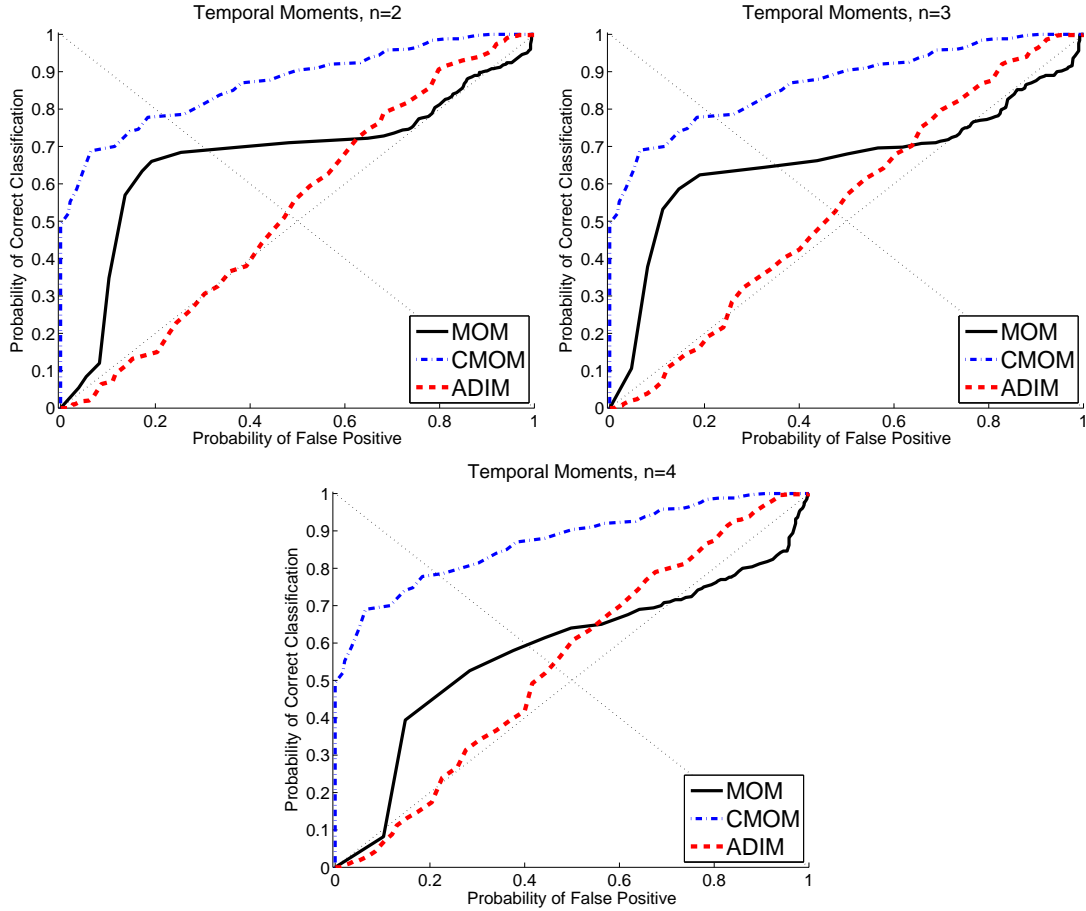


Figure 9: ROC curves showing classification performance of ordinary temporal moments (MOM), cepstral moments (CMOM), and attenuation and dispersion invariant temporal moments (ADIM) for $n = 2, 3$, and 4 in a wedge-shaped channel with exponential attenuation, $\beta = 10^{-8} \text{ m}^{-1} \text{ Hz}^{-1}$.

5.0 MOMENTS OF MOMENTS

In this chapter we investigate the effects of channel propagation on a set of features, namely the temporal and spectral moments of the received signal. We consider a channel model with frequency dependent propagation effects (which arise in shallow water channels, and in dispersive propagation in general), and we introduce randomness through uncertainty or random variations in the channel. Uncertainty and random variations in an ocean channel increase the variability of features computed from sonar echoes that have propagated in that channel, and the increased variability may have a negative effect on classification performance. In order to quantify this variability, we compute the statistics of potential features-the moments of the moment features of the wave. Ideally, the sonar echo from a particular target of interest would produce the same feature value each time the target was insonified. However, in practice this is not the case, as noise and other environmental factors cause the features to take on random values. For this work, we neglect the effect of noise and instead focus on variability introduced by the propagation channel.

The randomness of the moment features may be caused by two phenomena: uncertainty of the propagation channel and random variations within the channel itself. Uncertainty means that the parameters of the channel are assumed to be constant while the wave is propagating through the channel, but a new realization of the random parameters is encountered for each subsequent wave that passes through the channel. This type of random behavior could be caused by daily or seasonal weather cycles, or it could be caused by changes in the operating location. In a randomly varying channel, the parameters of the channel are fluctuating as the wave is passing through it. A major cause of these fluctuations in the

ocean is internal waves, which are responsible for changes in the water such as temperature, density, salinity, and velocity of the medium [18]. All of these changes affect acoustic propagation and can alter feature values.

In either case, the random fluctuations will affect the construction of a feature space from training data as well as the proper classification of observed data. It is, therefore, in the interest of improved classification to seek methods to quantify, approximate, or compensate for these random variations.

5.1 UNCERTAIN CHANNELS

In this section, the channel is modeled by a realization of a spatially-dependent impulse response defined by random parameters. Therefore, because a signal propagates through a single realization of a random channel, the features computed from that signal may be viewed as individual realizations of random variables. The purpose of this paper is to investigate the statistical properties of the features and derive expressions for the relationships between the random parameters of the channel and the random values of the features.

Liu and Yeh investigated the statistical properties of the temporal moments of optical pulses propagating through turbulent media and obtained expressions for the moments (i.e., ensemble averages) of the temporal moments of the pulses in terms of the two-frequency mutual coherence function [55, 34, 35]. The general concept of this chapter is similar – to obtain expressions for the moments of the temporal and spectral moment features of a propagating wave—but our approach is based on time-frequency methods because of the inherent nonstationarities of dispersive propagation.

5.1.1 Uncertain Channel Model

For the uncertain channel model, we let the channel be defined by realizations of random variables. For example, in the linear systems representation of the channel given in Eq. (2.42), the parameter x could be taken to be a random variable, representing uncertainty in

the target distance or how far the wave propagates. If the initial wave $u(0, t)$ is deterministic, then the propagation model in Eq. (2.51) becomes, in the ensemble sense,

$$\langle W_u(t, \omega; x) \rangle = W_u(t, \omega; 0) *_t \langle W_h(t, \omega; x) \rangle \quad (5.1)$$

where $*_t$ denotes time-domain convolution and the brackets $\langle \cdot \rangle$ denote the ensemble average. We use this propagation model to calculate the statistical behavior of the moment features of a propagating wave.

5.1.2 Moments of Moments of the Wigner Distribution

Following an approach similar to Liu and Yeh [35], we analyze the variability in moment features by calculating expected values of the temporal and spectral moment features; however, we do so from the Wigner distribution and approximation. In this section, we do not consider turbulent or random media, but rather a channel model characterized by random parameters. We note that, in this chapter, the variable m is used to denote the order of the moments of the channel. Because we are considering single mode propagation, we drop the m subscript from the dispersion relation that was used in previous chapters.

5.1.2.1 Temporal Moment Features The expected value of the temporal moments of the signal at x is given by

$$\langle \langle t_u^n \rangle_x \rangle = \int \int t^n \langle W_u(t, \omega; x) \rangle d\omega dt \quad (5.2)$$

and the second-order expectation of the temporal moment features follows from

$$\langle \langle \langle t_u^n \rangle_x^2 \rangle \rangle = \int \int (t_1 t_2)^n \langle W_u(t_1, \omega_1; x) W_u(t_2, \omega_2; x) \rangle dt_1 d\omega_1 dt_2 d\omega_2 \quad (5.3)$$

Higher-order expected values of the temporal moment features are given by

$$\begin{aligned} \langle \langle \langle t_u^n \rangle_x^i \rangle \rangle &= \int \int \int \int \dots \int \int (t_1 t_2 \dots t_i)^n \\ &\quad \langle W_u(t_1, \omega_1; x) W_u(t_2, \omega_2; x) \dots W_u(t_i, \omega_i; x) \rangle dt_1 d\omega_1 dt_2 d\omega_2 \dots dt_i d\omega_i \end{aligned} \quad (5.4)$$

We may write Eq. (5.4) in terms of the temporal moments of the initial wave (at $x = 0$) and the expected values of the temporal moments of the channel impulse response as

$$\begin{aligned} \langle \langle (t_u^n)_x \rangle^i \rangle &= \sum_{m_1, m_2, \dots, m_i=0}^n \binom{n}{m_1} \binom{n}{m_2} \dots \binom{n}{m_i} \int \int \dots \int \\ &\quad \langle \langle t_u^{n-m_1} \rangle_{0, \omega_1} \langle t_u^{n-m_2} \rangle_{0, \omega_2} \dots \langle t_u^{n-m_i} \rangle_{0, \omega_i} \rangle \langle \langle t_h^{m_1} \rangle_{x, \omega_1} \langle t_h^{m_2} \rangle_{x, \omega_2} \dots \langle t_h^{m_i} \rangle_{x, \omega_i} \rangle d\omega_1 d\omega_2 \dots d\omega_i \end{aligned} \quad (5.5)$$

The detailed derivation of this formula for $i = 1, 2$ is given in the Appendix.

The random quantities in Eq. (5.5) are the local temporal moments of the channel impulse response, which are given by

$$\langle t_h^m \rangle_{x, \omega} = \int t^m W_h(t, \omega, x) dt \quad (5.6)$$

The problem of solving for the statistics of the temporal moment features of the signal, then, essentially reduces to finding the ensembles of products of the moment features of the channel as given by Eq. (5.6). The per mode Wigner approximation for the channel, given in Eq. (2.53), may be utilized here to obtain approximate values of the temporal moment features of the channel:

$$\langle t_h^m \rangle_{x, \omega} \approx \int t^m e^{-2k_I(\omega)x} \delta(t - k'_R(\omega)x) dt = e^{-2k_I(\omega)x} (k'_R(\omega)x)^m \quad (5.7)$$

Ensemble averages of products of Eq. (5.7) may be used to obtain approximate moments of the temporal moment features of the signal. For example, if x is uncertain and described by the probability distribution $P(x)$, then the expected value of the moments is approximately given by

$$\langle \langle t_h^m \rangle_{x, \omega} \rangle \approx \int e^{-2k_I(\omega)x} (k'_R(\omega)x)^m P(x) dx \quad (5.8)$$

and the expected value of the product of i moments is approximately given by

$$\begin{aligned} \langle \langle t_h^{m_1} \rangle_{x, \omega_1} \langle t_h^{m_2} \rangle_{x, \omega_2} \dots \langle t_h^{m_i} \rangle_{x, \omega_i} \rangle &\approx \int e^{-2x(k_I(\omega_1) + k_I(\omega_2) + \dots + k_I(\omega_i))} \\ &\quad (k'_R(\omega_1))^{m_1} (k'_R(\omega_2))^{m_2} \dots (k'_R(\omega_i))^{m_i} P(x) dx \end{aligned} \quad (5.9)$$

We point out that the Wigner approximation is exact for exponential damping, $k_I(\omega) = b\omega$, and quadratic dispersion, $k_R(\omega) = \frac{1}{c}\omega + \gamma\omega^2$ [40]. Therefore, the moments of the features calculated using the expression in Eq. (5.9), which is based upon the approximation, are also exact for this case.

5.1.2.2 Frequency Moments The expected values of the frequency moment features are given by

$$\langle\langle\omega_u^n\rangle_x\rangle = \int \int \omega^n \langle W_u(t, \omega; x) \rangle d\omega dt \quad (5.10)$$

which generalizes to higher-order ensemble averages (i.e., moments of moment features) as

$$\begin{aligned} \langle\langle\langle\omega_u^n\rangle_x\rangle^i\rangle &= \int \int \int \int \dots \int \int (\omega_1 \omega_2 \dots \omega_i)^n \\ &\langle W_u(t_1, \omega_1; x) W_u(t_2, \omega_2; x) \dots W_u(t_i, \omega_i; x) \rangle dt_1 d\omega_1 dt_2 d\omega_2 \dots dt_i d\omega_i \end{aligned} \quad (5.11)$$

We may write Eq. (5.11) in terms of the squared magnitude of the initial wave and the squared magnitude of the channel as

$$\begin{aligned} \langle\langle\langle\omega_u^n\rangle_x\rangle^i\rangle &= \int \int \dots \int (\omega_1 \omega_2 \dots \omega_i)^n (|F(0, \omega_1)|^2 |F(0, \omega_2)|^2 \dots |F(0, \omega_i)|^2) \\ &\langle |H(x, \omega_1)|^2 |H(x, \omega_2)|^2 \dots |H(x, \omega_i)|^2 \rangle d\omega_1 d\omega_2 \dots d\omega_i \end{aligned} \quad (5.12)$$

The random quantity in Eq. (5.12) is the squared magnitude of the channel frequency response function, which is given by

$$|H(x, \omega)|^2 = \int W_h(t, \omega, x) dt \quad (5.13)$$

Using the Wigner approximation, we have

$$|H(x, \omega)|^2 \approx \int e^{-2k_I(\omega)x} \delta(t - k'_R(\omega)x) dt = e^{-2k_I(\omega)x} \quad (5.14)$$

which is, in fact, exact; hence, the spectral moments obtained using the approximation are exact.

We now consider two examples in which the distance to the target x is uncertain and modeled by a probability distribution. In the first example, the channel has dispersion only, and x is modeled by a uniform distribution. In the second example, the channel has a complex dispersion relation, and the distance x is modeled by a Gaussian distribution.

5.1.3 Example 1

For this example, we take a channel with dispersion only, no damping ($k_I(\omega) = 0$), and let x be a random variable, uniformly distributed on the interval $[0, X]$. This models a scenario where the channel is fixed, but the distance from the target is random.

First, we will find the approximate expected values of the temporal moment features, which are computed from Eq. (5.5) with $i = 1$. Using Eq. (5.8) with the uniform distribution on x , we have

$$\langle \langle t_h^m \rangle_{x,\omega} \rangle \approx \frac{(k'_R(\omega))^m}{X} \int_0^X x^m dx = \frac{(k'_R(\omega))^m}{X} \frac{1}{m+1} X^{m+1} = \frac{(k'_R(\omega)X)^m}{m+1} \quad (5.15)$$

Substituting this result into Eq. (5.5) with $i = 1$ allows us to calculate the expected values of the temporal moments of the signal. The general expression is given by

$$\langle \langle t_u^n \rangle_x \rangle = \sum_{m_1=0}^n \binom{n}{m_1} \int \langle t_u^{n-m_1} \rangle_{0,\omega_1} \frac{(k'_R(\omega_1)X)^{m_1}}{m_1+1} d\omega_1 \quad (5.16)$$

Accordingly, the expected value of the first temporal moment ($n = 1$) is

$$\langle \langle t_u \rangle_x \rangle = \int \langle t_u \rangle_{0,\omega_1} d\omega_1 + \int \frac{k'_R(\omega_1)X}{2} |F(0, \omega_1)|^2 d\omega_1 \quad (5.17)$$

$$= \langle t_u \rangle_0 + \frac{X}{2} \int k'_R(\omega_1) |F(0, \omega_1)|^2 d\omega_1 \quad (5.18)$$

We note that the integral term is the average group slowness [43].

The expected value of the second temporal moment ($n = 2$) is

$$\langle \langle t_u^2 \rangle_x \rangle = \int \langle t_u^2 \rangle_{0,\omega_1} d\omega_1 + 2 \int \langle t_u \rangle_{0,\omega_1} \frac{k'_R(\omega_1)X}{2} d\omega_1 + \int \frac{(k'_R(\omega_1)X)^2}{3} |F(0, \omega_1)|^2 d\omega_1 \quad (5.19)$$

$$= \langle t_u^2 \rangle_0 + X \int \langle t_u \rangle_{0,\omega_1} k'_R(\omega_1) d\omega_1 + \frac{X^2}{3} \int (k'_R(\omega_1))^2 |F(0, \omega_1)|^2 d\omega_1 \quad (5.20)$$

To find the approximate variances of the temporal moment features, we must do the calculation given in Eq. (5.5) for $i = 2$. First, we evaluate Eq. (5.9) with $i = 2$ to obtain

$$\langle \langle t_h^{m_1} \rangle_{x,\omega_1} \langle t_h^{m_2} \rangle_{x,\omega_2} \rangle = \frac{(k'_R(\omega_1))^{m_1} (k'_R(\omega_2))^{m_2}}{X} \int_0^X x^{m_1+m_2} dx \quad (5.21)$$

$$= \frac{(k'_R(\omega_1))^{m_1} (k'_R(\omega_2))^{m_2}}{X} \frac{1}{m_1+m_2+1} X^{m_1+m_2+1} \quad (5.22)$$

$$= \frac{(k'_R(\omega_1)X)^{m_1} (k'_R(\omega_2)X)^{m_2}}{m_1+m_2+1} \quad (5.23)$$

The general form of the second order expectation becomes

$$\langle\langle (t_u)_x \rangle^2 \rangle = \sum_{m_1, m_2=0}^n \binom{n}{m_1} \binom{n}{m_2} \int \int \langle t_u^{n-m_1} \rangle_{0, \omega_1} \langle t_u^{n-m_2} \rangle_{0, \omega_2} \langle \langle t_h^{m_1} \rangle_{x, \omega_1} \langle t_h^{m_2} \rangle_{x, \omega_2} \rangle d\omega_1 d\omega_2 \quad (5.24)$$

For the arrival time, which corresponds to the first-order moment feature ($n = 1$, or $\langle t_u \rangle_x$), we have

$$\begin{aligned} \langle\langle (t_u)_x \rangle^2 \rangle &= \int \int \langle t_u \rangle_{0, \omega_1} \langle t_u \rangle_{0, \omega_2} d\omega_1 d\omega_2 + \int \int \langle t_u \rangle_{0, \omega_1} \frac{k'_R(\omega_2)X}{2} |F(0, \omega_2)|^2 d\omega_1 d\omega_2 + \\ &\int \int \frac{k'_R(\omega_1)X}{2} |F(0, \omega_1)|^2 \langle t_u \rangle_{0, \omega_2} d\omega_1 d\omega_2 + \\ &\int \int \frac{k'_R(\omega_1)k'_R(\omega_2)X^2}{3} |F(0, \omega_1)|^2 |F(0, \omega_2)|^2 d\omega_1 d\omega_2 \end{aligned} \quad (5.25)$$

$$= \langle (t_u)_0 \rangle^2 + \langle t_u \rangle_0 X \int k'_R(\omega) |F(0, \omega)|^2 d\omega + \frac{X^2}{3} \left(\int k'_R(\omega) |F(0, \omega)|^2 d\omega \right)^2 \quad (5.26)$$

The variance of the arrival time is therefore approximately given by

$$\langle\langle (t_u)_x \rangle^2 \rangle - (\langle (t_u)_x \rangle)^2 \approx \frac{X^2}{12} \left(\int k'_R(\omega) |F(0, \omega)|^2 d\omega \right)^2 \quad (5.27)$$

$$\approx \frac{X^2}{12} (\langle k'_R(\omega) \rangle_0)^2 \quad (5.28)$$

If the propagation distance x was deterministic, the arrival time would also be deterministic (i.e., the variance would be zero). Therefore, Eq. (5.28) partially quantifies the uncertainty in the arrival time due to the uncertainty of the propagation distance. To fully characterize this uncertainty, we would compute the entire set of moments in order to compute the probability distribution function of the arrival time.

5.1.4 Example 2

We now derive approximate expressions for the first two moments of the moment features in a channel where the range x is uncertain and modeled by a Gaussian probability density function:

$$P(x) = \frac{1}{\sigma\sqrt{2\pi}} e^{-\frac{(x-\mu)^2}{2\sigma^2}} \quad (5.29)$$

where μ is the mean and σ^2 is the variance. The expected value of each of the temporal moments is given exactly by Eq. (5.5) with $i = 1$. Using Eq. (5.8), we have an approximate expression for the temporal moments of the channel,

$$\langle\langle t_h^m \rangle_{x,\omega}\rangle \approx (k'_R(\omega))^m \int x^m e^{-2k_I(\omega)x} P(x) dx \quad (5.30)$$

Inserting the density function for x given in Eq. (5.29) gives

$$\langle\langle t_h^m \rangle_{x,\omega}\rangle \approx \frac{(k'_R(\omega))^m}{\sigma\sqrt{2\pi}} \int x^m e^{-2k_I(\omega)x} e^{-\frac{(x-\mu)^2}{2\sigma^2}} dx \quad (5.31)$$

By completing the square in the exponent, the equation simplifies to

$$\langle\langle t_h^m \rangle_{x,\omega}\rangle \approx (k'_R(\omega))^m d_1(\omega) \left[\frac{1}{\sigma\sqrt{2\pi}} \int x^m e^{-\frac{(x-(\mu-2k_I(\omega)\sigma^2))^2}{2\sigma^2}} dx \right] \quad (5.32)$$

where $d_1(\omega) = e^{2k_I^2(\omega)\sigma^2 - 2k_I(\omega)\mu}$. The term in brackets is the expression for the moments of a Gaussian distribution with mean $(\mu - 2k_I(\omega)\sigma^2)$ and variance σ^2 . Accordingly, we have [20]

$$\langle\langle t_h^0 \rangle_{x,\omega}\rangle \approx d_1(\omega) \quad (5.33)$$

$$\langle\langle t_h \rangle_{x,\omega}\rangle \approx (k'_R(\omega)) d_1(\omega) [\mu - 2k_I(\omega)\sigma^2] \quad (5.34)$$

5.1.4.1 First Temporal Moment Feature The general expression for the expected value of the first temporal moment feature of the signal is given by Eq. (5.5) with $i = 1$ and $n = 1$:

$$\langle \langle t_u \rangle_x \rangle = \sum_{m_1=0}^1 \binom{1}{m_1} \int \langle t_u^{n-m_1} \rangle_{0,\omega_1} \langle \langle t_h^{m_1} \rangle_{x,\omega_1} \rangle d\omega_1 \quad (5.35)$$

$$= \int \langle t_u^1 \rangle_{0,\omega_1} \langle \langle t_h^0 \rangle_{x,\omega_1} \rangle d\omega_1 + \int \langle t_u^0 \rangle_{0,\omega_1} \langle \langle t_h^1 \rangle_{x,\omega_1} \rangle d\omega_1 \quad (5.36)$$

Utilizing the approximate expressions in Eqs. (7.37) and (5.34), we have

$$\langle \langle t_u \rangle_x \rangle \approx \int \langle t_u \rangle_{0,\omega_1} d_1(\omega_1) d\omega_1 + \int (k'_R(\omega_1)) d_1(\omega_1) [\mu - 2k_I(\omega_1)\sigma^2] |F(0, \omega_1)|^2 d\omega_1 \quad (5.37)$$

For the second moment of the first temporal moment feature, we must approximate

$\langle \langle t_h^{m_1} \rangle_{x,\omega_1} \langle t_h^{m_2} \rangle_{x,\omega_2} \rangle$:

$$\langle \langle t_h^{m_1} \rangle_{x,\omega_1} \langle t_h^{m_2} \rangle_{x,\omega_2} \rangle \approx \int e^{-2x(k_I(\omega_1)+k_I(\omega_2))} (k'_R(\omega_1)x)^{m_1} (k'_R(\omega_2)x)^{m_2} P(x) dx \quad (5.38)$$

$$\approx (k'_R(\omega_1))^{m_1} (k'_R(\omega_2))^{m_2} \frac{1}{\sigma\sqrt{2\pi}} \int x^{m_1+m_2} e^{-2x(k_I(\omega_1)+k_I(\omega_2))} e^{-\frac{(x-\mu)^2}{2\sigma^2}} dx \quad (5.39)$$

$$\approx (k'_R(\omega_1))^{m_1} (k'_R(\omega_2))^{m_2} d_2(\omega_1, \omega_2) \frac{1}{\sigma\sqrt{2\pi}} \int x^{m_1+m_2} e^{-\frac{(x-(\mu-2\sigma^2(k_I(\omega_1)+k_I(\omega_2))))^2}{2\sigma^2}} dx \quad (5.40)$$

where $d_2(\omega_1, \omega_2) = e^{2k_I^2(\omega_1)\sigma^2+4k_I(\omega_1)k_I(\omega_2)\sigma^2+2k_I^2(\omega_2)\sigma^2-2k_I(\omega_1)\mu-2k_I(\omega_2)\mu}$. The integral is the expression for the $(m_1 + m_2)$ -order moments of a Gaussian distribution with mean given by $(\mu - 2\sigma^2(k_I(\omega_1) + k_I(\omega_2)))$ and variance given by σ^2 . Therefore, we have

$$\langle \langle t_h^0 \rangle_{x,\omega_1} \langle t_h^0 \rangle_{x,\omega_2} \rangle \approx d_2(\omega_1, \omega_2) \quad (5.41)$$

$$\langle \langle t_h^0 \rangle_{x,\omega_1} \langle t_h^1 \rangle_{x,\omega_2} \rangle \approx k'_R(\omega_2) d_2(\omega_1, \omega_2) (\mu - 2\sigma^2(k_I(\omega_1) + k_I(\omega_2))) \quad (5.42)$$

$$\langle \langle t_h^1 \rangle_{x,\omega_1} \langle t_h^0 \rangle_{x,\omega_2} \rangle \approx k'_R(\omega_1) d_2(\omega_1, \omega_2) (\mu - 2\sigma^2(k_I(\omega_1) + k_I(\omega_2))) \quad (5.43)$$

$$\langle \langle t_h^1 \rangle_{x,\omega_1} \langle t_h^1 \rangle_{x,\omega_2} \rangle \approx k'_R(\omega_1) k'_R(\omega_2) d_2(\omega_1, \omega_2) \left[(\mu - 2\sigma^2(k_I(\omega_1) + k_I(\omega_2)))^2 + \sigma^2 \right] \quad (5.44)$$

The second-order expectation of the first-order temporal moment feature is given by

$$\begin{aligned}
\langle\langle (t_u)_x \rangle^2 \rangle &= \int \int \langle t_u \rangle_{0,\omega_1} \langle t_u \rangle_{0,\omega_2} \langle\langle t_h^0 \rangle_{x,\omega_1} \langle t_h^0 \rangle_{x,\omega_2} \rangle d\omega_1 d\omega_2 \\
&+ \int \int \langle t_u \rangle_{0,\omega_1} \langle t_u^0 \rangle_{0,\omega_2} \langle\langle t_h^0 \rangle_{x,\omega_1} \langle t_h^1 \rangle_{x,\omega_2} \rangle d\omega_1 d\omega_2 \\
&+ \int \int \langle t_u^0 \rangle_{0,\omega_1} \langle t_u \rangle_{0,\omega_2} \langle\langle t_h^1 \rangle_{x,\omega_1} \langle t_h^0 \rangle_{x,\omega_2} \rangle d\omega_1 d\omega_2 \\
&+ \int \int \langle t_u^0 \rangle_{0,\omega_1} \langle t_u^0 \rangle_{0,\omega_2} \langle\langle t_h^1 \rangle_{x,\omega_1} \langle t_h^1 \rangle_{x,\omega_2} \rangle d\omega_1 d\omega_2 \tag{5.45}
\end{aligned}$$

which may be approximated by substituting the approximate expressions from Eqs. (5.41)-(5.44):

$$\begin{aligned}
\langle\langle (t_u)_x \rangle^2 \rangle &\approx \int \int \langle t_u \rangle_{0,\omega_1} \langle t_u \rangle_{0,\omega_2} d_2(\omega_1, \omega_2) d\omega_1 d\omega_2 \\
&+ 2 \int \int \langle t_u \rangle_{0,d\omega_1} k'_R(\omega_2) d_2(\omega_1, \omega_2) \\
&(\mu - 2\sigma^2 (k_I(\omega_1) + k_I(\omega_2))) |F(0, \omega_2)|^2 d\omega_1 d\omega_2 \\
&+ \int \int k'_R(\omega_1) k'_R(\omega_2) d_2(\omega_1, \omega_2) \left[(\mu - 2\sigma^2 (k_I(\omega_1) + k_I(\omega_2)))^2 + \sigma^2 \right] \\
&|F(0, \omega_1)|^2 |F(0, \omega_2)|^2 d\omega_1 d\omega_2 \tag{5.46}
\end{aligned}$$

5.1.4.2 Second Temporal Moment Feature The expected value of the second temporal moment feature is given by Eq. (5.5) with $n = 2$ and $i = 1$:

$$\begin{aligned}
\langle\langle t_u^2 \rangle_x \rangle &= \sum_{m_1=0}^2 \binom{2}{m_1} \int \langle t_u^{n-m_1} \rangle_{0,\omega_1} \langle\langle t_h^{m_1} \rangle_{x,\omega_1} \rangle d\omega_1 \tag{5.47} \\
&= \int \langle t_u^2 \rangle_{0,\omega_1} \langle\langle t_h^0 \rangle_{x,\omega_1} \rangle d\omega_1 + 2 \int \langle t_u^1 \rangle_{0,\omega_1} \langle\langle t_h^1 \rangle_{x,\omega_1} \rangle d\omega_1 + \int \langle t_u^0 \rangle_{0,\omega_1} \langle\langle t_h^2 \rangle_{x,\omega_1} \rangle d\omega_1 \tag{5.48}
\end{aligned}$$

To find an approximate expression for this moment, we require the approximate temporal moments of the channel to second order. The zeroth and first order approximate moments are given in Eqs. (7.37) and (5.34), while the second order moment is approximately

$$\langle\langle t_h^2 \rangle_{x,\omega} \rangle \approx (k'_R(\omega))^2 d_1(\omega) \left[(\mu - 2k_I(\omega)\sigma^2)^2 + \sigma^2 \right] \tag{5.49}$$

Plugging these values into Eq. (5.48), we obtain the general expression

$$\begin{aligned} \langle \langle t_h^2 \rangle_{x,\omega} \rangle &\approx \int \langle t_u^2 \rangle_{0,\omega_1} d_1(\omega_1) d\omega_1 + 2 \int \langle t_u \rangle_{0,\omega_1} (k'_R(\omega_1)) d_1(\omega_1) [\mu - 2k_I(\omega_1)\sigma^2] d\omega_1 \\ &\quad + \int (k'_R(\omega_1))^2 d_1(\omega_1) [(\mu - 2k_I(\omega_1)\sigma^2)^2 + \sigma^2] |F(0, \omega_1)|^2 d\omega_1 \end{aligned} \quad (5.50)$$

The second-order expectation of the second temporal moment feature is given by Eq. (5.5) with $n = 2$ and $i = 2$:

$$\langle \langle (t_u^2)_x \rangle^2 \rangle = \sum_{m_1, m_2=0}^n \binom{2}{m_1} \binom{2}{m_2} \int \int \langle t_u^{n-m_1} \rangle_{0,\omega_1} \langle t_u^{n-m_2} \rangle_{0,\omega_2} \langle \langle t_h^{m_1} \rangle_{x,\omega_1} \langle t_h^{m_2} \rangle_{x,\omega_2} \rangle d\omega_1 d\omega_2 \quad (5.51)$$

By evaluating the summation and simplifying, we obtain

$$\begin{aligned} \langle \langle (t_u^2)_x \rangle^2 \rangle &= \int \int \langle t_u^2 \rangle_{0,\omega_1} \langle t_u^2 \rangle_{0,\omega_2} \langle \langle t_h^0 \rangle_{x,\omega_1} \langle t_h^0 \rangle_{x,\omega_2} \rangle d\omega_1 d\omega_2 \\ &\quad + 4 \int \int \langle t_u^2 \rangle_{0,\omega_1} \langle t_u^1 \rangle_{0,\omega_2} \langle \langle t_h^0 \rangle_{x,\omega_1} \langle t_h^1 \rangle_{x,\omega_2} \rangle d\omega_1 d\omega_2 \\ &\quad + 2 \int \int \langle t_u^2 \rangle_{0,\omega_1} \langle t_u^0 \rangle_{0,\omega_2} \langle \langle t_h^0 \rangle_{x,\omega_1} \langle t_h^2 \rangle_{x,\omega_2} \rangle d\omega_1 d\omega_2 \\ &\quad + \int \int \langle t_u^1 \rangle_{0,\omega_1} \langle t_u^1 \rangle_{0,\omega_2} \langle \langle t_h^1 \rangle_{x,\omega_1} \langle t_h^1 \rangle_{x,\omega_2} \rangle d\omega_1 d\omega_2 \\ &\quad + 4 \int \int \langle t_u^1 \rangle_{0,\omega_1} \langle t_u^0 \rangle_{0,\omega_2} \langle \langle t_h^1 \rangle_{x,\omega_1} \langle t_h^2 \rangle_{x,\omega_2} \rangle d\omega_1 d\omega_2 \\ &\quad + \int \int \langle t_u^0 \rangle_{0,\omega_1} \langle t_u^0 \rangle_{0,\omega_2} \langle \langle t_h^2 \rangle_{x,\omega_1} \langle t_h^2 \rangle_{x,\omega_2} \rangle d\omega_1 d\omega_2 \end{aligned} \quad (5.52)$$

The above exact expression may be approximated by plugging in approximations to $\langle \langle t_h^{m_1} \rangle_{x,\omega_1} \langle t_h^{m_2} \rangle_{x,\omega_2} \rangle$ for the various values of m_1 and m_2 . In addition to the expressions in Eqs. (5.41)-(5.44), the necessary expressions are:

$$\langle \langle t_h^0 \rangle_{x,\omega_1} \langle t_h^2 \rangle_{x,\omega_2} \rangle \approx (k'_R(\omega_2))^2 d_2(\omega_1, \omega_2) \left[(\mu - 2\sigma^2 (k_I(\omega_1) + k_I(\omega_2)))^2 + \sigma^2 \right] \quad (5.53)$$

$$\begin{aligned} \langle \langle t_h^1 \rangle_{x,\omega_1} \langle t_h^2 \rangle_{x,\omega_2} \rangle &\approx k'_R(\omega_1) (k'_R(\omega_2))^2 d_2(\omega_1, \omega_2) \\ &\quad \left[(\mu - 2\sigma^2 (k_I(\omega_1) + k_I(\omega_2)))^3 + 3\sigma^2 (\mu - 2\sigma^2 (k_I(\omega_1) + k_I(\omega_2))) \right] \end{aligned} \quad (5.54)$$

$$\begin{aligned} \langle \langle t_h^2 \rangle_{x,\omega_1} \langle t_h^2 \rangle_{x,\omega_2} \rangle &\approx (k'_R(\omega_1))^2 (k'_R(\omega_2))^2 d_2(\omega_1, \omega_2) \\ &\quad [(\mu - 2\sigma^2 (k_I(\omega_1) + k_I(\omega_2)))^4 + 6\sigma^2 (\mu - 2\sigma^2 (k_I(\omega_1) + k_I(\omega_2)))^2 \\ &\quad + 3\sigma^4] \end{aligned} \quad (5.55)$$

$$\begin{aligned}
\langle (\langle t_u^2 \rangle_x)^2 \rangle &= \int \int \langle t_u^2 \rangle_{0,\omega_1} \langle t_u^2 \rangle_{0,\omega_2} d_2(\omega_1, \omega_2) d\omega_1 d\omega_2 \\
&+ 4 \int \int \langle t_u^2 \rangle_{0,\omega_1} \langle t_u^1 \rangle_{0,\omega_2} k'(\omega_2) d_2(\omega_1, \omega_2) (\mu - 2\sigma^2 (k_I(\omega_1) + k_I(\omega_2))) d\omega_1 d\omega_2 \\
&+ 2 \int \int \langle t_u^2 \rangle_{0,\omega_1} \langle t_u^0 \rangle_{0,\omega_2} \langle \langle t_h^0 \rangle_{x,\omega_1} \langle t_h^2 \rangle_{x,\omega_2} \rangle d\omega_1 d\omega_2 \\
&+ \int \int \langle t_u^1 \rangle_{0,\omega_1} \langle t_u^1 \rangle_{0,\omega_2} k'(\omega_1) k'(\omega_2) d_2(\omega_1, \omega_2) \\
&\quad \left[(\mu - 2\sigma^2 (k_I(\omega_1) + k_I(\omega_2)))^2 + \sigma^2 \right] d\omega_1 d\omega_2 \\
&+ 4 \int \int \langle t_u^1 \rangle_{0,\omega_1} \langle t_u^0 \rangle_{0,\omega_2} \langle \langle t_h^1 \rangle_{x,\omega_1} \langle t_h^2 \rangle_{x,\omega_2} \rangle d\omega_1 d\omega_2 \\
&+ \int \int \langle t_u^0 \rangle_{0,\omega_1} \langle t_u^0 \rangle_{0,\omega_2} \langle \langle t_h^2 \rangle_{x,\omega_1} \langle t_h^2 \rangle_{x,\omega_2} \rangle d\omega_1 d\omega_2 \tag{5.56}
\end{aligned}$$

For the general case of an arbitrary complex dispersion relation, however, most of these integrals cannot be evaluated easily.

5.1.4.3 Real Dispersion Relation A channel model with a real dispersion relation is a channel that has dispersion only, no damping. For this special case,

$$k_I(\omega) = 0 \tag{5.57}$$

$$d_1(\omega) = 1 \tag{5.58}$$

$$d_2(\omega_1, \omega_2) = 1 \tag{5.59}$$

and the approximate expressions for the moments of the moment features simplify greatly.

The approximate expected value of the first temporal moment feature becomes

$$\langle \langle t_u \rangle_x \rangle \approx \int \langle t_u \rangle_{0,\omega_1} d\omega_1 + \int k'_R(\omega_1) \mu |F(0, \omega_1)|^2 d\omega_1 \tag{5.60}$$

$$\approx \langle t_u \rangle_0 + \mu \langle k'_R(\omega) \rangle_0 \tag{5.61}$$

The second order expectation of the first temporal moment feature is

$$\begin{aligned}
\langle (\langle t_u \rangle_x)^2 \rangle &\approx \int \int \langle t_u \rangle_{0,\omega_1} \langle t_u \rangle_{0,\omega_2} d\omega_1 d\omega_2 + 2\mu \int \int \langle t_u \rangle_{0,\omega_1} k'_R(\omega_2) |F(0, \omega_2)|^2 d\omega_1 d\omega_2 \\
&+ (\mu^2 + \sigma^2) \int \int k'_R(\omega_1) k'_R(\omega_2) |F(0, \omega_1)|^2 |F(0, \omega_2)|^2 d\omega_1 d\omega_2 \tag{5.62}
\end{aligned}$$

$$\approx (\langle t_u \rangle_0 + \mu \langle k'_R(\omega) \rangle_0)^2 + \sigma^2 (\langle k'_R(\omega) \rangle_0)^2 \tag{5.63}$$

and, therefore, the variance of the first temporal moment feature is

$$\langle (\langle t_u \rangle_x)^2 \rangle - \langle \langle t_u \rangle_x \rangle^2 = \sigma^2 (\langle k'_R(\omega) \rangle_0)^2 \quad (5.64)$$

For the second-order temporal moment feature, we have that the approximate expected value is given by

$$\langle \langle t_u^2 \rangle_x \rangle \approx \int \langle t_u^2 \rangle_{0,\omega_1} d\omega_1 + 2\mu \int \langle t_u \rangle_{0,\omega_1} (k'_R(\omega_1)) d\omega_1 \quad (5.65)$$

$$\begin{aligned} &+ (\mu^2 + \sigma^2) \int (k'_R(\omega_1))^2 |F(0, \omega_1)|^2 d\omega_1 \\ &\approx \langle t_u^2 \rangle_0 + 2\mu \langle tk'_R(\omega) \rangle_0 + (\mu^2 + \sigma^2) \langle (k'_R(\omega))^2 \rangle_0 \end{aligned} \quad (5.66)$$

and the second-order expectation of the second-order temporal moment feature is approximately given by

$$\langle (\langle t_u^2 \rangle_x)^2 \rangle \approx \int \int \langle t_u^2 \rangle_{0,\omega_1} \langle t_u^2 \rangle_{0,\omega_2} d\omega_1 d\omega_2 \quad (5.67)$$

$$\begin{aligned} &+ 4\mu \int \int \langle t_u^2 \rangle_{0,\omega_1} \langle t_u^1 \rangle_{0,\omega_2} k'_R(\omega_2) d\omega_1 d\omega_2 \\ &+ 2(\mu^2 + \sigma^2) \int \int \langle t_u^2 \rangle_{0,\omega_1} \langle t_u^0 \rangle_{0,\omega_2} (k'_R(\omega_2))^2 d\omega_1 d\omega_2 \\ &+ (\mu^2 + \sigma^2) \int \int \langle t_u^1 \rangle_{0,\omega_1} \langle t_u^1 \rangle_{0,\omega_2} k'_R(\omega_1) k'_R(\omega_2) d\omega_1 d\omega_2 \\ &+ 4(\mu^3 + 3\mu\sigma^2) \int \int \langle t_u^1 \rangle_{0,\omega_1} \langle t_u^0 \rangle_{0,\omega_2} k'_R(\omega_1) (k'_R(\omega_2))^2 d\omega_1 d\omega_2 \\ &+ (\mu^4 + 6\mu^2\sigma^2 + 3\sigma^4) \int \int \langle t_u^0 \rangle_{0,\omega_1} \langle t_u^0 \rangle_{0,\omega_2} (k'_R(\omega_1))^2 (k'_R(\omega_2))^2 d\omega_1 d\omega_2 \end{aligned}$$

$$\begin{aligned} \langle (\langle t_u^2 \rangle_x)^2 \rangle &\approx \langle t_u^2 \rangle_0^2 + 4\mu \langle t_u^2 \rangle_0 \langle tk'_R(\omega) \rangle_0 + 2(\mu^2 + \sigma^2) \langle t_u^2 \rangle_0 \langle (k'_R(\omega))^2 \rangle_0 \\ &+ (\mu^2 + \sigma^2) (\langle tk'_R(\omega) \rangle_0)^2 + 4(\mu^3 + 3\mu\sigma^2) \langle tk'_R(\omega) \rangle_0 \langle (k'_R(\omega))^2 \rangle_0 \\ &+ (\mu^4 + 6\mu^2\sigma^2 + 3\sigma^4) \left(\langle (k'_R(\omega))^2 \rangle_0 \right)^2 \end{aligned} \quad (5.68)$$

Therefore, the variance is given by

$$\begin{aligned} \langle (\langle t_u^2 \rangle_x)^2 \rangle - \langle \langle t_u^2 \rangle_x \rangle^2 &\approx \sigma^2 (\langle tk'_R(\omega) \rangle_0)^2 + 8\mu\sigma^2 \langle tk'_R(\omega) \rangle_0 \langle (k'_R(\omega))^2 \rangle_0 \\ &+ 2\sigma^2 (2\mu^2 + \sigma^2) \left(\langle (k'_R(\omega))^2 \rangle_0 \right)^2 \end{aligned} \quad (5.69)$$

5.2 RANDOM CHANNELS

The ocean environment is complex and fluctuating, and the random variations that occur in an ocean channel also induce variability to moment features. A major cause of ocean channel variability is internal waves, which are responsible for changes in the water such as temperature, density, salinity, and velocity of the medium, but other phenomena such as ocean currents and planetary waves also induce variability [18]. Using accepted models of random ocean acoustic propagation [18], we may extend the moments of moments approach described for uncertain channels to randomly varying channels. The expressions for the moments of the moment features are found in terms of the moments of the signal propagating in the corresponding deterministic channel and the two-frequency mutual coherence function. The two-frequency mutual coherence function is a commonly used measure to characterize fluctuating media [2], and its form is known and has been experimentally verified for ocean channels [18].

5.2.1 Randomly Varying Channels

We review the random propagation model given in [18]. The velocity of sound in the channel is given by

$$c = c_0 (1 + U_0(z) + \mu(\mathbf{x}, t)) \quad (5.70)$$

where c_0 is a constant, $U_0(z)$ represents the deterministic vertical dependence of the sound speed, and $\mu(\mathbf{x}, t)$ is the random variation of the sound speed in the medium. We generally define the correlation function of the random fluctuations in terms of the spatial and temporal separation, and also in terms of the average position (to account for anisotropic randomness) as

$$\rho\left(\mathbf{x} - \mathbf{x}', t - t', \frac{1}{2}(\mathbf{x} + \mathbf{x}')\right) = \langle \mu(\mathbf{x}, t) \mu(\mathbf{x}', t') \rangle \quad (5.71)$$

where the angle brackets represent an ensemble average. The nominal wavenumber is given by

$$k_0 = \frac{\omega}{c_0} \quad (5.72)$$

while the spatially dependent wavenumber is given by

$$k(\mathbf{x}) = \frac{\omega}{c_0(1 + U_0(z))} \quad (5.73)$$

The nature of the random variations in an ocean channel are described by two parameters that characterize the strength and the size of the variations. For simplicity, we will assume that the random variations of the channel are isotropic. The strength of the random fluctuations (denoted Σ) is characterized by the expected value of the squared integral of the variations:

$$\Sigma^2 = \left\langle \left(k_0 \int_0^R \mu dx \right)^2 \right\rangle \quad (5.74)$$

$$= k_0^2 \int_0^R \int_0^R \rho(|x - x'|) dx dx' \quad (5.75)$$

where R is the distance from the source to the receiver, the spatial dimensionality of the correlation function has been reduced because of the isotropic assumption, and, because the acoustic wave speed is significantly greater than the internal wave speed, we eliminate the temporal dependence of the correlation function [18].

The parameter describing the size of the fluctuations is defined as the average of the squared radius of the first Fresnel zone over the line connecting the source and receiver. The first Fresnel zone is the area within which refracted rays will constructively interfere with one another at the receiver. Assuming that the sound speed in the channel does not have a depth dependence, the radius can be found using the Pythagorean theorem. The radius of the Fresnel zone at x , denoted $R_F(x)$, is given by

$$R_F^2(x) = \frac{\lambda x(R - x)}{R} \quad (5.76)$$

The size parameter, Λ , is

$$\Lambda = \frac{1}{2\pi RL^2} \int_0^R (R_F(x))^2 dx \quad (5.77)$$

$$= \frac{R}{6k_0L^2} \quad (5.78)$$

where L is the correlation length of the fluctuations, as illustrated in Fig. 10 [18].

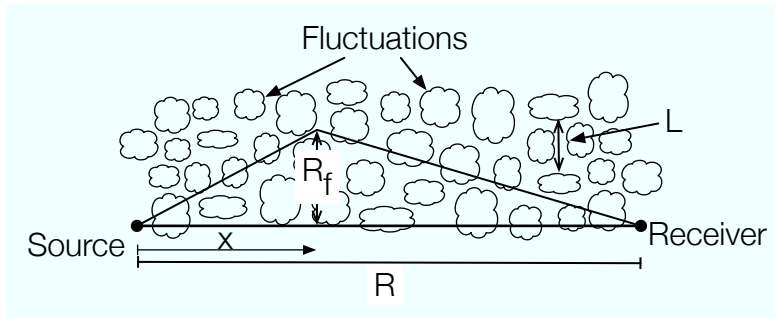


Figure 10: **Schematic of a fluctuating channel.**

We may now characterize a given fluctuating channel in terms of the size and strength parameters. The parameter space is divided into two regimes: *saturated* and *unsaturated*. In the saturated regime, the fluctuations will refract the energy significantly enough that multipath effects will appear. Multipath effects occur when several delayed and scaled copies of a signal arrive at the receiver. Because multiple delayed copies of the signal arrive at the receiver, the total energy undergoes a temporal spreading. In the unsaturated regime, the multipath effects may be present, but they are not significant. A special sub-region of the unsaturated regime is the geometrical optics regime, in which a single ray travels from source to receiver, but its path is perturbed by the fluctuations. The scattering regimes in the parameter space are shown in Fig. 11.

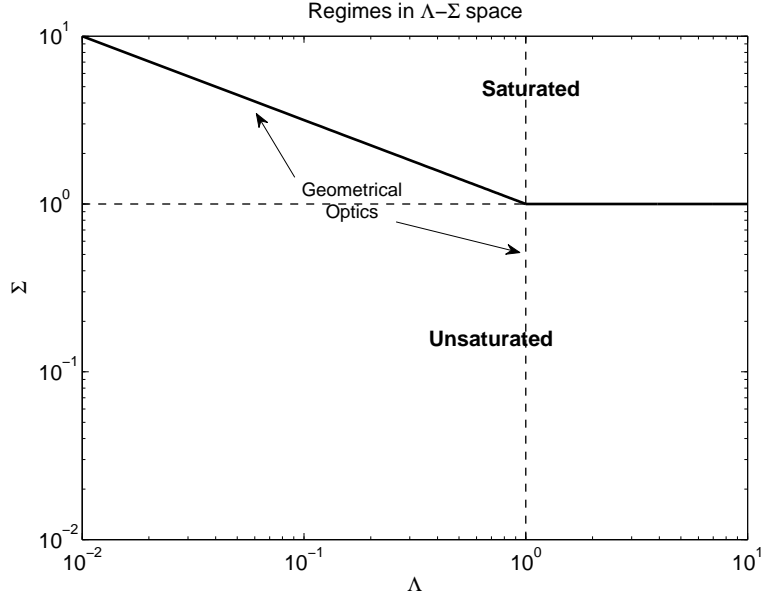


Figure 11: **Scattering regimes in Λ - Σ space.**

5.2.2 Pulse Propagation

For a deterministic channel, the signal at x is given by

$$u(x, t) = \int F(0, \omega) H(x, \omega) e^{-j\omega t} d\omega \quad (5.79)$$

where $H(x, \omega)$ is the deterministic transfer function. Analogously, a channel with randomly varying sound speed is modeled as

$$\hat{u}(x, t) = \int F(0, \omega) \hat{H}(x, \omega) e^{-j\omega t} d\omega \quad (5.80)$$

where \hat{H} is the random transfer function. We define the reduced wavefunction as the random transfer function normalized by the deterministic channel transfer function [18]

$$\hat{\psi}(x, \omega) = \frac{\hat{H}(x, \omega)}{H(x, \omega)} \quad (5.81)$$

and, substituting, we obtain an expression for the signal in a randomly varying channel in terms of the original spectrum, deterministic transfer function, and the reduced wavefunction:

$$\hat{u}(x, t) = \int F(0, \omega) H(x, \omega) \hat{\psi}(x, \omega) e^{-j\omega t} d\omega \quad (5.82)$$

This formulation of the signal at x will allow us to use the results of the previous section when deriving the moments of the moment features.

5.2.2.1 Wigner Distribution for Randomly Varying Channels The Wigner distribution of the signal at x is defined as

$$W_{\hat{u}}(t, \omega; x) = \frac{1}{2\pi} \int \hat{u}\left(x, t + \frac{\tau}{2}\right) \hat{u}^*\left(x, t - \frac{\tau}{2}\right) e^{j\omega\tau} d\tau \quad (5.83)$$

Substituting the expression from Eq. (5.82), we obtain the following relation:

$$W_{\hat{u}}(t, \omega; x) = W_u(t, \omega; 0) *_t W_H(t, \omega; x) *_t W_{\hat{\psi}}(t, \omega; x) \quad (5.84)$$

where $W_H(t, \omega; x)$ is the Wigner distribution of the deterministic transfer function of the channel, $W_{\hat{\psi}}(t, \omega; x)$ is the Wigner distribution of the reduced wavefunction, and $*_t$ represents convolution in the time domain. Because the initial wave is deterministic, the model becomes, in the ensemble sense,

$$\langle W_{\hat{u}}(t, \omega; x) \rangle = W_u(t, \omega; 0) *_t W_H(t, \omega; x) *_t \langle W_{\hat{\psi}}(t, \omega; x) \rangle \quad (5.85)$$

We may also write this model as

$$\langle W_{\hat{u}}(t, \omega; x) \rangle = W_u(t, \omega; x) *_t \langle W_{\hat{\psi}}(t, \omega; x) \rangle \quad (5.86)$$

where

$$W_u(t, \omega; x) = W_u(t, \omega; 0) *_t W_H(t, \omega; x) \quad (5.87)$$

is the Wigner distribution of the signal propagating in the deterministic channel. Writing the model as Eq. (5.86) will allow us to take advantage of the results of the previous chapters when deriving the moments of the moment features in the randomly varying channel model.

5.2.3 Moments of Moments

The moments of the temporal moment features of the Wigner distribution of the signal are given generally by

$$\langle\langle (t_{\hat{u}}^n/x)^i \rangle\rangle = \int \int \int \int \dots \int \int (t_1 t_2 \dots t_i)^n \langle W_{\hat{u}}(t_1, \omega_1; x) W_{\hat{u}}(t_2, \omega_2; x) \dots W_{\hat{u}}(t_i, \omega_i; x) \rangle dt_1 d\omega_1 dt_2 d\omega_2 \dots dt_i d\omega_i \quad (5.88)$$

which can be written equivalently in terms of the moments of the deterministic signal and moments of the reduced wavefunction as (see Eq. 5.89)

$$\langle\langle (t_{\hat{u}}^n/x)^i \rangle\rangle = \sum_{m_1, m_2, \dots, m_i=0}^n \binom{n}{m_1} \binom{n}{m_2} \dots \binom{n}{m_i} \int \int \dots \int \langle\langle t_u^{n-m_1} \rangle\rangle_{x, \omega_1} \langle\langle t_u^{n-m_2} \rangle\rangle_{x, \omega_2} \dots \langle\langle t_u^{n-m_i} \rangle\rangle_{x, \omega_i} \langle\langle t_{\hat{\psi}}^{m_1} \rangle\rangle_{x, \omega_1} \langle\langle t_{\hat{\psi}}^{m_2} \rangle\rangle_{x, \omega_2} \dots \langle\langle t_{\hat{\psi}}^{m_i} \rangle\rangle_{x, \omega_i} d\omega_1 d\omega_2 \dots d\omega_i \quad (5.89)$$

where $\langle\langle t_{\hat{\psi}}^n \rangle\rangle_{x, \omega}$ is the expected value of the n^{th} temporal moment of the reduced wavefunction, given by

$$\langle\langle t_{\hat{\psi}}^n \rangle\rangle_{x, \omega} = \int t^n \langle W_{\hat{\psi}}(t, \omega; x) \rangle dt \quad (5.90)$$

$$= \frac{1}{2\pi} \int \int t^n \langle \psi^* \left(x, \omega + \frac{\theta}{2} \right) \psi \left(x, \omega - \frac{\theta}{2} \right) \rangle e^{jt\theta} dt d\theta \quad (5.91)$$

If we introduce a variable substitution,

$$\omega_a = \omega - \frac{\theta}{2} \quad (5.92)$$

$$\omega_b = \omega + \frac{\theta}{2} \quad (5.93)$$

we find that the n^{th} moment is given by

$$\langle\langle t_{\hat{\psi}}^n \rangle\rangle_{x, \omega_b} = \frac{1}{2\pi} \int \int t^n \langle \hat{\psi}^*(x, \omega_a) \hat{\psi}(x, \omega_b) \rangle e^{jt(\omega_b - \omega_a)} dt d\omega_a \quad (5.94)$$

$$= j^n \int \delta^{(n)}(\omega_b - \omega_a) \langle \hat{\psi}^*(x, \omega_a) \hat{\psi}(x, \omega_b) \rangle d\omega_a \quad (5.95)$$

$$= j^n \left[\frac{\partial^n}{\partial \omega_a^n} \Gamma_2(x; \omega_a, \omega_b) \right]_{\omega_a = \omega_b} \quad (5.96)$$

where Γ_2 is the two-frequency mutual coherence function (MCF), defined as:

$$\Gamma_2(x; \omega_{a1}, \omega_{b1}) = \langle \hat{\psi}^*(x, \omega_{a1}) \hat{\psi}(x, \omega_{b1}) \rangle \quad (5.97)$$

The two-frequency MCF is widely used to characterize a fluctuating environment because it quantifies the coherence bandwidth and coherence time [2]. The definition of the two-frequency MCF generalizes to higher order as

$$\begin{aligned} \Gamma_{2i}(x; \omega_{a_1}, \omega_{b_1}, \omega_{a_2}, \omega_{b_2}, \dots, \omega_{a_i}, \omega_{b_i}) &= \langle \hat{\psi}^*(x, \omega_{a_1}) \hat{\psi}(x, \omega_{b_1}) \hat{\psi}^*(x, \omega_{a_2}) \hat{\psi}(x, \omega_{b_2}) \\ &\dots \hat{\psi}^*(x, \omega_{a_i}) \hat{\psi}(x, \omega_{b_i}) \rangle \end{aligned} \quad (5.98)$$

The $2i^{\text{th}}$ -frequency MCF will be used in the formulation of the moments of the moment features. For higher order expectations, Eq. (5.96) generalizes to

$$\begin{aligned} \langle \langle t_{\hat{\psi}}^{n_1} \rangle_x \langle t_{\hat{\psi}}^{n_2} \rangle_x \dots \langle t_{\hat{\psi}}^{n_i} \rangle_x \rangle &= j^{n_1+n_2+\dots+n_i} \\ &\left[\frac{\partial^{n_1}}{\partial \omega_{a_1}^{n_1}} \frac{\partial^{n_2}}{\partial \omega_{a_2}^{n_2}} \dots \frac{\partial^{n_i}}{\partial \omega_{a_i}^{n_i}} \Gamma_{2i}(x; \omega_{a_1}, \omega_{b_1}, \omega_{a_2}, \omega_{b_2}, \dots, \omega_{a_i}, \omega_{b_i}) \right] \end{aligned} \quad (5.99)$$

evaluated at $\omega_{a_1} = \omega_{b_1}, \omega_{a_2} = \omega_{b_2}, \dots, \omega_{a_i} = \omega_{b_i}$.

The form of the two-frequency MCF for the various scattering regimes is given in the literature (see, for example, Flatté [18]). However, because we need higher-order MCFs in the calculation of the moments of moments, we must use the approximation method given by Dashen to estimate the higher-order MCFs from the two-frequency MCF [19].

Assuming Gaussian statistics, we may approximate the $2i^{\text{th}}$ -frequency MCF as [19]

$$\Gamma_{2i}(x; \omega_{a_1}, \omega_{b_1}, \omega_{a_2}, \omega_{b_2}, \dots, \omega_{a_i}, \omega_{b_i}) \approx \sum_{\text{perms}} \prod_{m,n=1}^i \langle \hat{\psi}^*(x, \omega_{a_m}) \hat{\psi}(x, \omega_{b_n}) \rangle \quad (5.100)$$

where *perms* means that we sum over the permutations of the m s and n s. For example, for $i = 2$, we have

$$\begin{aligned} \Gamma_4(x; \omega_{a_1}, \omega_{b_1}, \omega_{a_2}, \omega_{b_2}) &\approx \langle \hat{\psi}^*(x, \omega_{a_1}) \hat{\psi}(x, \omega_{b_1}) \rangle \langle \hat{\psi}^*(x, \omega_{a_2}) \hat{\psi}(x, \omega_{b_2}) \rangle \\ &+ \langle \hat{\psi}^*(x, \omega_{a_1}) \hat{\psi}(x, \omega_{b_2}) \rangle \langle \hat{\psi}^*(x, \omega_{a_2}) \hat{\psi}(x, \omega_{b_1}) \rangle \end{aligned} \quad (5.101)$$

We use this approximation in the formulation of the moments of moments.

5.2.4 Example

In this section we compute expressions for the first two temporal moments of a signal propagating in a fluctuating channel. To maximize generality, we make no assumptions about the nature of the signal, the channel, or the fluctuations except to restrict the randomness to the geometrical optics regime. In this regime, the two-frequency MCF is given by [18]

$$\Gamma_2(x; \omega_1, \omega_2) = e^{-2\left(\frac{\omega_2 - \omega_1}{\omega_1 + \omega_2}\right)^2 \Sigma^2} \quad (5.102)$$

where Σ is the strength parameter given above. The expected value of first order temporal moment is given by

$$\begin{aligned} \langle \langle t_{\hat{u}} \rangle_x \rangle &= \int \langle t_u \rangle_{x, \omega_1} \langle \langle t_{\hat{\psi}}^0 \rangle_{x, \omega_1} \rangle d\omega_1 + \int \langle t_u \rangle_{x, \omega_1} \langle \langle t_{\hat{\psi}}^1 \rangle_{x, \omega_1} \rangle d\omega_1 \\ &= \langle t_u \rangle_x + \int \langle \langle t_{\hat{\psi}}^1 \rangle_{x, \omega_1} \rangle |F(x, \omega_1)|^2 d\omega_1 \end{aligned} \quad (5.103)$$

We must compute the expected value of the first temporal moment of the reduced wavefunction:

$$\langle \langle t_{\hat{\psi}}^1 \rangle_{x, \omega_1} \rangle = j \left[\frac{\partial}{\partial \omega_a} \langle \hat{\psi}^*(x, \omega_a) \hat{\psi}(x, \omega_b) \rangle \right]_{\omega_a = \omega_b} \quad (5.104)$$

$$= 0 \quad (5.105)$$

Therefore, we have that the first temporal moment of the wave in the random channel is equal to the first temporal moment of the wave propagating in the associated deterministic channel,

$$\langle \langle t_{\hat{u}} \rangle_x \rangle = \langle t_u \rangle_x \quad (5.106)$$

The second order expectation of the first order temporal moment is given by

$$\langle \langle \langle t_{\hat{u}} \rangle_x \rangle^2 \rangle = \sum_{m_1, m_2=0}^n \binom{1}{m_1} \binom{1}{m_2} \int \int \quad (5.107)$$

$$\begin{aligned} & \langle \langle t_u^{n-m_1} \rangle_{x, \omega_1} \langle t_u^{n-m_2} \rangle_{x, \omega_2} \rangle \langle \langle t_{\hat{\psi}}^{m_1} \rangle_{x, \omega_1} \langle t_{\hat{\psi}}^{m_2} \rangle_{x, \omega_2} \rangle d\omega_1 d\omega_2 \\ &= \int \int \langle \langle t_u^1 \rangle_{x, \omega_1} \langle t_u^1 \rangle_{x, \omega_2} \rangle \langle \langle t_{\hat{\psi}}^0 \rangle_{x, \omega_1} \langle t_{\hat{\psi}}^0 \rangle_{x, \omega_2} \rangle d\omega_1 d\omega_2 \\ &+ 2 \int \int \langle \langle t_u^1 \rangle_{x, \omega_1} \langle t_u^0 \rangle_{x, \omega_2} \rangle \langle \langle t_{\hat{\psi}}^0 \rangle_{x, \omega_1} \langle t_{\hat{\psi}}^1 \rangle_{x, \omega_2} \rangle d\omega_1 d\omega_2 \\ &+ \int \int \langle \langle t_u^0 \rangle_{x, \omega_1} \langle t_u^0 \rangle_{x, \omega_2} \rangle \langle \langle t_{\hat{\psi}}^1 \rangle_{x, \omega_1} \langle t_{\hat{\psi}}^1 \rangle_{x, \omega_2} \rangle d\omega_1 d\omega_2 \end{aligned} \quad (5.108)$$

which we write as

$$\langle (\langle t_{\hat{u}} \rangle_x)^2 \rangle = I_1(x) + 2I_2(x) + I_3(x) \quad (5.109)$$

where

$$I_1(x) = \int \int (\langle t_u^1 \rangle_{x,\omega_1} \langle t_u^1 \rangle_{x,\omega_2}) \langle \langle t_{\hat{\psi}}^0 \rangle_{x,\omega_1} \langle t_{\hat{\psi}}^0 \rangle_{x,\omega_2} \rangle d\omega_1 d\omega_2 \quad (5.110)$$

$$I_2(x) = \int \int (\langle t_u^1 \rangle_{x,\omega_1} \langle t_u^0 \rangle_{x,\omega_2}) \langle \langle t_{\hat{\psi}}^0 \rangle_{x,\omega_1} \langle t_{\hat{\psi}}^1 \rangle_{x,\omega_2} \rangle d\omega_1 d\omega_2 \quad (5.111)$$

$$I_3(x) = \int \int (\langle t_u^0 \rangle_{x,\omega_1} \langle t_u^0 \rangle_{x,\omega_2}) \langle \langle t_{\hat{\psi}}^1 \rangle_{x,\omega_1} \langle t_{\hat{\psi}}^1 \rangle_{x,\omega_2} \rangle d\omega_1 d\omega_2 \quad (5.112)$$

The expected value of the product of two zeroth order temporal moments of the reduced wavefunction is given by

$$\langle \langle t_{\hat{\psi}}^0 \rangle_{x,\omega_1} \langle t_{\hat{\psi}}^0 \rangle_{x,\omega_2} \rangle = \Gamma_4(x; \omega_1, \omega_1, \omega_2, \omega_2) \quad (5.113)$$

$$= 1 + \langle \hat{\psi}^*(x, \omega_1) \hat{\psi}(x, \omega_2) \rangle \langle \hat{\psi}^*(x, \omega_2) \hat{\psi}(x, \omega_1) \rangle \quad (5.114)$$

$$= 1 + e^{-4\left(\frac{\omega_2 - \omega_1}{\omega_1 + \omega_2}\right)^2 \Sigma^2} \quad (5.115)$$

and $I_1(x)$ then becomes

$$I_1(x) = \int \int (\langle t_u^1 \rangle_{x,\omega_1} \langle t_u^1 \rangle_{x,\omega_2}) \left[1 + e^{-4\left(\frac{\omega_2 - \omega_1}{\omega_1 + \omega_2}\right)^2 \Sigma^2} \right] d\omega_1 d\omega_2 \quad (5.116)$$

To find $I_2(x)$ we must evaluate

$$\langle \langle t_{\hat{\psi}}^1 \rangle_{x,\omega_1} \langle t_{\hat{\psi}}^0 \rangle_{x,\omega_2} \rangle = j \left[\frac{\partial}{\partial \omega_{a_1}} \Gamma_4(x; \omega_{a_1}, \omega_1, \omega_{a_2}, \omega_2) \right]_{\omega_{a_1} = \omega_1, \omega_{a_2} = \omega_2} \quad (5.117)$$

$$= j \left(\frac{\omega_2 (\omega_2 - \omega_1)}{\left(\frac{\omega_1 + \omega_2}{2}\right)^3} \right) \Sigma^2 e^{-4\left(\frac{\omega_2 - \omega_1}{\omega_1 + \omega_2}\right)^2 \Sigma^2} \quad (5.118)$$

and $I_2(x)$ is then

$$I_2(x) = \int \int (\langle t_u^1 \rangle_{x,\omega_1} \langle t_u^0 \rangle_{x,\omega_2}) \left[j \left(\frac{\omega_2 (\omega_2 - \omega_1)}{\left(\frac{\omega_1 + \omega_2}{2}\right)^3} \right) \Sigma^2 e^{-4\left(\frac{\omega_2 - \omega_1}{\omega_1 + \omega_2}\right)^2 \Sigma^2} \right] d\omega_1 d\omega_2 \quad (5.119)$$

Finally, for $I_3(x)$, we must find

$$\langle\langle t_{\hat{\psi}}^1 \rangle_{x,\omega_1} \langle t_{\hat{\psi}}^1 \rangle_{x,\omega_2} \rangle = j^2 \left[\frac{\partial}{\partial \omega_{a_1}} \frac{\partial}{\partial \omega_{a_2}} \Gamma_4(x; \omega_{a_1}, \omega_{b_1}, \omega_{a_2}, \omega_{b_2}) \right]_{\omega_{a_1}=\omega_{b_1}, \omega_{a_2}=\omega_{b_2}} \quad (5.120)$$

$$= \Sigma^4 \omega_1 \omega_2 \left(\frac{\omega_2 - \omega_1}{\left(\frac{\omega_1 + \omega_2}{2}\right)^3} \right)^2 e^{-4 \left(\frac{\omega_1 - \omega_2}{\omega_2 + \omega_1}\right)^2 \Sigma^2} \quad (5.121)$$

and $I_3(x)$ is then given by

$$I_3(x) = \int \int \langle\langle t_u^0 \rangle_{x,\omega_1} \langle t_u^0 \rangle_{x,\omega_2} \rangle \left[\Sigma^4 \omega_1 \omega_2 \left(\frac{\omega_2 - \omega_1}{\left(\frac{\omega_1 + \omega_2}{2}\right)^3} \right)^2 e^{-4 \left(\frac{\omega_1 - \omega_2}{\omega_2 + \omega_1}\right)^2 \Sigma^2} \right] d\omega_1 d\omega_2 \quad (5.122)$$

The variance is given by

$$\text{Var} \{ \langle t_{\hat{u}} \rangle_x \} = \langle\langle (t_{\hat{u}})_x \rangle^2 \rangle - (\langle\langle t_{\hat{u}} \rangle_x \rangle)^2 \quad (5.123)$$

While we cannot analytically evaluate these integrals without more information or assumptions, these results provide a recipe for a future numerical implementation of this framework. In general, as the variations of the medium increase in strength, the variability of the features will also increase. The Wigner distribution of the reduced wavefunction is related to the two-frequency MCF through a Fourier transform (Eqs. 5.90 and 5.91). As the strength parameter in Eq. (5.102) increases, the shape of the two-frequency MCF becomes more peaked. Because of the Fourier relation, the Wigner distribution of the reduced wavefunction will then become more broad, increasing the variability of the features.

6.0 FEATURE DISTRIBUTIONS

The process of automatically classifying a sonar echo can be organized into two steps: first, features that numerically describe characteristics of the received waveform are extracted from the wave; second, the features are fed to a classifier, which is typically a machine learning algorithm such as a Bayesian classifier, a neural network or a support vector machine [29]. The purpose of the classifier is to assign the observation to a class based upon knowledge learned from training data.

To improve classification performance under this paradigm, either the features or classifier must be improved. Our focus is on improving the features sent to the classifier, and in this chapter we explore how we may use the moments of moment features developed in the earlier chapters to improve classification performance. The method will use the estimates of the feature variability to design more effective and efficient feature sets. First, however, we review Bayesian classification in order to frame the discussion on classification performance.

6.1 BAYESIAN CLASSIFICATION

The process of training a classifier is the process of developing class specific probability distributions in the feature space. Traditionally, for the supervised learning case, this is done by feeding labelled training data examples to a classifier. The classifier uses this data to estimate the pdfs of the feature values for each class. A decision rule, such as maximum likelihood, is then applied over the pdfs in the feature space to determine decision thresholds. Future observations are then classified by their location in the feature space relative to the thresholds.

In order to simplify the discussion of Bayesian classification, we limit the discussion to the binary decision regime, with the two classes labeled as *target* and *clutter*. The concepts, however, generalize to any number of classes.

Because this is a two-class problem, we have two hypotheses: H_t is the target hypothesis, and H_c is the clutter hypothesis. The features are represented by the variable y . The likelihood that a feature value belongs to the target class is given by the conditional probability $p\{y|H_t\}$, and the likelihood that a feature value belongs to the clutter class is given by $p\{y|H_c\}$.

The likelihood is related to the *a posteriori* or posterior probability, given by $p\{H_t|y\}$, through Bayes' theorem, which is given by [53]

$$p\{H_t|y\} = \frac{p\{y|H_t\} p\{H_t\}}{p\{y\}} \quad (6.1)$$

where $p\{H_t\}$ is the *a priori* or prior probability of the target hypothesis, and $p\{y\}$ is the unconditional probability of the feature value.

The classifier in Bayesian classification can be represented by a likelihood ratio test (LRT):

$$\Lambda(y) \underset{H_c}{\overset{H_t}{>}} \eta \quad (6.2)$$

where $\Lambda(y)$ is the likelihood ratio and η is the threshold. The inequality notation indicates that if the likelihood ratio is greater than η the classifier assigns the target hypothesis to the observation, and if the likelihood ratio is less than η the classifier assigns the clutter hypothesis to the observation.

The maximum likelihood LRT is given by

$$\frac{p\{y|H_t\}}{p\{y|H_c\}} > 1 \quad (6.3)$$

Intuitively, this classifier chooses the hypothesis with the greater *a priori* likelihood.

The LRT for the *maximum a posteriori* (MAP) classifier is given by

$$\frac{p\{H_t|y\}}{p\{H_c|y\}} > 1 \quad (6.4)$$

This classifier chooses the more likely hypothesis given the feature value. Using Bayes' theorem, we have

$$\frac{p\{y|H_t\}}{p\{y|H_c\}} > \frac{p\{H_c\}}{p\{H_t\}} \quad (6.5)$$

If the hypotheses have equal priors, $p\{H_c\} = p\{H_t\}$, the MAP classifier is equivalent to the maximum likelihood classifier.

Given an observation and a decision by the classifier, there are four possible outcomes:

- **Hit** - The correct classification of a target; the probability of a hit is given by

$$P_H = \int_{\eta}^{\infty} p\{y|H_t\} dy \quad (6.6)$$

- **Miss** - The incorrect classification of a target as clutter; the probability of a miss is given by

$$P_M = \int_{-\infty}^{\eta} p\{y|H_t\} dy = 1 - P_H \quad (6.7)$$

- **False alarm** - The incorrect classification of clutter as a target; the probability of false alarm is given by

$$P_{FA} = \int_{\eta}^{\infty} p\{y|H_c\} dy \quad (6.8)$$

- **Correct rejection** - The correct classification of clutter as clutter; the probability of correct rejection is given by

$$P_{CR} = \int_{-\infty}^{\eta} p\{y|H_c\} dy = 1 - P_{FA} \quad (6.9)$$

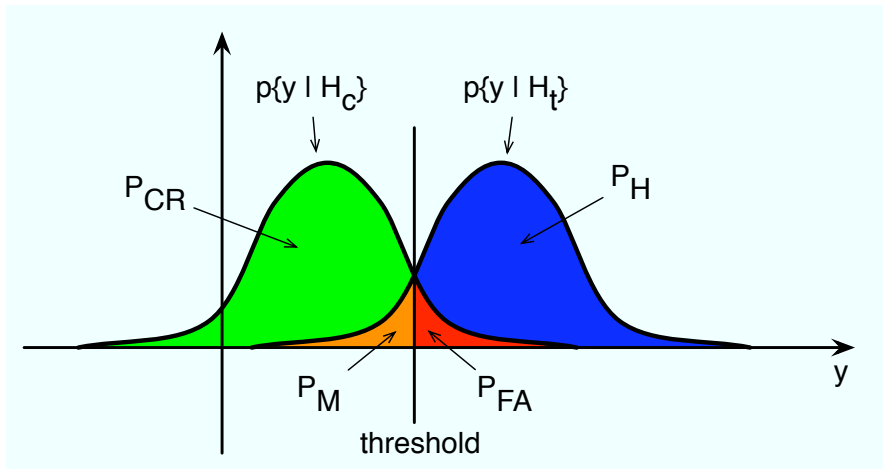


Figure 12: Feature distributions and possible outcomes of a likelihood ratio test.

The probability of each of these scenarios is illustrated in Fig. 12 for target and clutter distributions and a maximum likelihood threshold. Broadly speaking, to improve classification, we must reduce the overlap of the distributions. This can be done by reducing the width of each distribution or by moving them farther apart. In the remainder of this chapter, we discuss how we can estimate the probability distributions of moment features and then evaluate them for their class discriminability.

6.2 FEATURE DISTRIBUTIONS

The pdf of the feature conditioned on the target hypothesis is the likelihood of a feature value given that the signal originated in the target class. We may use the moments of moment features to estimate this likelihood. We write the likelihood as

$$p\{y|H_t\} = \frac{1}{2\pi} \int M_{H_t}(\theta) e^{-j\theta y} d\theta \quad (6.10)$$

where $M_{H_t}(\theta)$ is the characteristic function of the feature under the target hypothesis. The characteristic function and pdf are Fourier transform pairs, so we may write

$$M_{H_t}(\theta) = \int p\{y|H_t\} e^{j\theta y} dy \quad (6.11)$$

By expanding the exponential into a Taylor series, we have

$$M_{H_t}(\theta) = \int \sum_{m=1}^{\infty} \frac{(j\theta y)^m}{m!} p\{y|H_t\} dy \quad (6.12)$$

Switching the order of summation and integration and evaluating the integral, we find that the characteristic function may be constructed from the moments of the moment features [14]

$$M_{H_t}(\theta) = \sum_{m=0}^{\infty} \frac{j^m \theta^m}{m!} \langle y^m \rangle \quad (6.13)$$

The pdf may then be recovered via a Fourier transform as shown in Eq. (6.10). This procedure may also be used to estimate joint densities. The joint characteristic function is given by [14]

$$M_{H_t}(\theta_1, \theta_2) = \sum_{m_1, m_2=0}^{\infty} \frac{(j\theta_1)^{m_1} (j\theta_2)^{m_2}}{m_1! m_2!} \langle y_1^{m_1} y_2^{m_2} \rangle \quad (6.14)$$

and the joint pdf is then given by the two-dimensional Fourier transform:

$$p\{y_1, y_2|H_t\} = \left(\frac{1}{2\pi}\right)^2 \int \int M_{H_t}(\theta_1, \theta_2) e^{-j\theta_1 y_1 - j\theta_2 y_2} d\theta_1 d\theta_2 \quad (6.15)$$

The estimates of the pdfs obtained via this method, however, are just one of a potentially infinite set of pdfs that could satisfy the moments. Because we have arrived at this solution without specifying any requirements, there is no reason to believe that these are the ideal estimates.

A better estimate of the pdf would be obtained by following a procedure that specifically does not make any assumptions beyond the values of the moments; or, to put it another way, the most general pdf that still satisfies the moments. This estimate of the pdf is called the *maximum entropy* estimate [47, 31], and it has been well studied in this application, that is, in reconstructing the most general pdf from a finite set of moments. We review the main results [21, 41, 49].

The entropy of a pdf is given by

$$H(p|H_t) = - \int_a^b p\{y|H_t\} \ln p\{y|H_t\} dy \quad (6.16)$$

and it is typically understood to be a measure of randomness. The maximum entropy pdf is found via the method of Lagrange multipliers to be of the form

$$p\{y|H_t\} = \exp \left[- \sum_{r=0}^m \lambda_r y^r \right] \quad (6.17)$$

where λ_r are the multipliers whose exact values are chosen to satisfy the moment equation:

$$\int_a^b y^n \exp \left[- \sum_{r=0}^m \lambda_r y^r \right] dy = \langle y^n \rangle \quad (6.18)$$

As an example, for the case of $m = 2$, when we wish to estimate a pdf from only the first two moments, the maximum entropy pdf is the normal or Gaussian distribution.

In the example given in Section 5.1.4, we found expressions for the first two moments of the first temporal moment feature of an arbitrary initial signal propagating in a channel where propagation distance x was random and characterized by a normal distribution with mean μ and variance σ^2 . For the case of a real dispersion relation, we found the mean and variance of the first temporal moment to be approximately given by

$$\langle \langle t_u \rangle_x \rangle \approx \langle t_u \rangle_0 + \mu \langle k'_R(\omega) \rangle_0 \quad (6.19)$$

$$Var\{\langle t_u \rangle_x\} \approx \sigma^2 (\langle k'_R(\omega) \rangle_0)^2 \quad (6.20)$$

Therefore, the maximum entropy pdf of the first temporal moment feature is approximately given by the normal distribution with mean $\langle t_u \rangle_0 + \mu \langle k'_R(\omega) \rangle_0$ and variance $\sigma^2 (\langle k'_R(\omega) \rangle_0)^2$.

6.3 FEATURE SET DESIGN

Now that we have shown how the moments of the moment features are used to estimate the pdfs of the features, we explore how estimates of the pdfs of classification features can be used to design feature sets that will facilitate better classification performance. The individual features to be included in a feature set must be evaluated on the basis of two qualities: accuracy and redundancy. In general, there are three approaches to feature evaluation: distance measures, dependence measures, and information measures [3]. In this section we show how we can use these three measures to evaluate the accuracy and redundancy of features.

Feature selection is a topic that has received much interest in the machine learning community. This has been primarily motivated by the “curse of dimensionality,” which, with regard to classification, prescribes that the amount of training data required to properly characterize a feature space grows exponentially with the number of features used [17, 27]. In many realistic classification problems, training data is often limited; accordingly, the number of features used should be as small as possible, which motivates the designer of a sonar classification system to select the most effective features possible.

An effective feature set, therefore, consists of a small number of features that facilitate the separation of classes in the feature space while simultaneously not providing information that is redundant with respect to the other features in the set. Moreover, it is desirable that the within-class variability of a feature be small. This means, ideally, that identical objects have identical numerical values for a specific feature and other factors introduce minimal variability. In reality, objects within a class are rarely “identical.” Additionally, random variations arise due to factors such as noise and propagation effects that could be significant. It is nevertheless desirable, if possible, to mitigate the feature variability introduced by these latter factors. To address that goal, it is useful to quantitatively analyze the variability arising from such sources.

6.3.1 Accuracy

The accuracy of a feature is a measure of how well the feature discriminates between the target and clutter classes. A first-order estimate of the discriminability of a feature can be computed by calculating the Euclidean distance between the pdfs under the target and clutter hypotheses. This method requires only the first moment of the moment feature for each class, but it also ignores the variance and higher-order moments and, therefore, is not a very good measure of accuracy.

Accuracy may also be estimated via a dependence measure such as correlation. The correlation of a feature computed from a propagated echo with the expected free field feature value is given by

$$\rho_{y_1, y_{1ff}|H_t} = \frac{\langle y_1 y_{1ff} \rangle_{H_t} - \langle y_1 \rangle_{H_t} \langle y_{1ff} \rangle_{H_t}}{\sigma_{y_1|H_t} \sigma_{y_{1ff}|H_t}} \quad (6.21)$$

where y_{1ff} is the free field feature value, $\langle \cdot \rangle$ is the expected value, and σ is the standard deviation.

An additional quantity that may be used to evaluate accuracy is based upon the receiver operating characteristic (ROC) curve. A ROC curve is a plot of the probability of a hit (P_H) versus the probability of false alarm (P_{FA})—two classification metrics obtained from Eqs. (6.6) and (6.8), respectively. The classification performance as quantified by the ROC curve can be summarized by a single number by computing the area under the ROC curve (AUR). An AUR score of unity represents perfect classification while a score of 0.5 represents chance.

6.3.2 Redundancy

The amount of training data necessary to properly train a classifier grows exponentially with the dimensionality of the feature set, and typically for the sonar classification problem training data is not available in abundance. Therefore, it is important to construct feature sets with minimal redundancy. The within-class correlation of two features provides one measure of redundancy. The correlation coefficient is given by

$$\rho_{y_1, y_2} = \frac{\langle y_1 y_2 \rangle - \langle y_1 \rangle \langle y_2 \rangle}{\sigma_{y_1} \sigma_{y_2}} \quad (6.22)$$

where σ_{y_n} is the standard deviation of the feature y_n . Correlation coefficient values near unity indicate that the features are highly redundant. Similarly, values near negative one indicate anti-correlation, but this also indicates significant redundancy. Low redundancy is indicated by correlation coefficients near zero.

Mutual information can also be used to quantify the redundancy of two features. The mutual information between features y_1 and y_2 is given by

$$I(y_1, y_2|H_t) = \int \int p(y_1, y_2|H_t) \ln \left(\frac{p(y_1, y_2|H_t)}{p(y_1|H_t)p(y_2|H_t)} \right) dy_1 dy_2 \quad (6.23)$$

If two features have no mutual information, that is, $I(y_1, y_2|H_t) = 0$, then there is no redundancy and y_1 and y_2 are completely independent.

With these metrics established, the ideal feature set will be constructed by minimizing the amount of redundancy and maximizing the accuracy. This approach is called “minimum-redundancy-maximum-relevance” (mRMR) in the literature [36].

7.0 ACOUSTIC PROPAGATION IN A WEDGE-SHAPED OCEAN

The exact nature of propagation effects such as dispersion and damping is due to the specific geometry of the channel and the nature of the boundaries. Because of the complexity of the ocean environment, however, it is often not possible to implement exact models of a given shallow water channel. Highly accurate and useful approximations may be obtained by using simplified models. For many problems of interest, the range-independent parallel-plate waveguide is a sufficient approximation to a shallow-water ocean channel. A more accurate model is given by the range-independent Pekeris waveguide, which models acoustic interaction with bottom sediment in addition to propagation in the water column. Both of these models assume that the bottom is horizontal. In coastal regions, however, the ocean often has a sloping bottom, and thus a better approximation may be obtained by using a wedge shape as a model.

The solution of the wave equation in wedge-shaped environments has received considerable attention from researchers. Pierce studied the effect of dispersion on guided waves in waveguides with boundaries that vary slowly with the horizontal coordinate using the method of normal modes and an assumption of no coupling between modes [46]. Biot and Tolstoy gave the solution for the field in a rigid wedge due to a point source using the method of normal modes [4], and Chu then extended the method of Biot and Tolstoy to include the penetrable wedge [12, 13].

Buckingham used integral transform methods to solve for the sound field in both the perfectly reflecting wedge [6] and the penetrable-bottom wedge [7]. Harrison then generalized the method of Buckingham to include more complicated geometries [28].

Stakgold used the method of Riemann surfaces to obtain the solution of the Helmholtz equation within a wedge-shaped region with perfectly reflecting boundaries. The solution he

obtained is similar to the normal mode solution [48]. Kuznetsov recognized that the wave equation for the perfectly reflecting wedge is separable in cylindrical coordinates and used separation of variables to obtain a normal mode solution [33].

Our goal in this work is to obtain a solution of the acoustic field in a wedge and also an approximation to that solution that emphasizes propagation effects such as dispersion and damping in the time-frequency plane. To accomplish this, we initially follow an approach similar to that of Kuznetsov [33]. We analyze a simplified model of a sloping-bottom ocean channel, namely, a two-dimensional wedge with perfectly reflecting boundaries in polar coordinates. Via the method of separation of variables, we obtain an expression for the dispersion relation that couples radial frequency (ω) and spatial frequency (k) and highlight the similarities between the form of the dispersion relation for the wedge and the form of the dispersion relation for the two-plate waveguide. We compute the field in the wedge due to a point source at a given location and use this solution to obtain a per mode Wigner approximation of the acoustic field in the wedge. Finally, we give the results of simulations comparing the Wigner distribution of the exact solution to the result given by the Wigner approximation.

7.1 DISPERSION RELATION

Because our goal is to derive the Wigner approximation for the sloping-bottom waveguide, which will be defined in terms of the initial wave and the dispersion relation, we first derive the dispersion relation for the channel. The geometry and parameters relevant to the problem are given in Fig. 13. The angle of the wedge is denoted θ_0 . The source is located at (r', θ') and the receiver is located at (r, θ) . The ocean surface and bottom are assumed to be perfectly reflecting, that is, the solution of the wave equation goes to zero at the boundaries.

To find the dispersion relation, we begin with the unforced wave equation, given by [50]

$$\nabla^2 p(r, \theta, t) = \frac{1}{c^2} \frac{\partial^2 p(r, \theta, t)}{\partial t^2} \quad (7.1)$$

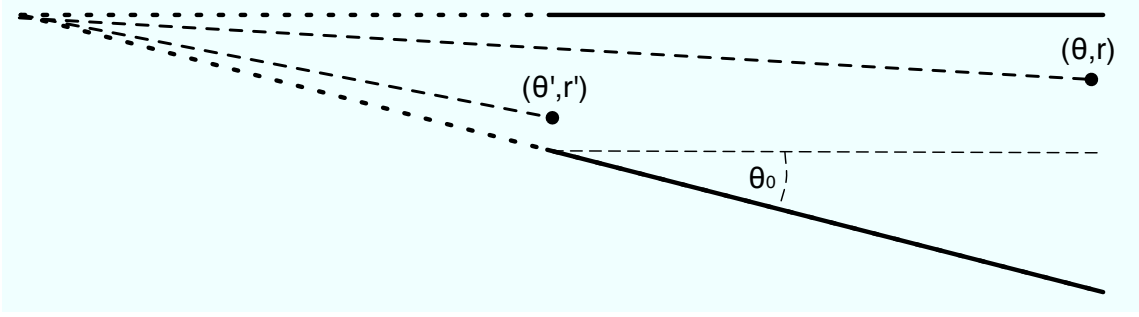


Figure 13: **Schematic of the perfect wedge.**

In polar coordinates, the Laplacian is defined as

$$\nabla^2 = \frac{1}{r} \frac{\partial}{\partial r} \left(r \frac{\partial}{\partial r} \right) + \frac{1}{r^2} \frac{\partial^2}{\partial \theta^2} \quad (7.2)$$

$$= \frac{\partial^2}{\partial r^2} + \frac{1}{r} \frac{\partial}{\partial r} + \frac{1}{r^2} \frac{\partial^2}{\partial \theta^2} \quad (7.3)$$

Eq. (7.1) then becomes

$$\frac{\partial^2 p}{\partial r^2} + \frac{1}{r} \frac{\partial p}{\partial r} + \frac{1}{r^2} \frac{\partial^2 p}{\partial \theta^2} = \frac{1}{c^2} \frac{\partial^2 p}{\partial t^2} \quad (7.4)$$

To obtain the Helmholtz equation, we plug in a solution with explicit time dependence, $p(r, \theta, t) = U(r, \theta)e^{j\omega t}$, giving

$$\frac{\partial^2 U}{\partial r^2} + \frac{1}{r} \frac{\partial U}{\partial r} + \frac{1}{r^2} \frac{\partial^2 U}{\partial \theta^2} + \frac{\omega^2}{c^2} U = 0 \quad (7.5)$$

This equation is separable, and thus we seek a solution of the form $U(\theta, r) = \Psi(\theta)\Phi(r)$.

Substituting this form of the solution into Eq. (7.5), we get

$$\frac{1}{\Phi(r)} \left[\frac{\partial^2 \Phi(r)}{\partial r^2} + \frac{1}{r} \frac{\partial \Phi(r)}{\partial r} \right] + \frac{1}{\Psi(\theta)} \left[\frac{1}{r^2} \frac{\partial^2 \Psi(\theta)}{\partial \theta^2} + \frac{\omega^2}{c^2} \Psi(\theta) \right] = 0 \quad (7.6)$$

Eq. (7.6) has two sets of differential terms dependent upon different variables; therefore, to satisfy the equation, the terms must be equal to the positive and negative values of a constant, which we call k_r^2 [32]. We then have the following two equations:

$$\frac{1}{\Phi(r)} \left[\frac{\partial^2 \Phi(r)}{\partial r^2} + \frac{1}{r} \frac{\partial \Phi(r)}{\partial r} \right] = -k_r^2 \quad (7.7)$$

$$\frac{1}{\Psi(\theta)} \left[\frac{1}{r^2} \frac{\partial^2 \Psi(\theta)}{\partial \theta^2} + \frac{\omega^2}{c^2} \Psi(\theta) \right] = k_r^2 \quad (7.8)$$

The two equations may be simplified algebraically to

$$\frac{\partial^2 \Phi(r)}{\partial r^2} + \frac{1}{r} \frac{\partial \Phi(r)}{\partial r} + k_r^2 \Phi(r) = 0 \quad (7.9)$$

$$\frac{\partial^2 \Psi(\theta)}{\partial \theta^2} + r^2 \left[-k_r^2 + \frac{\omega^2}{c^2} \right] \Psi(\theta) = 0 \quad (7.10)$$

Eq. (7.10) is equivalent to

$$\Psi''(\theta) + \mathcal{C}^2 \Psi(\theta) = 0 \quad (7.11)$$

where

$$\mathcal{C}^2 = r^2 \left[-k_r^2 + \frac{\omega^2}{c^2} \right] \quad (7.12)$$

The solution to Eq. (7.11) is a sinusoidal function. The vanishing boundary condition at $\theta = 0$ forces the solution to be of the form

$$\Psi(\theta) = A \sin(\mathcal{C}\theta) \quad (7.13)$$

and the vanishing boundary condition at $\theta = \theta_0$ requires that \mathcal{C} be given by

$$\mathcal{C} = \frac{m\pi}{\theta_0} \quad (7.14)$$

where m is an integer. The set of solutions given in Eq. (7.13) are called modes, and they have the property that they are orthonormal, that is

$$\int_0^{\theta_0} \Psi_m(\theta) \Psi_n(\theta) d\theta = \begin{cases} 1, & \text{if } m = n \\ 0, & \text{if } m \neq n \end{cases} \quad (7.15)$$

The dispersion relation is found by substituting the value for \mathcal{C} given in Eq. (7.14) into Eq. (7.12) and solving for k_r ,

$$k_r(\omega) = \frac{1}{c} \sqrt{\omega^2 - \left(\frac{m\pi c}{\theta_0 r} \right)^2} \quad (7.16)$$

The dispersion relation shows how wavenumber (k) and radial frequency (ω) are coupled. This coupling, as we will illustrate later, gives insight into how the time-frequency distribution of a wave evolves as it propagates.

7.1.1 Comparison to Parallel-Plate Waveguide

The dispersion relation for an ideal, isovelocity, parallel-plate waveguide with perfectly reflecting boundaries is given by [50]

$$k_r(\omega) = \frac{1}{c} \sqrt{\omega^2 - \left(\frac{m\pi c}{D}\right)^2} \quad (7.17)$$

where D is the depth of the waveguide (separation of the plates). Fig. 14 gives a visual comparison of the parameters for depth and range in the parallel-plate and sloping-bottom waveguides. The parameters x and D correspond to range and depth in the parallel-plate waveguide, respectively; while in the sloping-bottom waveguide the r parameter corresponds to range and the $\theta_0 r$ parameter corresponds to the arc length separating the two plates at range r .

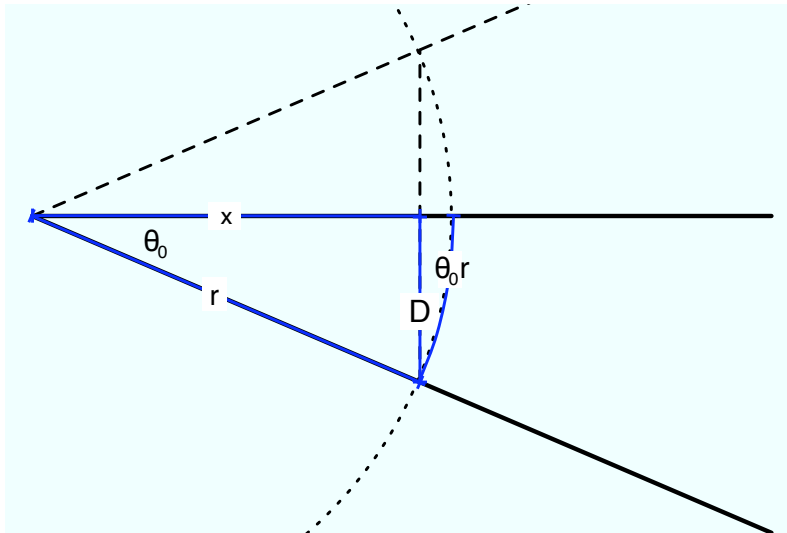


Figure 14: A comparison of the parameters for depth and range in the parallel-plate (D and x) and sloping-bottom ($\theta_0 r$ and r) waveguides.

Using basic trigonometry, we can relate the parameters of the parallel-plate waveguide to the parameters of the sloping-bottom waveguide as follows:

$$D = r \sin \theta_0 \quad (7.18)$$

$$x = r \cos \theta_0 \quad (7.19)$$

For small angles ($\theta_0 \ll 5^\circ$), we may use the approximation

$$\sin \theta_0 \rightarrow \theta_0 \quad (7.20)$$

$$\cos \theta_0 \rightarrow 1 \quad (7.21)$$

Therefore, for small angles,

$$D \rightarrow \theta_0 r \quad (7.22)$$

$$x \rightarrow r \quad (7.23)$$

Thus, as the angle of the slope of the bottom becomes smaller, we find that the form of the dispersion relation for the sloping-bottom waveguide given in Eq. (7.16) approaches the form of the dispersion relation for the parallel-plate waveguide. At exactly $\theta = 0$ the wedge would be closed, but we may obtain a channel of arbitrary depth as θ_0 becomes small (but greater than zero) by increasing the range from the apex.

7.2 ACOUSTIC FIELD DUE TO A POINT SOURCE

To find the acoustic field due to a point source in the waveguide, we derive the Helmholtz equation (Eq. 7.5) with an impulse located at (r', θ') , which is a point within the waveguide, i.e., $0 < r' < r$ and $0 < \theta' < \theta_0$. The inhomogeneous Helmholtz equation is

$$\frac{\partial^2 U}{\partial r^2} + \frac{1}{r} \frac{\partial U}{\partial r} + \frac{1}{r^2} \frac{\partial^2 U}{\partial \theta^2} + \frac{\omega^2}{c^2} U = -\frac{\delta(r - r')\delta(\theta - \theta')}{2\pi r} \quad (7.24)$$

We seek a solution in the form of an expansion in terms of the modes given by Eq. (7.13), or

$$U(\theta, r) = \sum_{m=1}^{\infty} \Psi_m(\theta)\Phi_m(r) \quad (7.25)$$

Plugging in this form of the solution, Eq. (7.24) then becomes

$$\sum_{m=1}^{\infty} \left[\frac{\partial^2 \Phi_m(r)}{\partial r^2} + \frac{1}{r} \frac{\partial \Phi_m(r)}{\partial r} \right] \Psi_m(\theta) + \left[\frac{1}{r^2} \frac{\partial^2 \Psi_m(\theta)}{\partial \theta^2} + \frac{\omega^2}{c^2} \Psi_m(\theta) \right] \Phi_m(r) = -\frac{\delta(r - r')\delta(\theta - \theta')}{2\pi r} \quad (7.26)$$

This equation may be simplified by using Eq. (7.8) to obtain

$$\sum_{m=1}^{\infty} \left[\frac{\partial^2 \Phi_m(r)}{\partial r^2} + \frac{1}{r} \frac{\partial \Phi_m(r)}{\partial r} + k_{rm}^2 \Phi_m(r) \right] \Psi_m(\theta) = -\frac{\delta(r-r')\delta(\theta-\theta')}{2\pi r} \quad (7.27)$$

We apply the operator $\int_0^{\theta_0} (\cdot) \Psi_n(\theta) d\theta$ to both sides of Eq. (7.27) and, because of the orthonormality of the modes (see Eq. 7.15), we now have [32]

$$\frac{\partial^2 \Phi_n(r)}{\partial r^2} + \frac{1}{r} \frac{\partial \Phi_n(r)}{\partial r} + k_{rn}^2 \Phi_n(r) = -\frac{\delta(r-r')\Psi_n(\theta')}{2\pi r} \quad (7.28)$$

The solution to this equation is given by the Hankel function [32],

$$\Phi_n(r) = \frac{j}{4} \Psi_n(\theta') H_0^{(1)}(k_{rn}(\omega) (r-r')) \quad (7.29)$$

where $k_{rn}(\omega)$ is given by Eq. (7.16). The total solution for the field is given by the sum of modes,

$$U(\theta, r) = \frac{j}{4} \sum_{m=1}^{\infty} \Psi_m(\theta) \Psi_m(\theta') H_0^{(1)}(k_{rm}(\omega) (r-r')) \quad (7.30)$$

The solution of the field due to a point source given in Eq. (7.30) is for a single frequency ω . The solution for a broadband pulse is found using Fourier synthesis. The spectrum of the field at r due to a broadband source located at r' is given by

$$F_n(r, \omega) = F(r', \omega) H_0^{(1)}(k_{rn}(\omega) (r-r')) \quad (7.31)$$

where $F(r', \omega)$ is the spectrum of the initial pulse at r' . Using the asymptotic form of the Hankel function we may write the spectrum as

$$F_n(r, \omega) \simeq e^{-j\frac{\pi}{4}} \sqrt{\frac{2}{\pi k_{rn}(\omega) (r-r')}} F(r', \omega) e^{jk_{rn}(\omega)(r-r')} \quad (7.32)$$

To obtain the pulse in the time domain, we inverse Fourier transform the spectrum at r , i.e.,

$$u_n(r, t) = \frac{1}{2\pi} \int F_n(r, \omega) e^{-j\omega t} d\omega \quad (7.33)$$

where $F_n(r, \omega)$ is given exactly by Eq. (7.31) or approximately in the asymptotic regime ($k_{rn}(\omega) (r-r') \gg 1$) by Eq. (7.32).

7.3 WIGNER DISTRIBUTION AND APPROXIMATION

The Wigner time-frequency distribution for the n^{th} mode is given by [14]

$$W_{un}(r, t, \omega) = \frac{1}{2\pi} \int F_n^* \left(r, \omega + \frac{\lambda}{2} \right) F_n \left(r, \omega - \frac{\lambda}{2} \right) e^{jt\lambda} d\lambda \quad (7.34)$$

By the properties of the Fourier transform, we have

$$F_n^* \left(r, \omega + \frac{\lambda}{2} \right) F_n \left(r, \omega - \frac{\lambda}{2} \right) = \frac{1}{2\pi} \int W_{un}(r, t, \omega) e^{-jt\lambda} dt \quad (7.35)$$

Using the asymptotic form of the spectrum at r given in Eq. (7.32), the Wigner distribution of the pulse due to a point source may be written as

$$W_{un}(r, t, \omega) = \frac{1}{\pi^2(r-r')} \int F^* \left(r', \omega + \frac{\lambda}{2} \right) F \left(r', \omega - \frac{\lambda}{2} \right) \frac{1}{\sqrt{k_{rn}^*(\omega + \frac{\lambda}{2})k_{rn}(\omega - \frac{\lambda}{2})}} e^{j(k_{rn}(\omega - \frac{\lambda}{2}) - k_{rn}^*(\omega + \frac{\lambda}{2}))(r-r')} e^{jt\lambda} d\lambda \quad (7.36)$$

Using the relation given in Eq. (7.35), we obtain

$$W_{un}(r, t, \omega) = \frac{1}{\pi^2(r-r')} \int \int W(r', t', \omega) \frac{1}{\sqrt{k_{rn}^*(\omega + \frac{\lambda}{2})k_{rn}(\omega - \frac{\lambda}{2})}} e^{j(k_{rn}(\omega - \frac{\lambda}{2}) - k_{rn}^*(\omega + \frac{\lambda}{2}))(r-r')} e^{j\lambda(t-t')} d\lambda dt' \quad (7.37)$$

where $W(r', t', \omega)$ is the Wigner distribution of the broadband source signal. We now write the dispersion relation in terms of its real and imaginary parts,

$$k_{rn}(\omega) = k_{Rrn}(\omega) + jk_{Irn}(\omega) \quad (7.38)$$

and Eq. (7.37) becomes

$$W_{un}(r, t, \omega) = \frac{1}{\pi^2(r-r')} \int \int W(r', t', \omega) \frac{1}{\sqrt{(k_{Rrn}(\omega + \frac{\lambda}{2}) - jk_{Irn}(\omega + \frac{\lambda}{2})) (k_{Rrn}(\omega - \frac{\lambda}{2}) + jk_{Irn}(\omega - \frac{\lambda}{2}))}} e^{-(k_{Irn}(\omega - \frac{\lambda}{2}) + k_{Irn}(\omega + \frac{\lambda}{2}))(r-r')} e^{j(k_{Rrn}(\omega - \frac{\lambda}{2}) - k_{Rrn}(\omega + \frac{\lambda}{2}))(r-r')} e^{j\lambda(t-t')} d\lambda dt' \quad (7.39)$$

Expanding the real and imaginary parts of the dispersion relation in the exponents into Taylor series gives [39]

$$k_{Irn} \left(\omega - \frac{\lambda}{2} \right) + k_{Irn} \left(\omega + \frac{\lambda}{2} \right) = \sum_{n=0}^{\infty} \frac{k_{Irn}^{(2n)}(\omega)}{(2n)!} \frac{\lambda^{2n}}{2^{2n-1}} \approx 2k_{Irn}(\omega) + \frac{1}{4}k_{Irn}''(\omega)\lambda^2 \dots \quad (7.40)$$

$$k_{Rrn} \left(\omega - \frac{\lambda}{2} \right) - k_{Rrn} \left(\omega + \frac{\lambda}{2} \right) = \sum_{n=0}^{\infty} \frac{k_{Rrn}^{(2n+1)}(\omega)}{(2n+1)!} \frac{\lambda^{2n+1}}{2^{2n}} \approx k'_{Rrn}(\omega)\lambda + \frac{1}{24}k_{Rrn}'''(\omega)\lambda^3 \dots \quad (7.41)$$

We may write the terms under the radical in Eq. (7.39) as

$$\begin{aligned} & \left(k_{Rrn} \left(\omega + \frac{\lambda}{2} \right) - jk_{Irn} \left(\omega + \frac{\lambda}{2} \right) \right) \left(k_{Rrn} \left(\omega - \frac{\lambda}{2} \right) + jk_{Irn} \left(\omega - \frac{\lambda}{2} \right) \right) = \\ & k_{Rrn} \left(\omega + \frac{\lambda}{2} \right) k_{Rrn} \left(\omega - \frac{\lambda}{2} \right) + jk_{Rrn} \left(\omega + \frac{\lambda}{2} \right) k_{Irn} \left(\omega - \frac{\lambda}{2} \right) \\ & - jk_{Rrn} \left(\omega - \frac{\lambda}{2} \right) k_{Irn} \left(\omega + \frac{\lambda}{2} \right) + k_{Irn} \left(\omega + \frac{\lambda}{2} \right) k_{Irn} \left(\omega - \frac{\lambda}{2} \right) \end{aligned} \quad (7.42)$$

Expanding each of these terms into Taylor series, we have

$$k_{Rrn} \left(\omega + \frac{\lambda}{2} \right) k_{Rrn} \left(\omega - \frac{\lambda}{2} \right) \approx (k_{Rrn}(\omega))^2 + \left(k'_{Rrn}(\omega) \frac{\lambda}{2} \right)^2 + \dots \quad (7.43)$$

$$\begin{aligned} jk_{Rrn} \left(\omega + \frac{\lambda}{2} \right) k_{Irn} \left(\omega - \frac{\lambda}{2} \right) & \approx jk_{Rrn}(\omega) k_{Irn}(\omega) - jk_{Rrn}(\omega) k'_{Irn}(\omega) \frac{\lambda}{2} \\ & + jk'_{Rrn}(\omega) \frac{\lambda}{2} k_{Irn}(\omega) - jk'_{Rrn}(\omega) k'_{Irn}(\omega) \left(\frac{\lambda}{2} \right)^2 + \dots \end{aligned} \quad (7.44)$$

$$\begin{aligned} jk_{Rrn} \left(\omega - \frac{\lambda}{2} \right) k_{Irn} \left(\omega + \frac{\lambda}{2} \right) & \approx jk_{Rrn}(\omega) k_{Irn}(\omega) + jk_{Rrn}(\omega) k'_{Irn}(\omega) \frac{\lambda}{2} \\ & - jk'_{Rrn}(\omega) \frac{\lambda}{2} k_{Irn}(\omega) - jk'_{Rrn}(\omega) k'_{Irn}(\omega) \left(\frac{\lambda}{2} \right)^2 + \dots \end{aligned} \quad (7.45)$$

$$k_{Irn} \left(\omega + \frac{\lambda}{2} \right) k_{Irn} \left(\omega - \frac{\lambda}{2} \right) \approx (k_{Irn}(\omega))^2 + \left(k'_{Irn}(\omega) \frac{\lambda}{2} \right)^2 + \dots \quad (7.46)$$

By keeping only the first order terms in each expansion, Eq. (7.42) is approximately equal to

$$\begin{aligned} & \left(k_{Rrn} \left(\omega + \frac{\lambda}{2} \right) - jk_{Irn} \left(\omega + \frac{\lambda}{2} \right) \right) \left(k_{Rrn} \left(\omega - \frac{\lambda}{2} \right) + jk_{Irn} \left(\omega - \frac{\lambda}{2} \right) \right) \\ & \approx (k_{Rrn}(\omega))^2 + (k_{Irn}(\omega))^2 \end{aligned} \quad (7.47)$$

Plugging the approximations into Eq. (7.39) gives

$$W_{un}(r, t, \omega) \approx \frac{e^{-2k_{Irn}(\omega)(r-r')}}{\pi^2(r-r')\sqrt{(k_{Rrn}(\omega))^2 + (k_{Irn}(\omega))^2}} \int \int W(r', t', \omega) e^{j\lambda(t-t' - k'_{Rrn}(\omega)(r-r'))} d\lambda dt' \quad (7.48)$$

We now evaluate the integrals to obtain the approximate expression:

$$W_{un}(r, t, \omega) \approx \frac{2e^{-2k_{Irn}(\omega)(r-r')}}{\pi(r-r')|k_{rn}(\omega)|} W(r', t - k'_{Rrn}(\omega)(r-r'), \omega) \quad (7.49)$$

This approximation provides a concise description of how the wave evolves in the time-frequency plane as it propagates. The energy of the wave undergoes a frequency-dependent time shift described by the first derivative of the real part of the dispersion relation. There is also frequency-dependent attenuation as described by the leading term, which is highly dependent upon the imaginary part of the dispersion relation.

7.4 NUMERICAL SIMULATIONS

To evaluate the accuracy of the approximation, we numerically compute the Wigner distribution of the exact result given in Eq. (7.31) and the Wigner approximation given in Eq. (7.49). We give two examples with different wedge geometries and source and receiver locations. For both examples, the sound channel is isovelocity at $1500 \frac{m}{s}$, the sampling frequency is 2000 Hz, and we simulate only the first propagating mode. The plots given are normalized to allow for easy comparison.

In the first simulation, the wedge angle is $\theta_0 = 0.5^\circ$, the source is located at $(r', \theta') = (3 \text{ km}, 0.25^\circ)$, and the receiver is located at $(r, \theta) = (7 \text{ km}, 0.3^\circ)$. Fig. 15 illustrates the geometry of the problem in Cartesian coordinates. Note that, in the Cartesian coordinate system, the source is at a depth of approximately 12 meters, and the channel at the source range is approximately 25 meters deep. The receiver is approximately 35 meters deep, while the channel at the receiver range is approximately 60 meters deep.

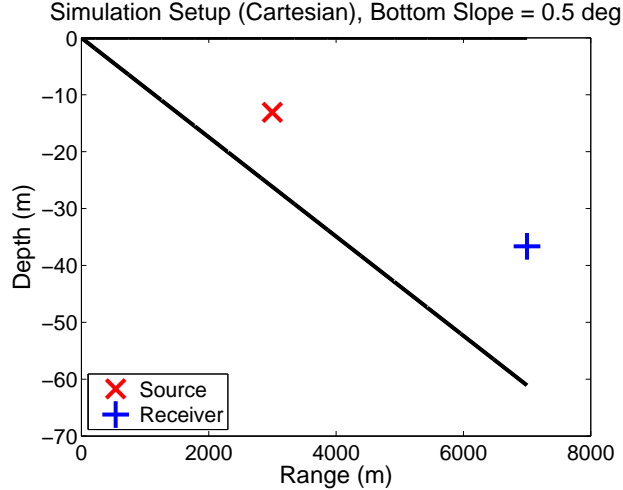


Figure 15: **Schematic diagram of the first example showing source (red x) and receiver (blue +) positions.**

Fig. 16 shows the results of the first numerical simulation. The Wigner distribution of the exact solution is shown in the top panel while the Wigner approximation is shown in the bottom panel. The approximation accurately captures the curvature induced by dispersion.

In the second simulation, the wedge angle is $\theta_0 = 0.1^\circ$, the source is located at $(r', \theta') = (10 \text{ km}, 0.05^\circ)$, and the receiver is located at $(r, \theta) = (15 \text{ km}, 0.05^\circ)$. Fig. 17 illustrates the geometry of the second simulation in Cartesian coordinates. Fig. 18 shows the results of the second numerical simulation. As in the previous example, the approximation accurately captures the frequency-dependent spreading of dispersion.

It is clear in both examples that the curvature caused by dispersion is similar in both the approximation and the exact solution. However, it is also clear that there are differences between the plots, most notably that broadband energy in the lower frequency range is present in the exact solution but not in the approximation. This energy is probably due to artifacts that arise in the numerical computation of the Wigner distribution. To demonstrate this fact, in Fig. 19 we compare the Wigner distribution of the exact solution to the spectrogram of the exact solution. In the spectrogram, the excess broadband energy is not present.

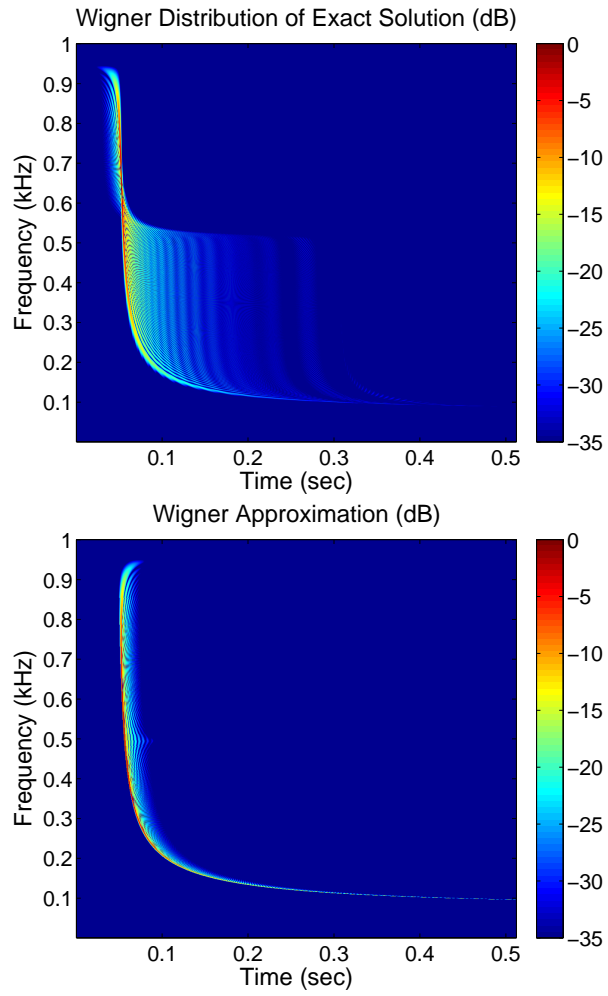


Figure 16: Normalized Wigner distribution of the exact solution (top panel) and normalized Wigner approximation (bottom panel) for the first example.

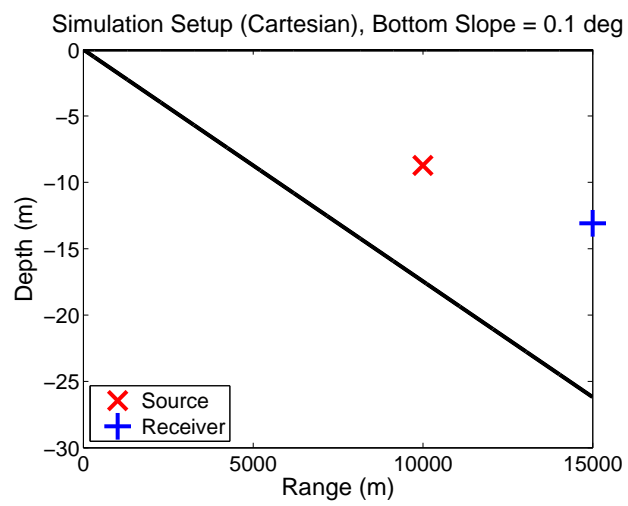


Figure 17: Schematic diagram of the second example showing source (red x) and receiver (blue +) positions.

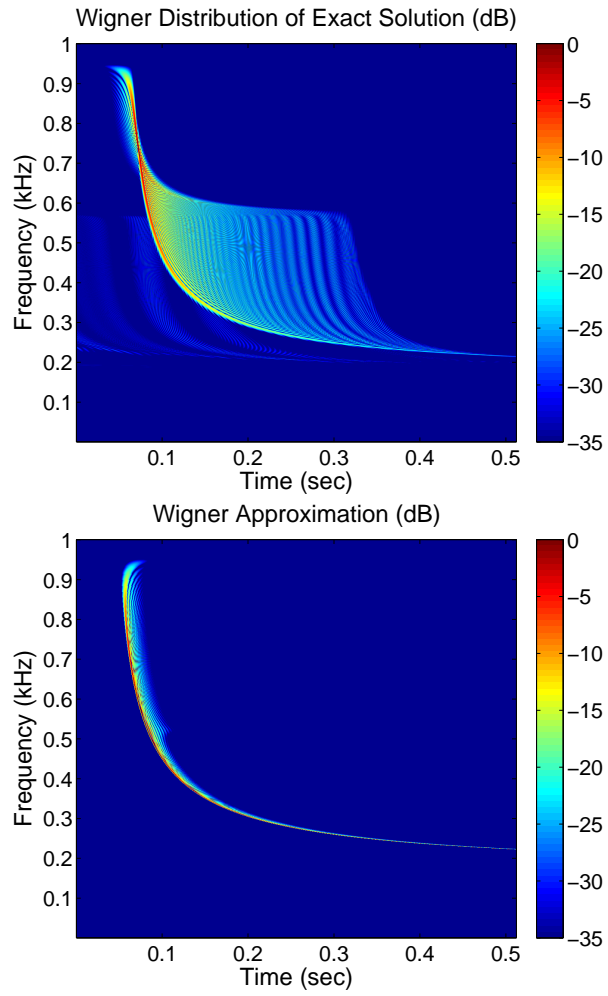


Figure 18: Normalized Wigner distribution of the exact solution (top panel) and normalized Wigner approximation (bottom panel) for the second example.

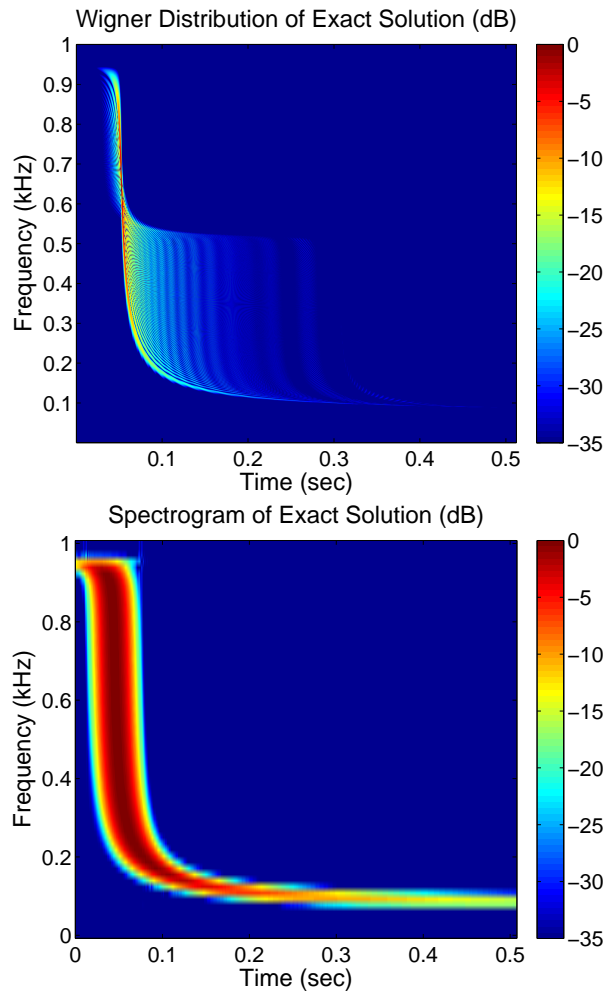


Figure 19: Normalized Wigner distribution of the exact solution (top panel) and normalized spectrogram of the exact solution (bottom panel) for the first example.

8.0 CONCLUSION

In this work we have presented a framework for estimating the variability of moment features calculated from signals propagating in shallow water channels using a phase space approximation method. In the process of developing this result, we have given the expression for the full-field Wigner approximation. The accuracy of the Wigner approximation was validated using the statistical moments, and we have shown that the Wigner approximation is more accurate than the stationary phase approximation for small propagation ranges. As the propagation range increases, the Wigner approximation approaches the stationary phase approximation.

Based upon the insights gained from the Wigner approximation, we have developed propagation-invariant moment-like classification features and have shown their usefulness through simulation. In classification problems where these features are not effective at separating the classes, however, other features may have to be used. In that case, it is important to be able to choose the best set of features, and to that end we developed a process for estimating the moments of the moment features. We then showed how the moments of moments could be used to estimate the pdfs of the features, and we gave two metrics with which a feature set should be evaluated in order to develop effective and environmentally robust feature sets.

Finally, we have extended the phase space approximation to the range-dependent propagation case. Using the technique of separation of variables, we have derived the exact modal solution of the acoustic field within a wedge-shaped region, and we used that exact solution to derive the Wigner approximation for the wedge.

8.1 FUTURE WORK

Many of the main results in this work, such as the moments of the Wigner approximation, the propagation-invariant moments, and the moments of the moment features, have been formulated for the range-independent propagation case. In the last chapter, we derived the solution and Wigner approximation for a range-dependent waveguide. An area for future work, then, is to develop those results for the wedge.

While the statistical moments are used as features to classify sonar signals in real world applications, it is only a small subset of the possible features that could be used. The general expression for moments of the Wigner distribution is given by

$$\langle g(t, \omega) \rangle = \int \int g(t, \omega) W(t, \omega) d\omega dt \quad (8.1)$$

In this work, we have studied the features where $g(t, \omega) = t^n$ or $g(t, \omega) = \omega^n$. However, any function of t and ω could be used for g . To make the framework presented here more useful, it would have to be extended to include more generalized features.

The propagation model used in this work is a one-way model. The initial signal in the model used in this work is considered to be the target response. This is a simplification, however. In active sonar, a pulse propagates from a source through the channel, interacts with the target, and then propagates through the channel again to a receiver. Therefore, a more accurate characterization of the pdfs of the features would be achieved by using a two-way propagation model that included the interaction with the target.

The expressions for the moments of the moment features are given in terms of the (deterministic) moments of the initial wave and the moments of the channel. Therefore, we may increase the separation between target and clutter distributions and simultaneously reduce within-class feature variability by designing outgoing signals to produce specific values for the moments of the initial wave. To illustrate this point, we return to the uncertain channel example given in Chapter 5. In the first example (Section 5.1.3), the variance of the arrival time of the signal was shown to be

$$\langle (\langle t_u \rangle_x)^2 \rangle - (\langle \langle t_u \rangle_x \rangle)^2 = \frac{X^2}{12} \left(\int \kappa'_R(\omega) |F(0, \omega)|^2 d\omega \right)^2 \quad (8.2)$$

The variance depends upon three terms: X , which quantifies the uncertainty of the distance of the receiver from the target; $\kappa'_R(\omega)$, which is determined by the channel; and $|F(0, \omega)|^2$, which is the initial target response. In active sonar, the target response is partially determined by the outgoing signal that interacts with the target. Therefore, in order to reduce the variance of the feature, the only parameter in Eq. (8.2) over which the system designer has any control is $|F(0, \omega)|^2$. To improve classification performance, the initial signal should be designed to increase the distance between the means of the target and clutter classes, while simultaneously reducing within-class variance.

APPENDIX

DERIVATIONS

A.1 TEMPORAL

The expected values of the temporal moment features are given by Eq. (5.2),

$$\langle\langle t_u^n \rangle_x\rangle = \int \int t^n \langle W_u(t, \omega; x) \rangle d\omega dt \quad (.1)$$

By substituting in Eq. (5.1) and using the standard definition of convolution, we obtain

$$\langle\langle t_u^n \rangle_x\rangle = \int \int \int t^n W_u(t - \tau, \omega; 0) \langle W_h(\tau, \omega; x) \rangle d\omega dt d\tau \quad (.2)$$

We then employ a change of variables,

$$\langle\langle t_u^n \rangle_x\rangle = \int \int \int (t + \tau)^n W_u(t, \omega; 0) \langle W_h(\tau, \omega; x) \rangle d\omega dt d\tau \quad (.3)$$

The binomial theorem is given by

$$(t + \tau)^n = \sum_{m=0}^n \binom{n}{m} t^{n-m} \tau^m \quad (.4)$$

Substituting this equation into Eq. (.3) gives

$$\langle\langle t_u^n \rangle_x\rangle = \sum_{m=0}^n \binom{n}{m} \int \int \int t^{n-m} \tau^m W_u(t, \omega; 0) \langle W_h(\tau, \omega; x) \rangle d\omega dt d\tau \quad (.5)$$

We may now do the integrals over t and τ , giving

$$\langle \langle t_u^n \rangle_x \rangle = \sum_{m=0}^n \binom{n}{m} \int \langle t_u^{n-m} \rangle_{0,\omega} \langle \langle t_h^n \rangle_{x,\omega} \rangle d\omega \quad (.6)$$

which gives the expected value of all temporal moments.

The second order expectations of the temporal moment features are given by Eq. (5.3),

$$\langle \langle \langle t_u^n \rangle_x \rangle^2 \rangle = \int \int \int \int t_1^n t_2^n \langle W_u(t_1, \omega_1, x) W_u(t_2, \omega_2, x) \rangle dt_1 dt_2 d\omega_1 d\omega_2 \quad (.7)$$

Proceeding analogously to the previous case, we substitute in Eq. (5.1) twice,

$$\begin{aligned} \langle \langle \langle t_u^n \rangle_x \rangle^2 \rangle = \\ \int \int \int \int t_1^n t_2^n \langle (W_u(t_1, \omega_1, 0) *_{t_1} W_h(t_1, \omega_1, x)) (W_u(t_2, \omega_2, 0) *_{t_2} W_h(t_2, \omega_2, x)) \rangle dt_1 dt_2 d\omega_1 d\omega_2 \end{aligned} \quad (.8)$$

We next use the standard definition of convolution twice and a change of variables to obtain

$$\begin{aligned} \langle \langle \langle t_u^n \rangle_x \rangle^2 \rangle = \int \int \int \int \int \int (t_1 + \tau_1)^n (t_2 + \tau_2)^n W_u(t_1, \omega_1, 0) W_u(t_2, \omega_2, 0) \\ \langle W_h(\tau_1, \omega_1, x) W_h(\tau_2, \omega_2, x) \rangle d\tau_1 d\tau_2 dt_1 dt_2 d\omega_1 d\omega_2 \end{aligned} \quad (.9)$$

The binomial theorem may be used twice here, giving,

$$\begin{aligned} \langle \langle \langle t_u^n \rangle_x \rangle^2 \rangle = \sum_{m_1, m_2=0}^n \binom{n}{m_1} \binom{n}{m_2} \int \int \int \int \int \int t_1^{n-m_1} \tau_1^{m_1} t_2^{n-m_2} \tau_2^{m_2} \\ W_u(t_1, \omega_1, 0) W_u(t_2, \omega_2, 0) \langle W_h(\tau_1, \omega_1, x) W_h(\tau_2, \omega_2, x) \rangle d\tau_1 d\tau_2 dt_1 dt_2 d\omega_1 d\omega_2 \end{aligned} \quad (.10)$$

We evaluate the integrals over t_1 and t_2

$$\begin{aligned} \langle \langle \langle t_u^n \rangle_x \rangle^2 \rangle = \sum_{m_1, m_2=0}^n \binom{n}{m_1} \binom{n}{m_2} \int \int \langle t_u^{n-m_1} \rangle_{0,\omega} \langle t_u^{n-m_2} \rangle_{0,\omega} \times \\ \int \int \tau_1^{m_1} \tau_2^{m_2} \langle W_h(\tau_1, \omega_1, x) W_h(\tau_2, \omega_2, x) \rangle d\tau_1 d\tau_2 d\omega_1 d\omega_2 \end{aligned} \quad (.11)$$

and finally evaluate the integrals over τ_1 and τ_2 , giving

$$\langle \langle \langle t_u^n \rangle_x \rangle^2 \rangle = \sum_{m_1, m_2=0}^n \binom{n}{m_1} \binom{n}{m_2} \int \int \langle t_u^{n-m_1} \rangle_{0,\omega} \langle t_u^{n-m_2} \rangle_{0,\omega} \langle \langle t_h^{m_1} \rangle_{x,\omega_1} \langle t_h^{m_2} \rangle_{x,\omega_2} \rangle d\omega_1 d\omega_2 \quad (.12)$$

A.2 FREQUENCY

The expected values of the frequency moment features are given by Eq. (5.10),

$$\langle\langle\omega_u^n\rangle_x\rangle = \int \int \omega^n \langle W_u(t, \omega; x) \rangle d\omega dt \quad (.13)$$

Substituting in the expression from Eq. (5.1), we obtain

$$\langle\langle\omega_u^n\rangle_x\rangle = \int \int \omega^n W_u(t, \omega; 0) *_t \langle W_h(t, \omega; x) \rangle d\omega dt \quad (.14)$$

We use the standard definition of convolution to get

$$\langle\langle\omega_u^n\rangle_x\rangle = \int \int \int \omega^n W_u(t - \tau, \omega; 0) \langle W_h(\tau, \omega; x) \rangle d\omega dt d\tau \quad (.15)$$

and by the integrating over t first, and then over τ we find

$$\langle\langle\omega_u^n\rangle_x\rangle = \int \omega^n |F(0, \omega)|^2 \langle |H(x, \omega)|^2 \rangle d\omega \quad (.16)$$

The second order expectation of the frequency moments is given by Eq. (5.11)

$$\langle\langle\omega_u^n\rangle_x^2\rangle = \int \int \int \int \omega_1^n \omega_2^n \langle W_u(t_1, \omega_1; x) W_u(t_2, \omega_2; x) \rangle d\omega_1 d\omega_2 dt_1 dt_2 \quad (.17)$$

Inserting the expression from Eq. (5.1) and organizing terms, we get

$$\begin{aligned} \langle\langle\omega_u^n\rangle_x^2\rangle &= \int \int \int \int \omega_1^n \omega_2^n W_u(t_1 - \tau_1, \omega_1; 0) W_u(t_2 - \tau_2, \omega_2; 0) \times \\ &\quad \langle W_h(\tau_1, \omega_1; x) W_h(\tau_2, \omega_2; x) \rangle d\omega_1 d\omega_2 dt_1 dt_2 d\tau_1 d\tau_2 \end{aligned} \quad (.18)$$

By the integrating over t first, and then over τ we obtain

$$\langle\langle\omega_u^n\rangle_x^2\rangle = \int \int \omega_1^n \omega_2^n |F(0, \omega_1)|^2 |F(0, \omega_2)|^2 \langle |H(x, \omega_1)|^2 |H(x, \omega_2)|^2 \rangle d\omega_1 d\omega_2 d\tau_1 d\tau_2 \quad (.19)$$

BIBLIOGRAPHY

- [1] R. A. Altes. Detection, estimation, and classification with spectrograms. *The Journal of the Acoustical Society of America*, 67(4):1232–1246, 1980.
- [2] L. C. Andrews and R. L. Phillips. *Laser Beam Propagation through Random Media, Second Edition (SPIE Press Monograph Vol. PM152)*. SPIE Publications, 2nd edition.
- [3] M. Ben-Bassat. *Use of Distance Measures, Information Measures and Error Bounds in Feature Evaluation*, chapter 35, pages 773–791. Elsevier Science Pub Co, March 1983.
- [4] M. A. Biot and I. Tolstoy. Formulation of wave propagation in infinite media by normal coordinates with an application to diffraction. In *Ocean Acoustics: Theory and Experiment in Underwater Sound*, pages 305–330. Acoustical Society of America, 1957.
- [5] L. M. Brekhovskikh. *Waves in layered media (Applied mathematics and mechanics)*. Academic Press, 1st edition.
- [6] M. J. Buckingham. Acoustic propagation in a wedge-shaped ocean with perfectly reflecting boundaries. In L. B. Felsen, editor, *NATO Advanced Research Workshop on Hybrid Formulation of Wave Propagation and Scattering*, pages 77–105, 1983.
- [7] M. J. Buckingham. Theory of three-dimensional acoustic propagation in a wedgelike ocean with a penetrable bottom. *The Journal of the Acoustical Society of America*, 82(1):198–210, 1987.
- [8] W. S. Burdic. *Underwater Acoustic System Analysis (Prentice-Hall Signal Processing Series)*. Prentice Hall, second edition, 1990.
- [9] P. Chestnut, H. Landsman, and R. W. Floyd. A sonar target recognition experiment. *The Journal of the Acoustical Society of America*, 66(1):140–147, 1979.
- [10] P. C. Chestnut and R. W. Floyd. An aspect-independent sonar target recognition method. *The Journal of the Acoustical Society of America*, 70(3):727–734, 1981.
- [11] P. Chevret, N. Gache, and V. Zimpfer. Time-frequency filters for target classification. *The Journal of the Acoustical Society of America*, 106(4):1829–1837, 1999.

- [12] D. Chu. Impulse response of density contrast wedge using normal coordinates. *The Journal of the Acoustical Society of America*, 86(5):1883–1896, 1989.
- [13] D. Chu. Exact solution for a density contrast shallow-water wedge using normal coordinates. *The Journal of the Acoustical Society of America*, 87(6):2442–2450, 1990.
- [14] L. Cohen. *Time Frequency Analysis : Theory and Applications (Prentice-Hall Signal Processing)*. Prentice Hall PTR, December 1994.
- [15] L. Cohen and P. Loughlin. Dispersion – its effects and compensation. In F. Sadjadi, editor, *Physics of Automatic Target Recognition*. Springer, 2007.
- [16] L. Cohen, P. Loughlin, and G. Okopal. Exact and approximate moments of a propagating pulse. *Journal of Modern Optics*, 55(19):3349–3358, 2008.
- [17] M. Dash and H. Liu. Feature selection for classification. *Intelligent Data Analysis*, 1:131–156, 1997.
- [18] R. Dashen, W. H. Munk, K. M. Watson, and F. Zachariasen. *Sound Transmission through a Fluctuating Ocean*. Cambridge University Press, 1 edition, June 1979.
- [19] Roger Dashen. Path integrals for waves in random media. *Journal of Mathematical Physics*, 20(5):894–920, 1979.
- [20] M. H. Degroot and M. J. Schervish. *Probability and Statistics, 3rd Edition*. Addison Wesley, 3rd edition, October 2001.
- [21] D. Dowson and A. Wragg. Maximum-entropy distributions having prescribed first and second moments (corresp.). *Information Theory, IEEE Transactions on*, 19(5):689–693, 1973.
- [22] L. Flax, L. R. Dragonette, and H. überall. Theory of elastic resonance excitation by sound scattering. *The Journal of the Acoustical Society of America*, 63(3):723–731, 1978.
- [23] A. P. French. *Vibrations and Waves (M.I.T. Introductory Physics Series)*. W. W. Norton, 1 edition, January 1971.
- [24] G. Gaunaurd. Transient acoustic scattering by fluid-loaded elastic shells. *International Journal of Solids and Structures*, 27(6):699–711, 1991.
- [25] G. C. Gaunaurd and D. Brill. Acoustic spectrogram and complex-frequency poles of a resonantly excited elastic tube. *The Journal of the Acoustical Society of America*, 75(6):1680–1693, 1984.
- [26] G. C. Gaunaurd and H. C. Strifors. Frequency- and time-domain analysis of the transient resonance scattering resulting from the interaction of a sound pulse with submerged elastic shells. *Ultrasonics, Ferroelectrics and Frequency Control, IEEE Transactions on*, 40(4):313–324, 1993.

- [27] I. Guyon and A. Elisseeff. An introduction to variable and feature selection. *Journal of Machine Learning Research*, 3:1157–1182, 2003.
- [28] C. H. Harrison. Wave solutions in three-dimensional ocean environments. *The Journal of the Acoustical Society of America*, 93(4):1826–1840, 1993.
- [29] T. Hastie, R. Tibshirani, and J. H. Friedman. *The Elements of Statistical Learning*. Springer, August 2001.
- [30] J. F. Hoffman. Classification of spherical targets using likelihood ratios and quadrature components. *The Journal of the Acoustical Society of America*, 49(1A):23–30, 1971.
- [31] E. T. Jaynes. Information theory and statistical mechanics. *Physical Review*, 106(4):620+, May 1957.
- [32] F. B. Jensen, W. A. Kuperman, M. B. Portor, and H. Schmidt. *Computational Ocean Acoustics (Modern Acoustics and Signal Processing)*. American Institute of Physics.
- [33] V. K. Kuznetsov. A new method for solving the problem of the sound field in a fluid wedge. *Soviet Physics - Acoustics*, 5:171–176, 1959.
- [34] C. H. Liu and K. C. Yeh. Pulse spreading and wandering in random media. *Radio Science*, 14(5):925–931, 1979.
- [35] C. H. Liu and K. C. Yeh. Statistics of pulse arrival time in turbulent media. *The Journal of the Optical Society of America*, 70(2):168–172, 1980.
- [36] H. Liu, E. R. Dougherty, J. G. Dy, K. Torkkola, E. Tuv, H. Peng, C. Ding, F. Long, M. Berens, L. Parsons, Z. Zhao, L. Yu, and G. Forman. Evolving feature selection. *IEEE Intelligent Systems*, 20(6):64–76, November 2005.
- [37] P. Loughlin. Wigner distribution approximation for filtered signals and waves. *Journal of Modern Optics*, 53(16):2387–2397, 2006.
- [38] P. Loughlin and L. Cohen. Moment features invariant to dispersion. volume 5426, pages 234–246. SPIE, 2004.
- [39] P. Loughlin and L. Cohen. Phase-space approach to wave propagation with dispersion and damping. volume 5559, pages 221–231. SPIE, 2004.
- [40] P. Loughlin and L. Cohen. A wigner approximation method for wave propagation. *The Journal of the Acoustical Society of America*, 118(3):1268–1271, 2005.
- [41] L. R. Mead and N. Papanicolaou. Maximum entropy in the problem of moments. *Journal of Mathematical Physics*, 25(8):2404–2417, 1984.
- [42] G. Okopal and P. Loughlin. Feature extraction for classification of signals propagating in channels with dispersion and dissipation. volume 6566, pages 65660G+. SPIE, 2007.

- [43] G. Okopal, P. Loughlin, and L. Cohen. Recognition of propagating vibrations and invariant features for classification. volume 6234, pages 623415+. SPIE, 2006.
- [44] G. Okopal, P. Loughlin, and L. Cohen. Dispersion-invariant features for classification. *The Journal of the Acoustical Society of America*, 123(2):832–841, 2008.
- [45] A. V. Oppenheim, R. W. Schaffer, and J. R. Buck. *Discrete-Time Signal Processing (2nd Edition)*. Prentice Hall, February 1999.
- [46] A. D. Pierce. Extension of the method of normal modes to sound propagation in an almost-stratified medium. *The Journal of the Acoustical Society of America*, 37(1):19–27, 1965.
- [47] C. E. Shannon. A mathematical theory of communication. *SIGMOBILE Mob. Comput. Commun. Rev.*, 5(1):3–55, January 2001.
- [48] I. Stakgold. *Boundary Value Problems of Mathematical Physics Vol 2*. Macmillan, January 1968.
- [49] A. Tagliani. On the application of maximum entropy to the moments problem. *Journal of Mathematical Physics*, 34(1):326–337, 1993.
- [50] I. Tolstoy and C. S. Clay. *Ocean Acoustics : Theory and Experiment in Underwater Sound*. Acoustical Society of America, 1987.
- [51] C. Y. Tsui, G. N. Reid, and G. C. Gaunard. Resonance scattering by elastic cylinders and their experimental verification. *The Journal of the Acoustical Society of America*, 80(2):382–390, 1986.
- [52] R. J. Urick. *Principles of Underwater Sound 3rd Edition*. Peninsula Pub, August 1996.
- [53] H. L. Van Trees. *Detection, Estimation, and Modulation Theory, Part I*. Wiley-Interscience, 1 edition, September 2001.
- [54] A. D. Waite. *Sonar for Practising Engineers*. Wiley, 3 edition, November 2001.
- [55] K. C. Yeh and C. H. Liu. An investigation of temporal moments of stochastic waves. *Radio Science*, 12(5):671–680, 1977.